Università degli Studi di Genova

Università
di Genova

PhD Thesis

IDENTIFICATION OF NOVEL BIGUANIDE BASED-COMPOUNDS AS ANTI TUMOR AGENTS FOR GLIOBLASTOMA: PHARMACOLOGICAL ASSESSMENT IN 3D CULTURE MODELS

Ph.D. Course in NEUROSCIENCE

Cycle XXXIV (2018-2021)

Curriculum: Clinical and experimental Neuroscience

Candidate:

Dr. Alessia Graziana Bosio

Tutor:

Prof. Tullio Florio

Index

Abstract

Glioblastoma (GBM) is the most common malignant and aggressive adult brain tumour characterized by its clinical behaviour, with high growth rate, diffuse invasiveness, and low response to therapies. Despite of multimodal treatment, which consists in extensive surgery followed by radiotherapy and chemotherapy (temozolomide, TMZ) the mean life expectancy for patients with GBM is less than 2 years. Although remarkable research efforts have been done in the last decades, no significant improvement in patient survival have been obtained from 2005, also due to the lack of appropriate models to study the role of cellular heterogeneity and microenvironment in GBM growth, invasiveness and drug response.

Among the main causes of therapeutic failure there is the ability of GBM cells to rapidly invade the brain parenchyma, greatly limiting successful surgical tumour debulking and the presence of cancer stem cells (CSC, also called tumour-initiating cells, TICs) which were identified over a decade ago also in GBM. Cancer stem cells are responsible for the malignant properties of tumours, have stem properties (self-renewal and differentiation), chemo-/radio-resistance and are able to expand to re-initiate tumours, promoting tissue infiltration, metastasis and relapse. CSC display cellular plasticity that is the ability to move between cell states to efficiently adapt to signals from the tumour microenvironment, such as terminal differentiation into a non-tumorigenic state, transition into an invasive mesenchymal phenotype (epithelial–mesenchymal transition, EMT), or trans-differentiation into endothelial-like cells, leading to tumour angiogenesis. Conventional chemotherapies can eliminate bulk tumour cells while CSC evade most therapies, thus in order to GBM eradication, it will be crucial to find compounds able to effectively target CSC.

Metformin, a widely used antidiabetic drug shows an antiproliferative effect on GBM CSC (GSC), via the inhibition of the CLIC-1 (Chloride Intracellular Channel 1) mediated ion current. Since other biguanides (both linear or cyclic) have demonstrated to act via CLIC-1 inhibition, this mechanism of action has been proposed to be a pharmacological class effect.

Thus, we tested novel biguanide derivatives to enhance the metformin antitumour effect and pharmacological profile. Firstly, we performed a screening of the antiproliferative activity (by MTT assay and cell count) of the novel biguanide in-vitro, on patient-derived GSC and to assess the absence of off-target activity we used umbilical cord mesenchymal stem cells. We identified two compounds, Q54 (IC50 0.43 mM) and Q48 (IC50 0.083 mM) which exhibit a more potent antiproliferative effect as compared to metformin, the absence of off-target activity and the selectivity towards CLIC-1 (tested by electrophysiology recordings). Conversely, Q46 which didn't show any significant effect was chosen as a positive control. By Boyden chambers assay and Matrigel™ invasion assay, we assessed the impairment of migration and invasion. In zebrafish, Q54 nor Q48 display aspecific toxicity, but Q54 was able to reduce the proliferation of GSCs xenotransplanted in their hindbrain. Moreover, we characterized two 3D models (GSC 3D cultures and tumoroids) by assessing cell proliferation (by EdU labelling), cell subpopulations and drug response. Q54 and Q48 were able to inhibit cell proliferation on GSC 3D cultures.

By screening our GSC cultures for the CLIC-1 protein content we found that 2 cultures which spontaneously express low CLIC-1, were able to grow in vivo and to retain stem-like phenotype and functional features in vitro, but in these cultures, Q48 and Q54 displayed reduced potency and efficacy as antiproliferative agents as compared to high CLIC-1-expressing tumours.

Thus, this data highlight the potential of Q48 and Q54 to target GSC with a better pharmacological profile as compared to metformin in CLIC-1 expressive culture; indeed, CLIC-1 acts as a booster for GSC proliferation but it is not required for GBM development. In addition, our compounds were tested on three different models that allow us to obtain different information that integrate each other, aiming to obtain more predictive results of what could happen in a GBM. We suggest that this approach could be useful in order to try to overcome the lack of reliable models in GBM research.

Introduction

1. Brain tumours

The American Cancer Society (ACS) and the International Agency for Research on Cancer (IARC) in 2020, have estimated that 1 out of 5 persons will develop cancer during their lifetime, thus cancer represents one of the main problems for the healthcare system worldwide. [1]

Brain tumours are a subgroup of tumours that arise within the central nervous system (CNS), affecting young, adult and elderly. Brain tumours could be primary brain tumours (benign or malign), which originate from brain cells, or they could be metastases from other neoplasia (breast, lung, melanoma). Focusing on primary brain tumours, they represent the most commonly diagnosed solid malignancy among children (0-19) accounting for 20% of the newly diagnosis. Meningioma, glioblastomas and astrocytomas represent more than half of all CNS tumours considering all age groups; their incidence peaks in the elderly. [2]

In Italy, 6122 tumours of the CNS have been diagnosed in 2020, representing the 1.6% of the total new cancer diagnosis. Brain tumours accounts for more than 2% of the deaths caused by malignancies in adults (data from 2017) [3].

The frequent presence of non-specific symptoms that could delay the diagnosis, and the vulnerability of the CNS, patients' quality of life and prognosis is seriously affected also in case of benign neoplasm, making them among the most lethal and debilitating tumours.

1.2 Classification

The World Health Organization (WHO) in 2016 classified brain tumours according to localization, histological and molecular parameters.[4]

WHO classification of tumours of the central nervous system

Diffuse astrocytic and oligodendroglial tumours	
Diffuse astrocytoma, IDH-mutant	9400/3
Gemistocytic astrocytoma, IDH-mutant	9411/3
Diffuse astrocytoma, IDH-wildtype	*9400/3*
Diffuse astrocytoma, NOS	9400/3
Anaplastic astrocytoma, IDH-mutant	9401/3
Anaplastic astrocytoma, IDH-wildtype	*9401/3*
Anaplastic astrocytoma, NOS	9401/3
Glioblastoma, IDH-wildtype	9440/3
Giant cell glioblastoma	9441/3
Gliosarcoma	9442/3
Epithelioid glioblastoma	*9440/3*
Glioblastoma, IDH-mutant	9445/3*
Glioblastoma, NOS	9440/3
Diffuse midline glioma, H3 K27M–mutant	9385/3*
Oligodendroglioma, IDH-mutant and 1p/19q-codeleted	9450/3
Oligodendroglioma, NOS	9450/3
Anaplastic oligodendroglioma, IDH-mutant and 1p/19q-codeleted	9451/3
Anaplastic oligodendroglioma, NOS	*9451/3*
Oligoastrocytoma, NOS	*9382/3*
Anaplastic oligoastrocytoma, NOS	*9382/3*
Other astrocytic tumours	
Pilocytic astrocytoma	9421/1
Pilomyxoid astrocytoma	9425/3
Subependymal giant cell astrocytoma	9384/1
Pleomorphic xanthoastrocytoma	9424/3
Anaplastic pleomorphic xanthoastrocytoma	9424/3
Ependymal tumours	
Subependymoma	9383/1
Myxopapillary ependymoma	9394/1
Ependymoma	9391/3
Papillary ependymoma	9393/3
Clear cell ependymoma	9391/3
Tanycytic ependymoma	9391/3
Ependymoma, *RELA* fusion–positive	9396/3*
Anaplastic ependymoma	9392/3
Other gliomas	
Chordoid glioma of the third ventricle	9444/1
Angiocentric glioma	9431/1
Astroblastoma	9430/3
Choroid plexus tumours	
Choroid plexus papilloma	9390/0
Atypical choroid plexus papilloma	9390/1
Choroid plexus carcinoma	9390/3
Neuronal and mixed neuronal-glial tumours	
Dysembryoplastic neuroepithelial tumour	9413/0
Gangliocytoma	9492/0
Ganglioglioma	9505/1
Anaplastic ganglioglioma	9505/3
Dysplastic cerebellar gangliocytoma (Lhermitte–Duclos disease)	9493/0
Desmoplastic infantile astrocytoma and ganglioglioma	9412/1
Papillary glioneuronal tumour	9509/1
Rosette-forming glioneuronal tumour	9509/1
Diffuse leptomeningeal glioneuronal tumour	
Central neurocytoma	9506/1
Extraventricular neurocytoma	9506/1
Cerebellar liponeurocytoma	9506/1
Paraganglioma	8693/1
Tumours of the pineal region	
Pineocytoma	9361/1
Pineal parenchymal tumour of intermediate differentiation	9362/3
Pineoblastoma	9362/3
Papillary tumour of the pineal region	9395/3
Embryonal tumours	
Medulloblastomas, genetically defined	
Medulloblastoma, WNT-activated	9475/3*
Medulloblastoma, SHH-activated and *TP53*-mutant	9476/3*
Medulloblastoma, SHH-activated and *TP53*-wildtype	9471/3
Medulloblastoma, non-WNT/non-SHH	9477/3*
Medulloblastoma, group 3	
Medulloblastoma, group 4	
Medulloblastomas, histologically defined	
Medulloblastoma, classic	9470/3
Medulloblastoma, desmoplastic/nodular	9471/3
Medulloblastoma with extensive nodularity	9471/3
Medulloblastoma, large cell / anaplastic	9474/3
Medulloblastoma, NOS	9470/3
Embryonal tumour with multilayered rosettes, C19MC-altered	9478/3*
Embryonal tumour with multilayered rosettes, NOS	*9478/3*
Medulloepithelioma	9501/3
CNS neuroblastoma	9500/3
CNS ganglioneuroblastoma	9490/3
CNS embryonal tumour, NOS	9473/3
Atypical teratoid/rhabdoid tumour	9508/3
CNS embryonal tumour with rhabdoid features	*9508/3*
Tumours of the cranial and paraspinal nerves	
Schwannoma	9560/0
Cellular schwannoma	9560/0
Plexiform schwannoma	9560/0

Melanotic schwannoma	9560/1
Neurofibroma	9540/0
Atypical neurofibroma	9540/0
Plexiform neurofibroma	9550/0
Perineurioma	9571/0
Hybrid nerve sheath tumours	
Malignant peripheral nerve sheath tumour	9540/3
Epithelioid MPNST	9540/3
MPNST with perineurial differentiation	9540/3
Meningiomas	
Meningioma	9530/0
Meningothelial meningioma	9531/0
Fibrous meningioma	9532/0
Transitional meningioma	9537/0
Psammomatous meningioma	9533/0
Angiomatous meningioma	9534/0
Microcystic meningioma	9530/0
Secretory meningioma	9530/0
Lymphoplasmacyte-rich meningioma	9530/0
Metaplastic meningioma	9530/0
Chordoid meningioma	9538/1
Clear cell meningioma	9538/1
Atypical meningioma	9539/1
Papillary meningioma	9538/3
Rhabdoid meningioma	9538/3
Anaplastic (malignant) meningioma	9530/3
Mesenchymal, non-meningothelial tumours	
Solitary fibrous tumour / haemangiopericytoma**	
Grade 1	8815/0
Grade 2	8815/1
Grade 3	8815/3
Haemangioblastoma	9161/1
Haemangioma	9120/0
Epithelioid haemangioendothelioma	9133/3
Angiosarcoma	9120/3
Kaposi sarcoma	9140/3
Ewing sarcoma / PNET	9364/3
Lipoma	8850/0
Angiolipoma	8861/0
Hibernoma	8880/0
Liposarcoma	8850/3
Desmoid-type fibromatosis	8821/1
Myofibroblastoma	8825/0
Inflammatory myofibroblastic tumour	8825/1
Benign fibrous histiocytoma	8830/0
Fibrosarcoma	8810/3
Undifferentiated pleomorphic sarcoma / malignant fibrous histiocytoma	8802/3
Leiomyoma	8890/0
Leiomyosarcoma	8890/3
Rhabdomyoma	8900/0
Rhabdomyosarcoma	8900/3
Chondroma	9220/0
Chondrosarcoma	9220/3
Osteoma	9180/0
Osteochondroma	9210/0
Osteosarcoma	9180/3
Melanocytic tumours	
Meningeal melanocytosis	8728/0
Meningeal melanocytoma	8728/1
Meningeal melanoma	8720/3
Meningeal melanomatosis	8728/3
Lymphomas	
Diffuse large B-cell lymphoma of the CNS	9680/3
Immunodeficiency-associated CNS lymphomas	
AIDS-related diffuse large B-cell lymphoma	
EBV-positive diffuse large B-cell lymphoma, NOS	
Lymphomatoid granulomatosis	9766/1
Intravascular large B-cell lymphoma	9712/3
Low-grade B-cell lymphomas of the CNS	
T-cell and NK/T-cell lymphomas of the CNS	
Anaplastic large cell lymphoma, ALK-positive	9714/3
Anaplastic large cell lymphoma, ALK-negative	9702/3
MALT lymphoma of the dura	9699/3
Histiocytic tumours	
Langerhans cell histiocytosis	9751/3
Erdheim–Chester disease	9750/1
Rosai–Dorfman disease	
Juvenile xanthogranuloma	
Histiocytic sarcoma	9755/3
Germ cell tumours	
Germinoma	9064/3
Embryonal carcinoma	9070/3
Yolk sac tumour	9071/3
Choriocarcinoma	9100/3
Teratoma	9080/1
Mature teratoma	9080/0
Immature teratoma	9080/3
Teratoma with malignant transformation	9084/3
Mixed germ cell tumour	9085/3
Tumours of the sellar region	
Craniopharyngioma	9350/1
Adamantinomatous craniopharyngioma	9351/1
Papillary craniopharyngioma	9352/1
Granular cell tumour of the sellar region	9582/0
Pituicytoma	9432/1
Spindle cell oncocytoma	8290/0
Metastatic tumours	

The morphology codes are from the International Classification of Diseases for Oncology (ICD-O) [742A]. Behaviour is coded /0 for benign tumours; /1 for unspecified, borderline, or uncertain behaviour; /2 for carcinoma in situ and grade III intraepithelial neoplasia; and /3 for malignant tumours. The classification is modified from the previous WHO classification, taking into account changes in our understanding of these lesions.
*These new codes were approved by the IARC/WHO Committee for ICD-O.
Italics: Provisional tumour entities. **Grading according to the 2013 *WHO Classification of Tumours of Soft Tissue and Bone*.

Figure 1 Who classification of tumours of the central nervous system (2016) [4]

Focusing on astrocytic tumours (or gliomas), a group of brain tumours that arise from astrocytes, they are historically classified into four groups with increasing malignancy, in line with the histological presentation.

Pilocityc astrocytoma (WHO Grade I): oftener affects children, has the best long-term survival among gliomas due to its lesser malignancy and the possibility of a successful surgical resection.

Diffuse astrocytoma (WHO Grade II): slow growth gliomas with a mild grade of nuclear atypia. Despite its low level of malignancy and slow growth it can infiltrate the surrounding parenchyma, relapse after surgical resection and evolve to a high-grade glioma over time.

Anaplastic astrocytoma (WHO Grade III): it has greater cellularity and mitotic activity as compared to grade II gliomas. Tumours cells rapidly invade the surrounding normal brain tissue and migrate, thus the surgical resection is often ineffective and led to a rapid relapse.

Glioblastoma (WHO Grade IV): is the most aggressive and malignant form. It is characterized by fast replication, high infiltrative ability and strong nuclear atypia. Moreover, it shows areas of haemorrhage, necrosis and endothelial proliferation. Glioblastoma may derive from the evolution of a lower grade glioma.

The 2016 WHO classification takes also into account the Isocitrate Dehydrogenase (IDH) mutation status: each grade of astrocytomas could be either IDH-mutant or IDH-wild type. In particular, referring to the same astrocytoma grade, IDH-mutant status confers a better prognosis as compared to the IDH-wild type. The reason for the better prognosis confers by the IDH mutant is unknown: some researchers have hypothesized that IDH mutation results in decreasing the NADPH and α-ketoglutarate concentrations, thus affecting different cellular pathways.

It is now expected a new classification of brain tumour by WHO, in which the condition IDH-wild type became crucial for the classification as a glioblastoma, instead IDH-mutant will be classified as IDH-mutant astrocytoma, an entirely different category[5].

1.3 Glioblastoma

Glioblastoma (GBM) is the most aggressive and lethal form of primary brain tumour in adults, with a mean survival of 15 months, mostly due to high cell heterogeneity within the tumour mass, which leads to failure of the current standard of care. GBM can arise anywhere within the central nervous system but it is commonly located in the frontal or temporal lobes. According to the mutation of the IDH-1 gene, WHO classification distinguishes GBM into two types: IDH-wild type and IDH-mutant. The former subtype accounts for 90% of the cases, typically occurring in older patients as a de-novo GBM, while the latter classify GBMs which may results from a progression of lower grade diffuse glioma and is usually associated with a better prognosis[6]. The overall GBM annual incidence is 3-5 per 100,000 individuals with a mean age at the diagnosis of 64 years[2]. Despite no increase in brain tumour has observed since 1985, GBM represent an exception whereas it has been observed an increased incidence in several countries[7]. Unfortunately, the increasing incidence is not associated with an ameliorated prognosis: survival hasn't changed in the last decades, attending on an overall survival rate at 5 years of 5%, remarking the urgent need for new effective therapies against this neoplasia. With regard to gender, GBM frequency is slightly higher in males than female[2]. There is no evidence of risk factors for tumour development, except for history of ionising radiation exposure, or patients with familial cancer syndrome as Li-Fraumeni syndrome, Lynch syndrome and others[8].

1.3.1 Histological and Molecular features

From a histological point of view, GBM is characterized by pleomorphic astrocytes associated with marked nuclei atypia and high mitotic activity. A distinguishing mark of GBM is prominent angiogenesis mediated by a high level of VEGF expression. Despite the high neoangiogenesis, GBM also shows hypoxic and necrotic areas, commonly surrounded by crowded tumour cells forming pseudopalisading edges.

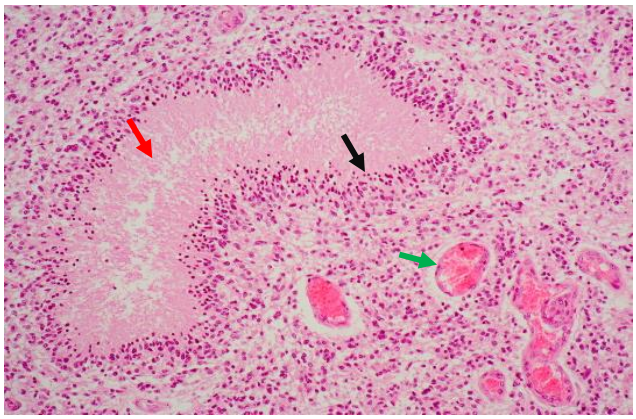

Figure 2 Histopathological image of a glioblastoma. Black arrow indicates the pseudopalisading edge with necrosis of neoplastic cells (red arrow) along with microvascular proliferation (green arrow) [9].

Glioblastoma presents a marked genetic instability and multiple alterations on different genes as TERT promoter, TP53, EGFR and PTEN, MGMT promoter; in particular, the latter is predictive for the response to alkylating agents[10,11]. On the basis of their genomic alteration and their gene expression profile, GBM have been proposed to be classified into 4 molecular subgroups: classical, mesenchymal, neural and proneural[12]. This classification has also clinical implications, for instance younger patients were mostly represented by the proneural subtype, which led to a longer survival. Classical and mesenchymal

subtype tumours will better respond to aggressive treatments, as compared to the other class[13].

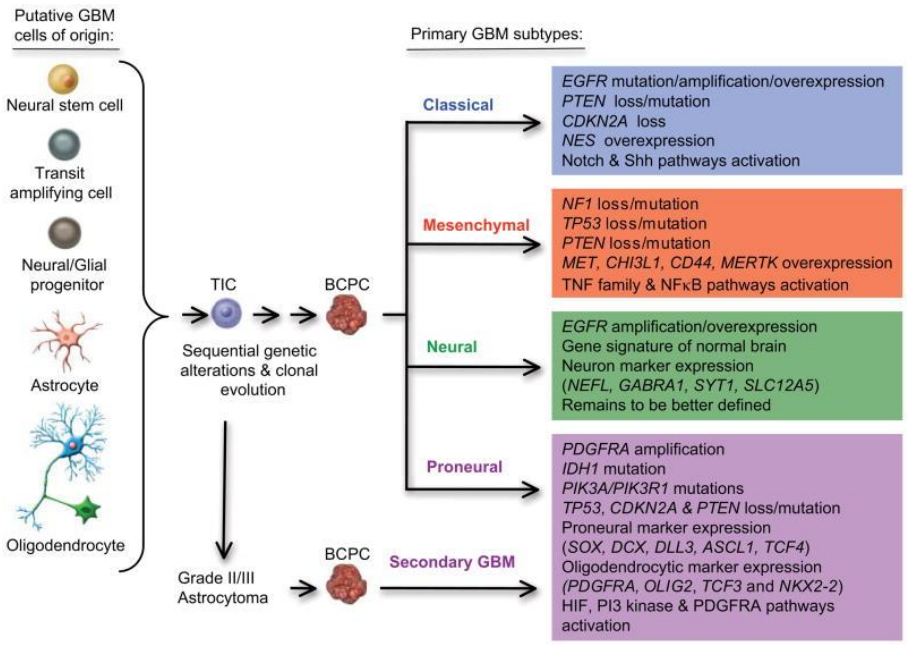

Figure 3 Genetic changes in different glioblastoma subtypes [12]

1.3.2 Clinical Presentation

The clinical presentation can vary according to tumour size, localization and brain region involved. Typically, the most common symptoms are related to the increased intracranial pressure and include headache, nausea, vomiting, dizziness, lethargy. In relation to the brain region involved, patients could experience neurological disorders such as weakness, numbness, hemiparesis, loss of vision or language alterations, but behavioural alterations are also frequent, especially in the early time of the disease. However, due to the non-specific nature of the symptoms at presentation, the diagnosis could be delayed and when the manifestation gets worse, the infiltrative nature of the tumour may have already colonized a wider area of the brain. The diagnosis is made accordingly to the brain imaging and biopsy.

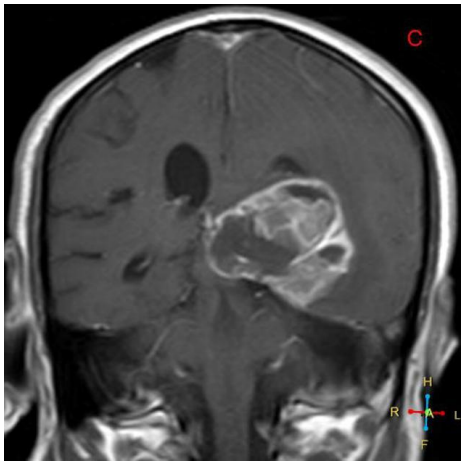

Figure 4 Brain MRI showing the presence of a Glioblastoma [14]

1.3.3 Standard of care

To date, the current standard of care is based on neurosurgery (whereas possible), chemo- and radiotherapy. The goal of the surgery is to obtain the maximal debulking of the tumour mass, while minimizing the injury to the surrounding normal brain, to reduce the patient's symptoms and increase the efficacy of the following therapy. However, due to the high infiltrative nature of GBM cells, which can migrate away from the mass in the early phases of tumour development, total resection is rarely obtainable. After the surgery, the main standard treatment offers to the patients is radiotherapy, which has been demonstrated to improve the mean survival rate, as compared to best supportive care[15–17]. Radiotherapy often led to a remission phase, in which remaining mass stop its growth or slightly decrease in size, improving the patient's symptoms. Nevertheless, not all patients are responsive to radiotherapy, and above all, tumour commonly relapses in one year leading to a worsening of the clinical condition and chance of survival. Concerning chemotherapy, the agents whose introduction shows a significant although small change in life-span rate is temozolomide (TMZ)[18]; this is an oral alkylating agent with a good penetration through the blood brain-barrier, generally well tolerated by patients. At physiological pH TMZ is rapidly

converted in the active compound 5-(3-Methyl-1-triazeno) imidazole-4-carboxamide (MTIC), whose antineoplastic activity is achieved by the alkylation of the guanine residues O^6 when DNA is in the replicative phase[19,20]. Unfortunately, tumour very often relapses even the TMZ therapy, indicating the presence of chemo-resistant cells. To date, the main known mechanism of TMZ resistance is the overexpression of O^6-methylguanine methyltransferase (MGMT), a DNA repairing enzyme, which eliminate the methyl residues, thus repairing the DNA and leading to a successful cell's replication[20–22].

In case of glioblastoma relapse, the chances of therapy are limited, patients could follow second line chemotherapy or be enrolled in a trial study or when resection is still possible, they could receive GliaSite, GammaTile, Gliadel wafers or similar, that are dispositive able to focus their action (irradiation or drug release) directly in the tumour cavity. In particular, GliSite is an inflatable balloon catheter able to deliver radiation by an aqueous solution of organically bound iodine-12 introduced into the balloon via a subcutaneous port; GliaSite is placed in the resection cavity at the time of tumour debulking; GammaTile, which is a more recent approach is a brachytherapy platform consisting of Cesium-131 (131Cs) seeds embedded with an absorbable collagen matrix. Instead, Gliadel is made by wafers that contains the chemotherapeutic drug carmustine, and are implanted in the tumour cavity during the surgical procedure, soon after the removal of the tumour mass.

To summarize, the first approach to a newly diagnosed glioblastoma is surgical resection (if possible), radio and chemotherapy, according to the Stupp protocol (fractionated radiotherapy plus TMZ, followed by adjuvant TMZ)[18]. To note, this protocol was the best improvement of glioblastoma's patient life-span rate, which unfortunately remains about 15 months from the diagnosis, with a deterioration in the quality of life. Since 2005, despite huge research efforts, no significant improvements have been obtained.

2. Cancer Stem Cells

The definition of stem cells specifically refers to a population of undifferentiated cells that retain the ability to renew themselves indefinitely and differentiate into a broad range of specialized cells. As far as cancer is concerned, tumour mass is mostly constituted by a larger differentiated population, usually with fast but time-limited growth, and a rare subpopulation of cancer stem cells (CSC) characterized by a slow but limitless cell-division[23]. CSCs exhibit, as the normal counterpart, peculiar characteristics:

- Self-renewal: The ability to generate by asymmetric division an identical progeny, in order to fuel the stem cells pool, and one that comes into differentiation processes.
- Multi-lineage Differentiation: The potentiality to differentiate into various cell types.
- Drug resistance: A high activity of DNA repairing enzyme and membrane drug extrusion pump.
- Expression of distinct stem-like cell biomarkers: Nestin, CD44, CD133, among others [24].
- Tumorigenic potential: Ability to generate a tumour upon intra-cranial transplantation in nude mice, that recapitulates the cellular heterogeneity of the parental tumour, which reflect a tumor-initiating cell activity of this subpopulation. [24,25]

CSCs were firstly identified and isolated in leukaemia in the '90[26], and then identified and isolated in several blood and solid tumours, such as breast, pancreatic, colorectal and brain cancers, among others[27–29]. CSC identification and isolation is based on the observation of phenotypic properties, and the expression of characteristic markers, that allow scientists to distinguish them

from the remaining cell populations of the tumour mass. Initially, the marker's pattern was thought to be peculiar for each specific tumour, for example, breast cancer CSCs are CD44 positive, while melanoma CSC show high expression of CD20. However, subsequent studies identified a large markers' overlap in different tumour histotypes. Therefore, is still difficult to identify the CSC population in different tumours by a validate methods: the marker's expression must always be correlated by the observation of the cells behaviour[24].

Historically, theories of tumorigenesis were based on the stochastic model, which propose that all cells within the whole cancer mass retain the same tumorigenic ability: cells have the same probability to acquire genetic mutations that lead to aberrant cell behaviour, thus giving rise to the tumour mass. After the evidence of the cancer stem cells existence, the stochastic model has been substituted by the hierarchical model, by which only a small cell subpopulation within the mass (CSC) acquires, by aberrant mutations, growth advantages and malignant properties that give rise to the primary neoplasm and its metastasis; in fact, the tumorigenic ability is demonstrated by the experiment according to which when CSC are implanted in nude mice the neoplasia is able to easily and quickly regrowth (also called TIC-Tumour initiating cells) [30,31].

CSC may originate from normal stem cells, that undergo genetic and/or epigenetic mutations, or may derive from a de-differentiation of epithelial cells (EMT-epithelial-mesenchymal transition)[32]. In both cases, the micro-environment (niche) plays a crucial role: several studies highlighted the importance of the niche in normal tissue homeostasis [33]. In cancer, tissue homeostasis is impaired due to different causes, including tissue inflammation processes, anomalous expression of the extracellular proteins, hypoxia. aberrant stimuli from the niche promote the development of cancer stem cell

phenotype and their malignant properties, such as sustainment of tumour progression and migration for metastasis propagation[31].

The identification of CSCs has important implication for patient survival and prognosis for two main reasons: on one hand, their high content within the tumour mass is prognostic and predictive for poor patient's outcome and survival, as studies show for breast cancer or colon cancer; on the other hand, their resistance to therapies make them the main responsible for metastasis and tumour relapse[31,34,35]. In light of this observation, it is crucial to consider CSC eradication while studying new and old antitumor agents and find therapeutic strategies able to effectively remove the pull of CSC.

2.1 Glioblastoma stem cells

The presence of CSCs in glioblastoma has been demonstrated by several groups starting the 2000s[36–38]. Soon after, their resistance to the standard of care therapies has been shown [39,40], thus becoming clear that one of the main reasons for GBM relapse and mortality is the persistence of CSCs. In particular, it has been observed that glioblastoma cancer stem cells (GSC), are able to implement the DNA repairing machinery in response to radiation therapy[39]. Moreover, GSCs activate several pathways that mediate cytotoxic drug resistance as DNA damage checkpoints, NOTCH, and PARP. Thus the persistence of GSC after administration of cytotoxic agents is not mediated by a single mechanism, but it is the result of the development and integration of several molecular pathways. To note, the resistance mechanisms could also be acquired by micro-environmental stimuli, hypoxia or metabolic alteration[41].

GSC origin is not clear: they could derive from normal neural stem cells, that undergoes genetic mutation, or from more differentiated progenitors that reacquire self-renewal and tumorigenic abilities[42].

Pathways regulating GSC activity involve the integration of several intrinsic and extrinsic factors. Among the intrinsic factors, there is genetic and epigenetic modifications, altogether with metabolic alterations. In particular, is well known that GBM shows important genetic inter-tumour and intra-tumour heterogeneity, displaying a broad range of mutations (including EGFR, IDH1, PTEN, TP53, ATRX…) which, together with acquired epigenetic alterations, contribute to regulate CSC survival and development. Moreover, GBM heterogeneity also make challenging to define the clonal complexity of this tumour, whose apex relies on CSC, responsible for GBM genesis and evolution. Metabolic alterations are mainly caused by restrictions of nutrients and oxygen intake, which lead to the activation and overexpression of self-renewal, proliferation and survival pathways. Extrinsic factors that promote stemness, include niche-derived stimuli, such as the NOTCH signalling mediated through the binding of Tenascin C with cell surface integrin, extracellular matrix stiffness, secreted chemokines, redundant activation of VEGF signalling, overexpression of metalloproteinase (important mediator of invasion). Regarding the immune system, on one side tumour-associated macrophages stimulate GSC tumorigenicity and growth, on the other side, GSCs are able to evade the control and elimination by the immune system through a variety of immunosuppressive mechanism. The combination of all these factors (genetic, epigenetic and metabolic alterations, micro-environmental factors and immune crosstalk) rules the growth of GSC and the maintenance of their stemness features[24,41,42].

To sum up, the complexity of GSC biology requires, in order to effectively eradicate the pool of GSC, a multi-target approach therapy is required, able to affects both their metabolism and the interactions with the niche; it is crucial to deeply study GSC regulation and metabolism to identify new therapeutic targets and possibly, more effective therapies.

2.1.1 Glioblastoma stem cells markers

One of the issues limiting the study of GSC biology derives from the lack of markers able to distinguish GSC from neural stem and progenitor cells (NSPC). Indeed, some of the most utilized markers are expressed by both cell populations, like the transcription factors Sox-2, Olig-2, and Nanog, or the intermediate filament protein Nestin. All these proteins are intracellular, therefore classical characterization techniques such as flow cytometry are hardly suitable, representing another limitation in the study of GSCs. The lack of exclusive markers, reliable and validate analysis techniques, make the isolation of this population challenging. In order to find out cell surface markers, several molecules have been proposed**:** CD133 (prominin-1) a glycoprotein of neural stem cells, CD44 (a cell surface glycoprotein), integrin α6, CD15/SSEA-1. To note, these markers are useful but are not fully specific and sensitive for GSC. Another assay to identify GSC in vitro is based on their ability to form neurospheres in a serum-free medium, based on the self-renewal abilities of these cells. To date, to characterize a culture of glioblastoma cell-enriched in cancer stem cells is essential to integrate a marker analysis with functional observation, as spherogenic assays[41,42].

3. New therapeutic approaches for Glioblastoma

The perspective of the life of glioblastoma patients from the diagnosis is less than two years, despite the combination of neurosurgery, radiotherapy and TMZ. The main cause of the bad prognosis in GBM patients is the rapid relapse, whereby the therapies are mostly ineffective and fail to control the neoplasia growth. The new cytotoxic approaches are directed to target several intracellular pathways, among them, those activated by tyrosine kinase receptors (RTKs) EGFR, PDGFR and VEGFR have been widely studied. Unfortunately, these agents didn't display a remarkable efficacy. For instance,

agents which target EGFR show limited effectiveness in glioblastoma due to the genetic variability among patients and their efficacy has been shown to be limited to the patients whose tumour co-express EGFRvIII and PTEN[43]. Recently, the REGOMA study reports that patients with recurrent high-grade glioma treated with regorafenib, an oral multi-target RTK inhibitor, demonstrated a significantly longer survival such as compared to standard therapy (lomustine) and a good safety profile, without significant dependence on MGMT expression and IDH status [44].

New approaches include the involvement of molecules that acts using monoclonal antibodies, as bevacizumab which acts against VEGF and has shown an important radiological response in patients with high-grade recurrent gliomas, targeting another of the landmarks of glioblastoma, the neo-angiogenesis[45], but without additional benefit to the patient life span rate[46]. Promising trials are ongoing also to study the efficacy of vaccines against different tumour cell surface receptors based on the administration of autologous dendritic cells[47], which present the enormous advantage to be patient-specific but at the same time, the present production difficulties.

In the last years the tumour-treating field (TT field) system has been developed, an electric field applied to the scalp at 200 kHz frequency, which demonstrate to give small survival advantages (few months) with concomitant TMZ treatment, likely through the disruption of the cells' mitosis[48]. TT field system shows a good safety profile but it requires the direct contact of the arrays with the shaved scalp for 22 hours per day, resulting in possible skin rashes, irritation, and ulcers, which could impair patients' adherence. [49]

In light of the dependence of tumour relapse by GSC survival and self-renewal, several studies are trying to target GSC intracellular pathways or membrane integrins. In the latter case cilengitide, an oral-agents acting on integrin subtypes $\alpha v\beta 3$, $\alpha v\beta 5$ and $\alpha 5\beta 1$, has been studied in several clinical trials, but

results are still controversial and seem to be influenced by the methylation status of the MGMT gene[50,51].

To sum up, thus far, no significant improvements in the standard therapies are accomplished and glioblastoma patients still don't have hope for a cure, even though several novel approach clinical trials are ongoing. Anyhow, to positively impact on survival rate, new discovered molecules should impact on GSC survival or be able to enhance the toxicity of classical chemotherapy agents. In order to find out new targets, basic research on GSC biology will be crucial to deeply study their pathways and molecular profile.

3.1 Innovative GSCs target: Chloride intracellular channel 1 (CLIC-1)

The chloride intracellular channel 1 (CLIC-1) belongs to a family of related genes (CLIC-1-6). This family of proteins is well conserved among the vertebrates suggesting their involvement in essential biological functions. Differently from the classical chloride channels, which only reside in the plasma membrane, the CLIC family exists as cytoplasmic soluble proteins, which, in response to different stimuli as pH change or redox status imbalance, assemble as integral membrane multimeric ion channel[52]. In particular, CLIC-1 expression and membrane activity has been reported to be increased and have a role in cell cycle progression, proliferation, migration and apoptosis in several human cancer as breast ductal carcinoma[53], gastric cancer[54], ovarian cancer[55], hepatocellular carcinoma[56] and glioblastoma[57], thus representing a possible tumour biomarker and new pharmacological target. In glioblastoma cells, CLIC-1 is overexpressed both at mRNA and protein level and the upregulation of the active trans-membrane conformation correlates with GBM aggressiveness[58]. The mechanism by which CLIC-1 mediates its activity is not well understood yet, the main hypothesis states that its functional upregulation

promotes Cl^- inward current which regulates ROS production and pH balance, resulting in cell cycle promotion[59]. In GSCs, CLIC-1 is overexpressed and constitutively located at the membrane level, showing high ionotropic activity. Interestingly, CLIC-1 silencing by siRNA, impairs in vitro proliferation and self-renewal ability of glioblastoma cancer stem cells; moreover, when CLIC-1 silenced cells are injected in nude mice, impaired tumorigenicity is observed with augmented mice survival as compared to those injected with non-silenced CSC. In GBM differentiated cells, which compose the great part of the tumour bulk, and in normal stem cells (i.e. mesenchymal stem cells), CLIC-1 activity doesn't seem to be crucial for proliferation and survival, as demonstrated by lack of significant effects after its pharmacological inhibition[60]. Thus it was proposed that GBM CSC proliferation and tumorigenesis depends on CLIC-1 activity[58]. Whether CLIC-1 activity is crucial for the survival of GBM CSC, then it could represent a new promising target to selectively impairs CSC viability.

3.2 Drug repositioning

Drug repositioning is defined as the identification of alternative therapeutic indications for already approved drugs, meaning that whereby a drug shows a potential effect on a different pathological condition, it will be reinvestigated for that aim. Different ways could lead to drug repositioning: serendipity, adverse events observation, epidemiological consideration, targeted research, deep investigation on drug mechanism of action or pathogenic mechanisms. Drug repositioning can extend the use of a molecule within the same therapeutic area of the already registered use (e.g. capecitabine utilized in tumours different from the original approved type) or even to another therapeutic field. This approach has huge advantages as compared to the "classical" de-novo drug discovery: it is cheaper, faster and more efficient, mostly because safety profile of the studied molecule in human has already been assessed and doesn't require new investigations, and the scale-up from

the industry to the clinic has already been performed. Clearly, drug repositioning still represents a drug development thus exhibit some "risky points" that pharmaceutical industries and researcher must take into account and overcome. Indeed, patients will present different pathological conditions which may uncover unexpected toxicities, the drug could be delivered by new or different delivery system or formulation, the dosing and the timing of the therapy could be different from the approved use, especially when the required dose is higher. These conditions could highlight adverse events unseen before, therefore these issues must be addressed with appropriate safety studies before proceeding in register the new therapeutic use[61]. In the history of drug discovery and development, there are several examples of "drug-repositioning", thalidomide, for example, was used as a sedative and antinausea during pregnancy but subsequently abandoned for its severe adverse events (impairment in limbs formation, due to lack of vascularization) that now are exploited to beat multiple myeloma (inhibition of tumour-related angiogenensis)[62,63]; sildenafil firstly designed as an antihypertensive drug, failed in this goal, but collateral effects showed efficacy in erectile dysfunction and pulmonary hypertension[64], indications that are now registered[65] and allow the use of a molecule which was first considered as inadequate; acetylsalicylic acid (ASA, aspirin), widely used as an anti-inflammatory drug, is now registered also as an anti-aggregation drug at a lower, safer dosage. This indication was based on the observation of a high rate of bleeding events in patients treated with aspirin that lead Craven in the 1950[s] to daily administer ASA in previously heart attacked patients, observing a clinical benefit[66]. This observation was later confirmed by the discovery of the COX-mediated mechanism of action. Moreover, studies are ongoing also for its potential anticancer activity[67,68].

As regards the oncology field, drug repositioning could represent a valid approach to integrate classical drug discovery. Indeed, the classical path "from the bench to the bedside" is particularly long, expensive and not efficient, as demonstrated by the small number of molecules that each year achieve the approval for the clinical use and from the number of compounds that pass the phase I of the clinical trial, but subsequently don't reveal the expected efficacy[69,70].

For glioblastoma therapy, several "new" and "old" molecules have been preclinically tested in vitro and/or in vivo, and some of them reached a further development in clinical trials either as single drug or in combination with other treatments[61]. Among the new developing drugs, for example, bevacizumab or regorafenib, originally approved for other tumours, are now undergoing trials also for glioblastoma[44,45]. As far as "old" drugs is concerned, there are different examples such as disulfiram that shows anti-proliferative activity in preclinical studies on GBM cell lines and on GSC, hence is now investigated in different clinical trials[61], or chloroquine which inhibits autophagy and in clinical trials increased the median overall survival when added to conventional therapies[71].

A remarkable example of drug repositioning, in oncology and in particular in glioblastoma new potential therapy is the antidiabetic drug metformin: starting from the observation that there was a positive correlation between the chronic consumption of metformin and a lower incidence and mortality for various types of cancer, as respected as both diabetic or nondiabetic subjects, metformin is being "re-studied" for its antineoplastic properties[72–74].

3.2.1 Metformin

Metformin is a biguanide molecule, widely used for the treatment of type II diabetes for more than 50 years. Metformin causes an impairment of hepatic glucose production, reduces intestinal absorption of glucose, reduces the lipolysis in adipocyte thus increasing and improving insulin sensitivity. The molecular mechanism through which metformin exploit its antidiabetic effects is not fully clarified and seems to involve lots of intracellular pathways, triggered by the direct modulation of the 5-adenosine monophosphate-activated protein kinase (AMPK): it acts by the suppression of the mitochondrial respiratory chain, increases the activity of the insulin receptor, and stimulate the GLUT4 transporter to the plasma membrane[61,72] . Thus, the activation of AMPK in particular, results in the regulation of cells metabolism and homeostasis, contribute to the euglycemic effect mediated by metformin[75].

Metformin is now under evaluation in different preclinical and clinical trials for its potential anticancer activity, due to the epidemiological observation of a positive correlation between metformin consumption and incidence of cancer[73]. Several in vitro studies show antiproliferative effects of metformin in various tumour type, such as pancreatic[76] and breast carcinomas[77,78], and glioma[79,80], alone or in combination with other chemotherapeutic agents. Particularly, in glioblastoma metformin is able to potentiate the pro-apoptotic TMZ effects, acting activate the 5-adenosine monophosphate-activated protein kinase (AMPK)[79].

Metformin exerts its antiproliferative effects through the regulation of insulin and glucose intake but also acts directly on tumour growth and survival. Among several hypotheses of the mechanism of action for the metformin-mediated antiproliferative effects, AMPK activation seems to have a central role, mostly due to the inhibition of mTOR pathway which results in the

impairment of cancer cell growth[72]. Nevertheless, different studies demonstrate AMPK independent metformin antiproliferative effects, for example through the modulation of the hexokinase I and II in triple-negative breast cancer[81], or the inhibition of K-ras pathway[82], or directly modulating the activity of $CD8^+$ tumour-infiltrating lymphocytes[83].

Noteworthy, metformin is able to selectively impair proliferation in CSC, as demonstrated in breast CSC and subsequently in different tumour types, including GBM, and shows synergistic effects with classical cytotoxic drugs[25,84–87]. The reason behind the higher sensitivity to metformin of CSC is under investigation: studies report the involvement of different pathways, from the hyperglicolitc metabolism, thus more sensitive to metformin, to the inhibition of CSC pro-inflammatory pathways which lead to cell growth arrest[61]. In particular, as regard GSC, metformin has been demonstrated to directly acts on CLIC-1. Indeed, metformin is able to reduce the Cl^- current by the interaction with the extracellular portion of CLIC-1 (possibly with Arg29) which lead to the antiproliferative effect by the cell cycle arrest in G1 phase. Interestingly, this modulation only occurs in GSC and not in normal stem cells (umbilical cord-derived mesenchymal stem cells -MSCs) where CLIC-1 localization is mainly confined to the cytoplasm[60]. In light of this evidence, CLIC-1 has been proposed to be a direct target of metformin action and thus, a target to pharmacologically impair GSC growth and survival[52,88]. However, high metformin concentration (up to 10mM) is required to induce GSC growth arrest in vitro, therefore this could prevent its translation into a clinical setting. Since other biguanides (both linear and cyclic) have demonstrated to act via CLIC-1 inhibition, this mechanism of action has been proposed to be a pharmacological class effect[88].

4. In-vitro research models

In the last years, accurate tumour-genome studies allowed a precise molecular classification of glioblastoma and the identification of different alterations driving its growth and spread. Even if several new possible pharmacological targets have been identified, in the short term probably a significant enhancement for patient survival is not expected, thus there is an urgent need to research in this field. To date, a critical factor in glioblastoma research, which has made both drug- and target-discovery complex and often a failure, is the lack of reliable models able to reproduce the marked intra-tumour heterogeneity and microenvironment interaction, which is well-known to have a critical role in GBM development and growth. Indeed, even if the discovery of cancer stem cells in GBM provide a huge advantage in GBM research, it is still difficult to model GBM developmental cellular hierarchy, the simultaneous presence and interplay between stem cells progenitors, differentiated tumour cells, non-tumour cells and immune system components (microglia and infiltrating macrophages)[89,90]. For instance, tumour-infiltrate immune system promotes GBM growth and invasion[91,92], or astrocytes which are very abundant in normal brain tissue where they carry out different role such as taking part to the blood brain barrier or sustain the neuronal survival, but they plays a key role also in GBM progression forming a peri-vascular space fundamental for GBM invasion[93]. In addition to the cell-cell interactions, it is important to consider the interactions between glioblastoma and ECM components. It has been demonstrated that GBM can remodel its microenvironment increasing the presence of tenascin-C, osteopontin, vitronectin and hyaluronic acid (HA), facilitating its infiltration ability along with the overexpression of CD44 (HA receptor), matrix metalloproteinase-9 (MMP-9) and hyalorinadase[94,95]. Moreover, GBM expresses high levels of RGD-binding integrins, which interact with ECM-proteins to promote cell

infiltration[50]. Thus, it will be crucial to model these intermolecular connections to better mimic this complex and dynamic communication network to obtain a more reliable picture of glioblastoma heterogeneity and pharmacological response.

4.1 2D models for glioblastoma research

Currently, the most widely used models in GBM research are GBM cell lines or patient-derived GSCs, in 2D cultures. These models have several limitations which result in alterations of cell phenotype, intracellular signalling, and drug response. In this culture condition, cells are grown as a monolayer on plastic or on an ECM-like layer, thus they are unable to recapitulate the 3D structure which affects cell-cell interaction, spatial organization, exposure to nutrients and oxygen. Moreover, this model doesn't reiterate the cellular heterogeneity and ECM interaction. Nevertheless, 2D culture model presents also several advantages which made it the most used model in pre-clinical research: it is easy to expand and maintain good reproducibility, allows good cell imaging both for morphology monitoring or cell staining with different antibodies, gives information about the growth and drug toxicity thanks to different assay that have been developed to assess proliferation in 2D models.

4.1.1 Glioma cell line

Glioma cell lines are commercially available lines of a homogenous cell population from human GBM, which can be expanded indefinitely and, to date, represent the most used tool in GBM research. However, they present several issues in the translation of the results in clinical settings, thus do not represent the best way to investigate GBM complexity. Indeed, culture passages of cell lines can result in genotypic and phenotypic variation[96], and

among literature, have been reported over 20 different culture conditions, making difficult the comparison of the studies. Genetic and phenotypic changes due to the culture passages or to the culture conditions (i.e. high foetal serum concentrations), make them unreliable models and distant from the features of patients' tumours, thus also lacking in reproducing inter-tumour heterogeneity[90,97]. In the last years, due to the lack of reliability of the data obtained on cell lines, scientists are trying to replace them with a more appropriate model.

4.1.2 Glioblastoma stem cell cultures

To date, the most reliable model to study glioblastoma features are patient-derived glioblastoma stem cell-enriched cultures, which were demonstrated to better recapitulate the characteristics of the original primary tumour[98]. Glioblastoma stem cell cultures (GSCs) are obtained from neurosurgical specimen's and cultured in a serum-free medium that contains specific nutrient mix, including essential growth factors such as EGF (epidermal growth factor) and bFGF (basic fibroblast growth factor)[25]. Once established and characterized, these conditions allow a long-term culture that recapitulate the key features of stem cells (self-renewal, marker expression, multipotent differentiation, tumour-initiating ability, therapy resistance)[41]. GSCs can grow as a neurosphere in suspension or as a monolayer on a thin layer of ECM proteins mixture[25]. When GSCs have been discovered, the growth as a neurosphere was considered as a sufficient condition to identify glioblastoma stem cells, but then has been demonstrated that it wasn't a defining feature nor it was essential for their long term expansion[90]. In addition, neurospheres make the culture less homogeneous and cell imaging harder to be performed, thus growth in monolayer, which is more manageable and reliable, is now preferred

even if also this model presents some issues. Indeed, GSCs in 2D cultures are plated on plastic flasks which represents an abnormally stiffer surface. Moreover, the ECM mixture, which is fundamental to guarantee the cells adhesion, is enriched in collagen and laminin, which can interact with the cells possibly influencing their biological behaviour[90]. To date, thanks to new technologies developed in cell studies and imaging, what was considered as disadvantages of the neurosphere culture, as the necrotic core, oxygen and nutrients gradients, cell-cell and cell-matrix tight interactions, and reduced cell homogeneity, is now considered as worth to be studied in order to better recapitulate tumour heterogeneity as occurs in the in-vivo conditions. To support this hypothesis, studies show different cellular behaviour in 2D as compared to 3D GSC culture conditions[99], even if, studying neurospheres from 68 patients, the analysis of gene expression failed to overlap the results observed in the original tumours[100]. In conclusion, both 2D and 3D GSC monocultures present some pitfalls, mostly due to the absence of the normal cells counterpart and the microenvironment, which are known to establish a reciprocal communication that influence each other behaviour. These limits are serious determinants causing the frequent failing in predict in-vivo drug response.

4.2 Development of 3D models

3D culture technologies are a recent developing field aimed to reproduce an organ-like structure in a dish, in order to model human development and disease. The development of 3D culture technologies employ researchers from different field, from developmental biology to engineering, it comprehends different techniques such as organoids (and tumoroids), microfluidics system, 3D printed and functionalized scaffold and the "organ-on-a-chip" technology. The definition of the term "organoid" implies that it must contain more than one cell type of the organ it models, it must exhibit some specific function of that organ and, lastly, the cells must organize themselves in a way similar to what happens in the organ itself[101]. Organoids can be grown from two main types of stem cells: pluripotent embryonic stem cells (ES) and their synthetic induced pluripotent stem cells (iPS) counterparts, and from organ-restricted adult stem cells[102]. Organoid technology represents a new model, placed in-between cell cultures and in-vivo studies, to investigate developmental biology, basic cell functions, and gene expression but also represent a new promising platform for translational research. In particular, as regards translational approaches, organoids have been successfully used to model infectious disease (human kidney organoids infected with SARS-COV-2[103], human mini-brain infected with the zika virus[104], or human stomach organoids infected with helicobacter pylori[105]), hereditary diseases, toxicology studies and cancer (for example, introducing mutations in normal organoids to study carcinogenesis). Remarkably, organoids hold big promises in the personalized-medicine field because patient-derived organoids theoretically allow rapid in-vivo testing of drug response in different human conditions, ranging from cancer to rare diseases[102]. Thus far, organoids likely represent a turning point in biomedical research, even though they also have some limitations. Indeed, the current organoid models, fails in recapitulate mature stage of development,

they do not present innervation, immune system, microbiome, and vascularization, which impairs nutrients supply and growth. Recently, researchers are working to overcome these drawbacks (for example integrating different 3D technologies) in order to try to in-vitro recapitulates the in-vivo complexity[106].

4.2.1 Organoids

Since 2008, many organoid models have been developed worldwide to resemble gut, kidney, brain, retina, lung, thyroid, among others. Generally, researchers start from ES or iPS and, following strict protocols (in terms of different media, growth factors, matrix and days exposure) they obtain the differentiation and self-organization of the organ structure "in a dish"[101,102].

- "Mini-Brain": Lancaster and Knoblich developed a protocol to obtain a single neural organoid containing the representation of different brain regions. Briefly, their approach starts from floating embryoid bodies embedded in Matrigel (a laminin and collagen enriched matrix secreted by the Engelbreth-Holm-Swarm tumour cell line). This allows the growth of large neuroepithelial buds, which develop into different brain regions. Mini-brain can reach a few millimeters in size and they are cultures in spinning bioreactors. Single cell RNA sequencing confirms that gene expression programs of cortical cells in organoids are similar to those found in the correspondent fetal tissue[107]. Brain organoids have huge potential to study brain cancer or neurodevelopmental disorders

such as autism or neurodegenerative diseases which are impossible or very difficult to model in animals[101].

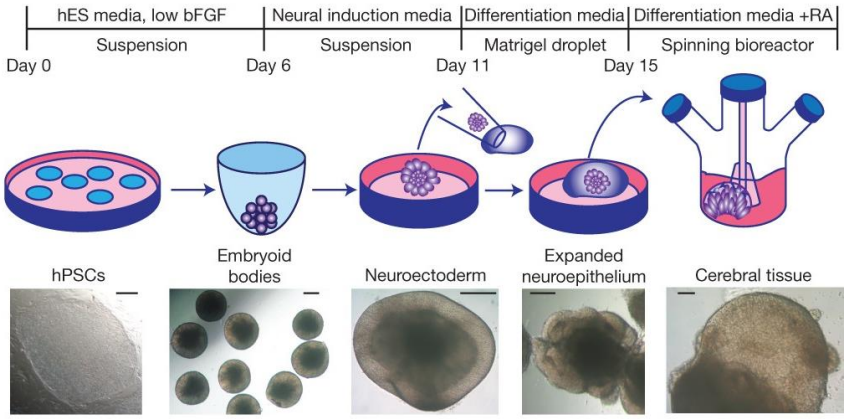

Figure 5 Schematic summary of the "mini-brain" establishment method (Lancaster, 2013) [107]

- "Mini-gut": Sato, Clevers and colleagues developed a culture system to obtain an epithelial organoid from a single $Lgr5^+$ stem cell or by a fragment of the intestinal crypt, starting from the observation that $Lgr5^+$ cells could go through thousands of cell divisions in vivo. Stem cells are suspended in Matrigel and cultures in a serum-free media supplemented with three different proteins: R-Spondin1 (a ligand of Lgr5 which activate the Wnt signalling), EGF, and Noggin (to obtain colon organoids it must be added also Wnt3a). The result is a highly polarized epithelium with a central lumen, both genetically and phenotypically stable[108,109]. An outstanding application of colon organoids in personalized medicine is the colon organoid-based cystic fibrosis test. Organoids can be obtained in a few weeks after the biopsy and drug tests could be performed. This approach has been already utilized for the identification of the appropriate drug combination to successfully treat a patient with a very rare CFTR mutation, who otherwise have difficulties in finding in a short time an effective therapy[102,110].

4.2.2 Tumoroids

Tumoroids are "tumour-like organoids", that means that they are organoids obtained by tissue resections or biopsies from cancer patients[111]. Tumoroids show better conservation of genetic and phenotypic features of the original tumour, which, together with a relatively easy in-vitro expansion, open the possibilities to generate living biobanks of different tumours, such as colorectal[112], breast[113] or gastric[114] carcinomas. Biobanks could be a crucial tool for drug screening and development, in order to test drug response and theoretically, correlate it with the tumour genetic features. Clearly, tumoroids will be also a platform for the purposes of personalized medicine, indeed they can directly grow from patient biopsy and in few weeks drug screening could be performed to predict patients responses[106].

4.3 Glioblastoma 3D models

In the last years, attempting to reproduce glioblastoma heterogeneity as a tool to better study its features and drug response, several laboratories worldwide are trying to applicate 3D technologies to the investigation on this lethal tumour. The first 3D models have been developed from stabilized glioblastoma cell lines grew on different scaffold (with or without the coating by specific proteins) or hydrogels, highlighting an increased expression of stemness marker and therapy resistance, similar to what found in patients[90]. Moreover, studies underline that modifying the scaffold or hydrogel stiffness, it increases the expression of mediator of different pathways, suggesting a possible involvement of the stiffness changing in the observed cellular response[115]. Subsequently, with the emerging of the organoid model, scientists they were introduced also in the glioblastoma research.

Some of the approaches recently proposed are reported below (*figure 6*).

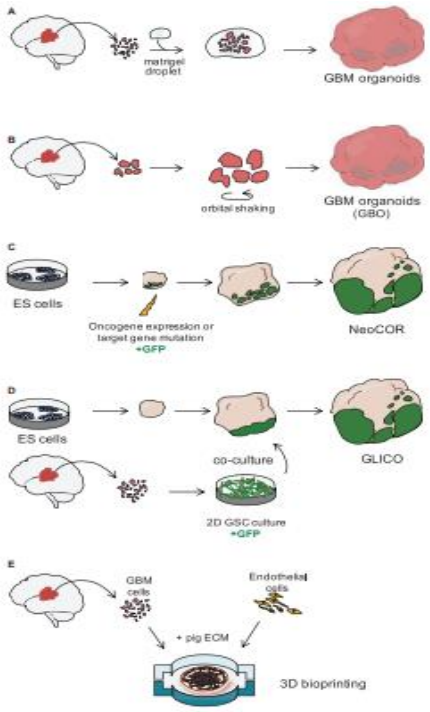

Figure 6 Glioblastoma organoid models. A: GSCs embedded in Matrigel, B: GBO, Glioblastoma fragments in orbital shaker without Matrigel, C:NeoCOR-Neoplastic Cerebral Organoid, D: Glico, GSCs co-cultured within brain organoid, E:GBM cells and endothelial cells seeded on a chip with a bioprinted pig extracellula matrix. (Azzarelli,2020 [89])

4.3.1 Glioblastoma organoids from primary tissue

In 2016, Hubert and colleagues[116] cultured 3D organoids from patient-derived glioblastoma stem cells or from finely minced GBM specimens. Cells, embedded in Matrigel, were kept in culture for over a year. In the first two months, organoids reached a size of 3-4 mm, but after that, their growth slows down, probably due to limited nutrients diffusion caused by the increased size. After several months in culture, they generate daughter spheres, which subsequently fuse with the main organoid, thus indicating stable viability of the organoid over months without passaging. This model shows a hypoxic gradient, similar to the one occurring in vivo within the tumour mass, and

correlated to a gradient of stem cell density. Indeed, $Sox2^{+}$ cells have been found in the periphery of the organoid showing a high proliferating activity, while the hypoxic core was characterized by lower abundance of stem-like cells. Interestingly, Sox2+ cells from the core exhibit different molecular properties as compared to the ones from the organoid periphery, resulting mainly quiescent. This suggests that distinct stem cells subpopulations (or functional state) can be found inside individual organoids and that their distribution may be influenced by the microenvironment. This system is highly promising for translational cancer research, even if it still requires further characterization and validation. Moreover, it is difficult to use it for wide drug screening due to the relatively long time necessary to establish the organoid culture. In 2020 Jacob and colleagues[117] developed a faster method (1-2 weeks) to generate GBM organoid, called GBO, and they established a GBO biobank of 70 samples from 53 patients, which, thanks to the faster culture methods, could be extremely useful for the personalized medicine approach, to preclinically test drugs, correlating the response with particular genotypes, and eventually, enrol patients in specific clinical trials; indeed, their potential translational application has already been proposed. The GBO methods imply that surgical specimens are cut in 1 mm size fragments and cultured in an orbital shaker without Matrigel and in a serum-free and EGF-bFGF-free medium, to preserve intra e inter-tumour heterogeneity. GBOs maintain genetic and molecular features of the parental tumours, even if the long term analyses showed variable results. As the organoid model proposed by Hubert, GBO shows the hypoxic gradient but they can be cut to obtain a propagation of the culture and avoid extensive core necrosis. Thawed GBO can recover and continue their growth, representing a big advantage in order to establish biobanks.

4.3.2 Genetic engineered brain organoids to study tumour development: the NeoCOR model

Besides all the already mentioned possible applications of the mini-brain model, they have been also applied in brain cancer research with the NeoCOR model (Neoplastic organoid model). Scientists overexpressed known oncogenes and/or deleted tumour suppressor genes at an early stage of organoid development along with inducing the expression of GFP (to be able to follow the cells that carry the genetic alterations). By introducing single mutation, it is possible to identify and follow the key alterations that led to organoids overgrowth, finding that they are similar to the genetic alteration often found in glioblastoma. Interestingly, by the induction of different genetic alterations, it is possible to resemble different GBM subtypes, for example, the mesenchymal subtype can be reproduced by activating HRasG12V and disrupting p53[118,119]. To date, if it is possible to recapitulate all the GBM subtypes and whether they are comparable to the patient-derived cell and organoid is still to be elucidated[89].

4.3.3 Co-culture of GBM cells with brain organoids

The GLICO model (GLIoma Cerebral Organoids) is constituted by different patient-derived GSC cell lines, marked with GFP, co-cultured with a fully developed 3D brain organoid. GSC can proliferate and are able to invade and integrate within the organoid. Interestingly, each cell lines invade the surrounding "normal" organoid in a unique way, showing different invasion and proliferation patterns. Moreover, cell lines that show higher invasiveness in organoid are the ones that exhibit a higher infiltrative ability when transplanted in mice, likely reflecting patient-specific properties. Genetic studies confirm that key genetic aberrations of the native tumour are maintained in the GLICO model[120,121].

4.3.4 3D GBM models via Bio-printing technology

The organ-on-a-chip model is constituted by small engineered devices (chips) in which the key functions of the organ are recapitulated and different compartments can communicate thanks to microfluidic channels[122]. In the GBM-on-a-chip model[123], endothelial cells and patient-derived cancer cells are embedded in decellularized pig brain extracellular matrix and bio-printed into two different chambers of the chip: endothelial cells are seeded on the outside of the chip, while patient-derived cancer cells are seeded in the core of the chip. Compartmentalization establishes a radial oxygen gradient recapitulating important features of the tumour, leading to a necrotic core. This model resembles the perivascular niche and it shows a higher number of $Sox2^+$ cells at the periphery of the core of the chip. This model is faster to establish as compared to other GBM organoid models (1-2 weeks), but requires advanced technologies. Even if it doesn't reproduce a 3D spatial organization, it provides a comparable microenvironment of the original in vivo tumour and promote cell-cell and cell-matrix interaction.

Rationale and Aims of the Thesis

GSC, which represent a small subpopulation into the tumour mass, have been demonstrated to be responsible for GBM chemo-radio resistance and relapse, thus their removal it's crucial to maximize the efficacy of the neurosurgery and avoid GBM relapse. Thus, new therapies able to target also GSC are currently needed. Among the recently proposed approach, metformin has been demonstrated to directly target GSC and few clinical trials are evaluating its safety and efficacy as adjuvant therapy for GBM patients. The high dose that would be required in-vivo to recapitulate the in-vitro antiproliferative effects, is one of the main issues that limits the administration of metformin in cancer patients.

Thus, starting from the observation that metformin and other biguanide compounds as phenformin and cycloguanil, are able to target GSC via the inhibition of the CLIC-1 mediated ion current, we screened nine newly synthesized compound which shares the biguanide moiety (cyclic or linear) in order to enhance the pharmacological profile of metformin.

We selected two compounds (Q48 and Q54) in light of their enhanced activity as compared to metformin, selectivity towards GSC and the ability to acts on CLIC-1. The lack of reliability of models is a drawback for GBM pharmacological research because each model shows some pitfalls (i.a. 2D culture lack in recapitulating the cell-cell interaction and cell-matrix interaction; in-vivo models are rarely suitable for high-throughput drug screening; 3D model, to date, lacks in reproducibility and they quite difficult to handle and work with), therefore these compounds have been tested on three different models: patient-derived GSC cultures, in-vivo on zebrafish models and on 3D GSC cultures. This approach aims to integrate information

from each model to obtain more predictive information of what could happen in a GBM. To summarize the aims of this work are:

- To enhance metformin antitumour effects and pharmacological profile by screening newly biguanide compounds
- To define the relevance of CLIC-1 as a key regulator of GSC's susceptibility to biguanide compounds
- To characterize two 3D models
- To test the selected compounds on different GBM models (zebrafish and 3D)

Results

GSC isolation and characterization of the differentiation ability

In the past years, the laboratory directed by Prof. Florio, in which I worked during my PhD, have optimized a preclinical model for GBM research consisting in patient-derived GSC culture. GSC isolation and in-vitro expansion have been performed as previously described (see "Material and Methods"). Along with the in-vivo tumorigenesis test, to verify that the stem cell enrichment was effective, the expression of different stemness marker was measured by Western blot, RT-PCR (data not shown) and immunofluorescence. The staminal phenotype was compared to cells model of the component of the tumour mass characterized by a more differentiated phenotype, which is induced in GSC by changing the culture conditions (see "Materials and Methods"). Within two weeks from the culture media switch, cells take a neuron/astrocyte-like morphology (*Figure 7-A*) and the content of the astrocytic differentiation marker (GFAP) increase, while Sox-2 decreases in these conditions, confirming the shift towards a differentiated phenotype (*Figure 7-B*). To corroborate the western blot results, the expression of Sox-2 and GFAP was analysed also by immunofluorescence staining (*Figure 7-C*).

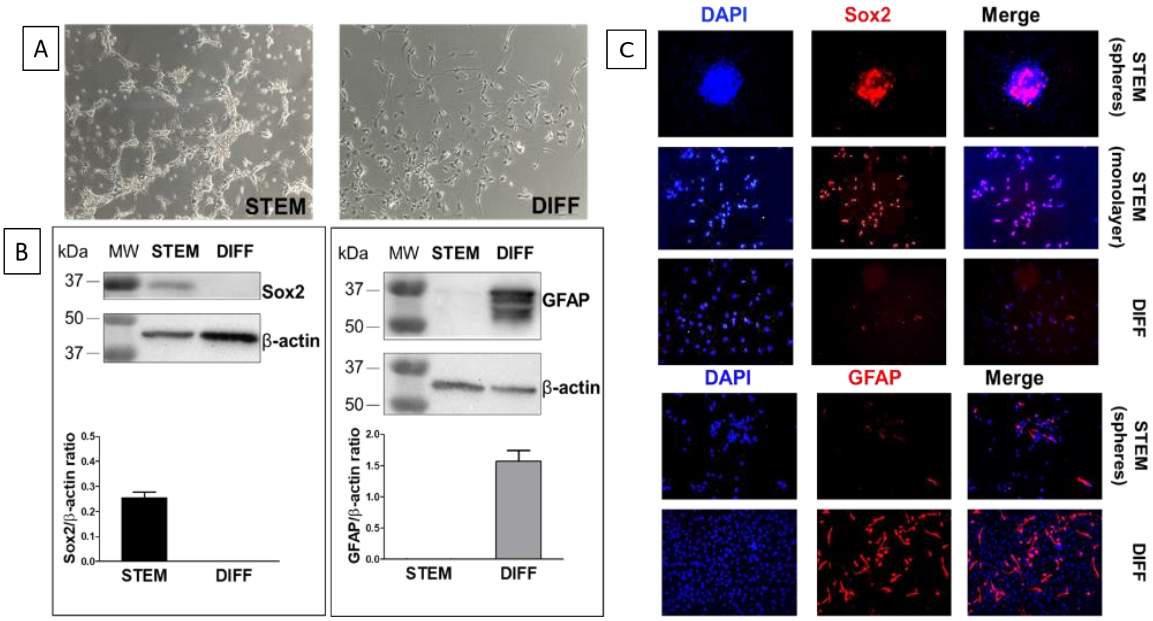

Figure 7 Representative characterization of GSC cultures. A: morphology of GSC grown in stem cell-permissive medium (STEM) or after shifting for 2 weeks in 10% FBS-containing medium (DIFF). Photos were obtained by a phase-contrast microscope. (bar =10 µm) B: western blots performed on GSCs and differentiated cell lysates of stem cell marker, Sox-2 (left) and for the astrocytic differentiation marker GFAP (right). β-actin was detected on the same membrane and used as a reference for protein loading. The densitometric analysis is reported in the histograms as mean ± S.D. of densitometric values of Sox-2 and GFAP normalized with β-actin content. C-Upper panels: Immunofluorescence analysis of Sox-2 expression (red) in GSC spheroids (upper pictures, bar = 200 µm), GSC monolayers (middle pictures, bar = 100 µm) and differentiated GBM cells (lower pictures, bar = 100 µm). Nuclei were counterstained with DAPI (blue). C-Lower panels: Immunofluorescence analyses of GFAP expression (red). Nuclei were counterstained with DAPI (blue). Bar = 200 µm.

Screening of novel biguanide derivatives: synthesis and antiproliferative activity

Biguanide compounds both linear, as metformin or phenformin, and cyclic, as cycloguanil, have demonstrated to act as antiproliferative agents on GSC by the inhibition of the CLIC-1 mediated ion current. Even if cycloguanil IC50 is 50 fold lower as compared to metformin it exerts its toxicity also in normal stem cells, thus its selectivity profile it's not adequate. On the other hand, metformin is more selective towards GSC, but it requires high concentrations to impair GSC viability that are difficult to reach in patients, thus preventing its translation in the clinical setting[124]. To develop new antitumour agents with an improved pharmacological profile, metformin and cycloguanil were chosen as chemotypes. In collaboration with the Department of Pharmacy of the University of Genoa, we obtained two series of biguanides compounds: aryl-biguanides (named Q42, Q46, Q48, Q49, and Q50) and cycloguanil-like derivatives (Q51, Q52, Q53, and Q54) introducing substitutions on aromatic rings (molecular structure reported in *Figure 8-A*). Antiproliferative effect of the novel biguanide compounds was tested on GSCs, ucMSCs, and on Non-Stem GBM cells to test their potency and selectivity. Cell viability was assessed

by MTT assay treating the cells for 48 h, in concentration-response experiments. As regards GSCs, molecules were tested on five independent GSC cultures (GBM3, 5, 19, 23, and 37) to overcome GBM heterogeneity. Metformin confirms its high efficacy and low potency (max. Inhibition − 82% and average IC50 9.78 mM, *Table 1*) in the inhibition of GSC proliferation[88]. Q42, Q48, Q50 and Q54 exhibit a higher potency than metformin, showing mean IC50 values within the μM range, mean IC50 of Q49, Q51 and Q53 was in the low mM range (showing only a small improvement of metformin potency), while Q46 and Q52 did not reach an adequate inhibitory activity to allow the IC50 calculation. The efficacy of the novel compounds was obtained by the comparison to the maximal antiproliferative effect at 3 mM: efficacy of all active biguanide ranged between − 71 and − 83% (metformin show an -82% efficacy at a concentration of 30 mM, 30 fold higher as compared to the novel biguanide), while Q46 (− 27%), Q51 (− 61%) and Q52 (− 56%) showed the lowest activity (*Table 1*). On differentiated cells, obtained by shifting the culture condition of GSC to an FBS containing medium, Q46, Q48, Q51, Q52, Q53 and Q54 showed reduced antiproliferative effect when used in the IC50 range, as compared to the inhibition of proliferation in the respective GSCs culture (*Figure 8-B*). Conversely, Q42, Q49 and Q50 show similar efficacy and potency observed in GSC. Similar results were obtained in four independently isolated ucMSC cultures, where Q42, Q49 and Q50 impaired cell viability while Q46, Q48, Q51, Q52, Q53 and Q54 exhibited only a modest inhibitory effect (*Figure 8-C*). These data suggest that Q42, Q49 and Q50 show off-target activity because they exert their antiproliferative effects not only on GSC.

Taken together, the results of this screening indicate that Q48 (mean IC50 = 0.082 mM) and Q54 (mean IC50 = 0.43 mM) show the highest potency *(Figure 8-A and Table 2)* and lowest off-target effect, and thus were selected for

subsequent investigations (*Figure 8-B,C*), while Q46, which didn't display any significant antiproliferative activity, was used as negative controls.

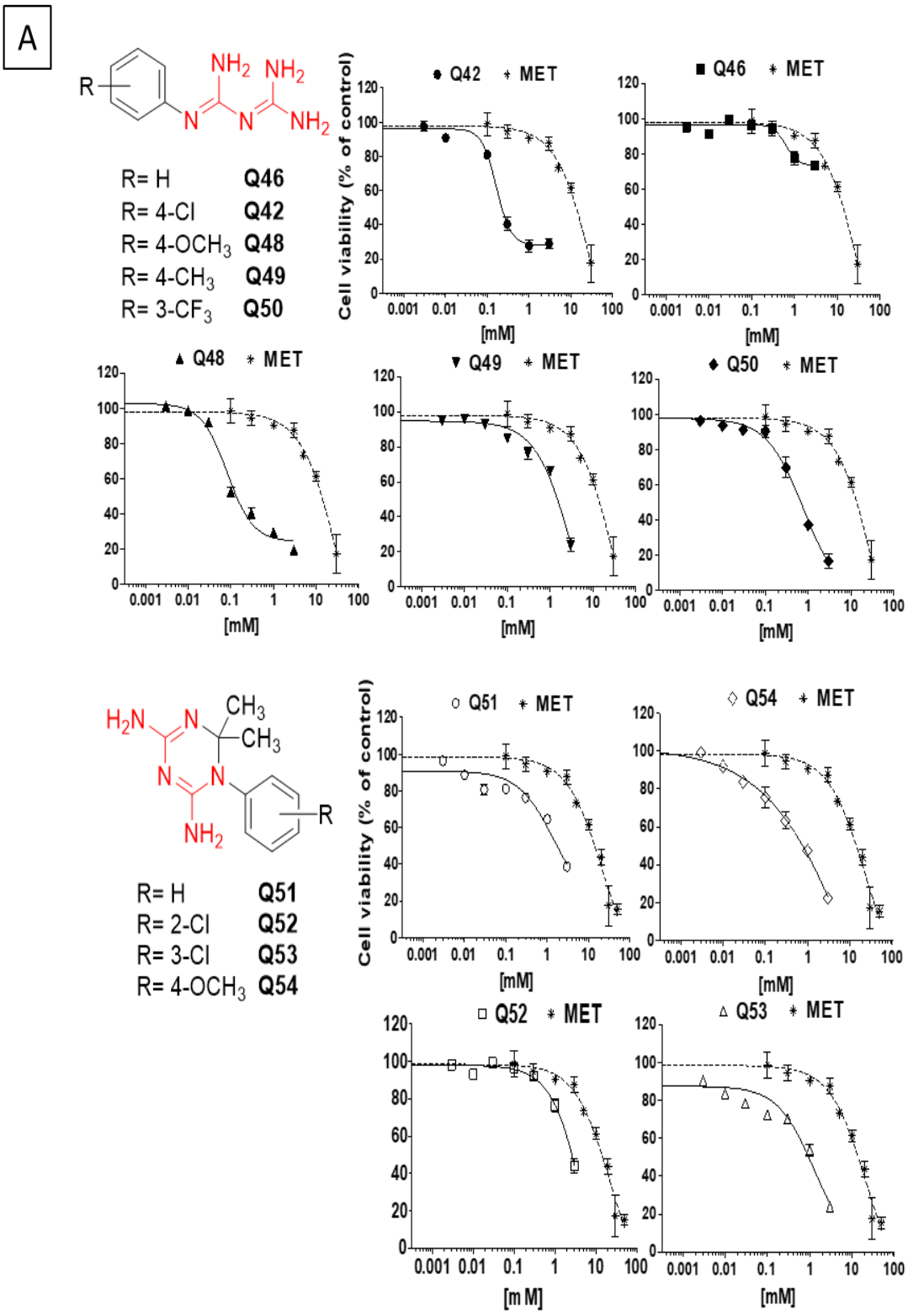

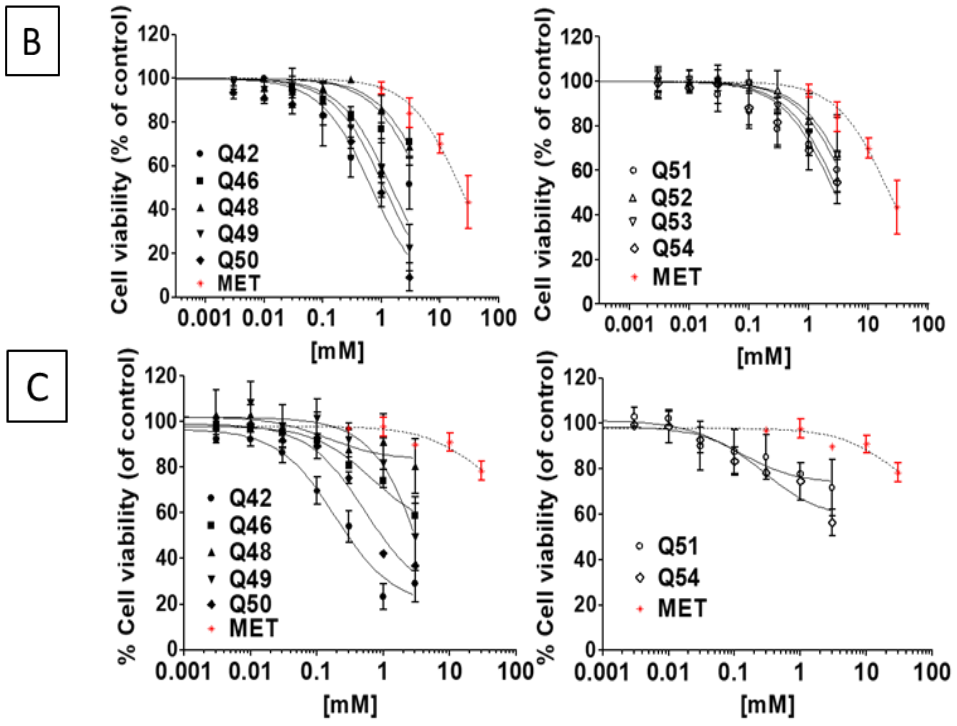

Figure 8 Novel biguanide derivatives concentration-response curves in comparison with metformin on GSC (A) Non-stem GBM cells (non-GSC) (B) and ucMSC (C). A: Upper panel- Chemical structure of linear biguanides (biguanide moiety highlighted in red) antiproliferative activity of Q42, Q46, Q48, Q49, and Q50 as compared with metformin activity. Lower panel- Chemical structure of cyclic biguanides (biguanide moiety highlighted in red) antiproliferative activity of Q51, Q52, Q53, and Q54 as compared to metformin activity. Cell viability was evaluated by MTT assay after 48 h of treatment. Data are reported as average of replica experiments in multiple GSC cultures (mean ± S.E.M. of at least three independent experiments for each culture).
Figure 8B: Left graph: antiproliferative activity of Q42, Q46, Q48, Q49, and Q50 as compared to metformin activity (in red). Right graph: antiproliferative activity of Q51, Q52, Q53, and Q54 as compared to metformin activity (in red). Cell viability was evaluated by MTT assay after 48 h of treatment. Non-stem GBM cells were obtained by the same GSC cultures tested in A, by shifting culture conditions in FBS containing medium. Data are reported as average of replica experiments in multiple differentiated glioblastoma cell cultures (mean ± S.E.M. of at least three independent experiments for each culture). C: Left graph: antiproliferative activity of Q42, Q46, Q48, Q49, and Q50 as compared to metformin activity (in red) on ucMSC cultures. Right graph: antiproliferative activity of Q51, Q52, Q53, and Q54 in comparison with metformin activity (in red). Cell viability was evaluated by MTT assay after 48 h of treatment. Data are reported as average of replica experiments in independently isolated ucMSC cultures (mean ± S.E.M. of at least three independent experiments for each culture).

TABLE 1. IC_{50} AND EFFICACY VALUES OF THE ANTIPROLIFERATIVE ACTIVITY OF BIGUANIDE DERIVATIVES ON MULTIPLE GSC CULTURES

# Linear com-pounds	n	Mean IC_{50} (mM)°	Efficacy [3mM]*	# Cyclic com-pounds	n	Mean IC_{50} (mM)°	Efficacy [3mM]*
Q42	3	0.18	71%	**Q51**	5	1.48	61%
Q46	3	n.r.	27%	**Q52**	5	n.r.	56%
Q48	5	0.082	81%	**Q53**	5	1.29	76%
Q49	5	3.34	76%	**Q54**	5	0.43	78%
Q50	3	0.79	83%				
Metformin: mean IC_{50} =9.78 mM°; efficacy = 82% (30mM)*							

n = number of GSC cultures tested; *maximal inhibition of cell viability (%); °overall mean values from pooled concentration-response curves; n.r.= not reached

Table 1 The table reports the number of GSC cultures tested for each compound and potency and efficacy calculated.

Selectivity of Q54 and Q48 towards GSC

To demonstrate the selectivity of the treatment with the novel biguanide compounds toward GSCs, we measured Sox-2 expression after treatment with Q48 (100 μM), Q54 (300 μM), and metformin (10 mM). These concentrations were chosen according to the range of the respective IC50 values previously identified. Sox-2 expression was evaluated by Western-blotting on GBM3 GSC lysates after 48h treatment (*Figure 9*). Q48, Q54 and metformin reduced Sox-2 levels clearly indicating a reduction of stem-like cell content after treatment. No changes in Sox-2 content was observed after Q46 treatment thus confirming the specificity of the observed effects.

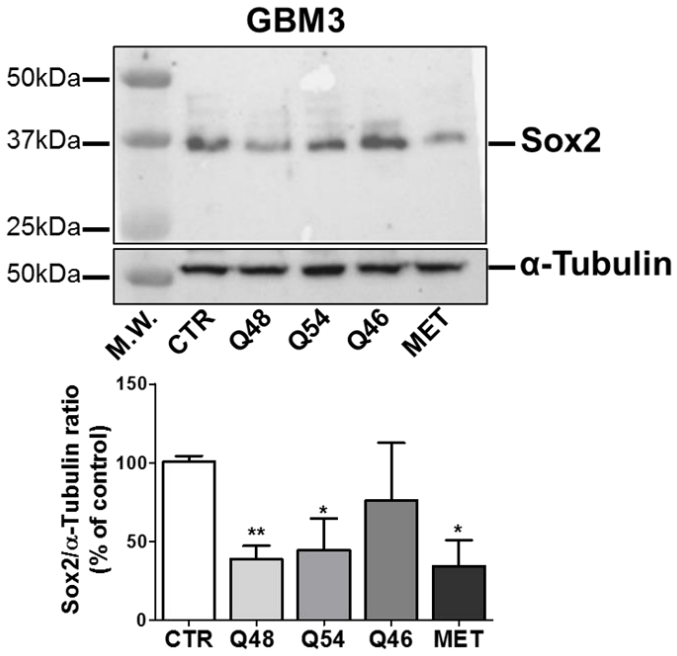

*Figure 9 Biguanide treatment selectively reduces Sox2+ cell content. Representative Western blot of Sox2 levels in GSCs cultures (GBM3) in control conditions (CTR) or after treatment with Q48 (100 μM), Q54 and Q46 (300 μM), and metformin (10 mM) for 48 h. α-tubulin was used as a reference for protein loading. Q48 and Q54 significantly reduced Sox2 expression. Quantification by densitometric analysis is normalized for α-tubulin expression and it is reported as the average of two independent analyses (lower panel). * = p < 0.05; ** = p < 0.01.*

Effects of novel biguanide compounds (Q54 and Q48) on proliferation rate evaluated by cell count

The antiproliferative efficacy of Q48, Q54, and Q46 (10 and 100 μM) was tested on GSC growth rate by Trypan blue exclusion assay, which allows to directly measure cell number and viability (see "Material and methods"). Cell counts were performed after 48-72 h treatment of GSC cultures from GBM3, GBM23 and GBM19; both concentrations of Q48 and Q54 significantly decreased the number of viable cell, without differences among GSC cultures (*Figure 10*). Hundred μM was the most effective concentration both for Q54 and Q48, after 48 and 72 hrs of treatment (Q48 viable cell reduction: 75–93%; Q54 of viable cells reduction 76–92%). Q46 confirmed its low activity in all the cultures.

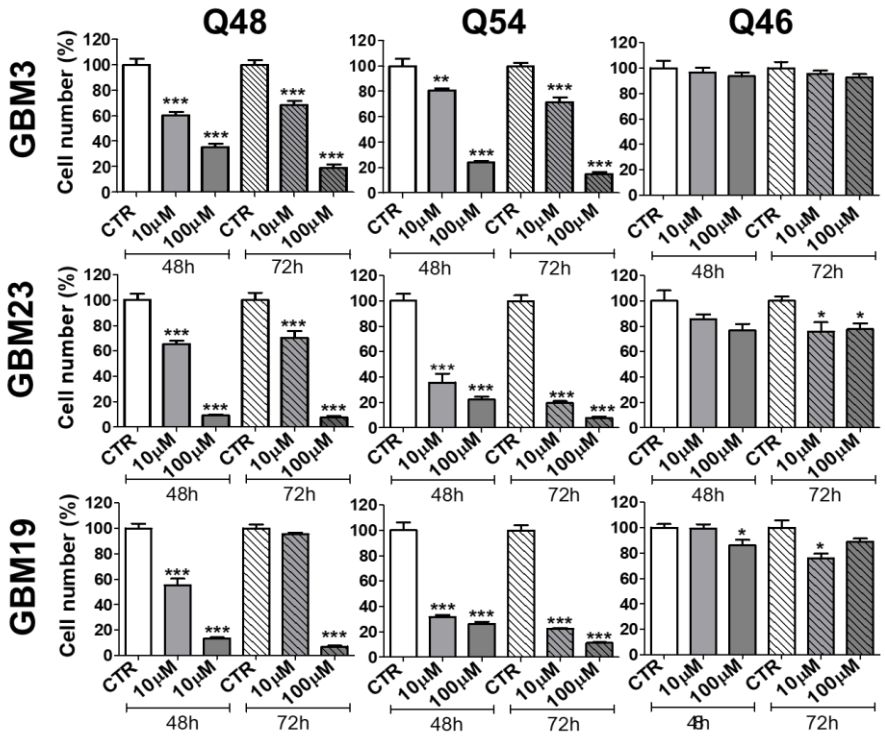

*Figure 10 Antiproliferative activity of Q48, Q54, and Q46 on GBM3, 19 and 23 evaluated by cell count. The effects of Q48, Q54 and Q46 (10 and 100 μM) on cell counting was evaluated by Trypan-blue exclusion assay, 48-72h after treatment. Data represent the mean ± S.E.M. of 3 independent experiments performed in quadruplicate. Cell count confirmed the high efficacy and potency of Q48 and Q54, while Q46 was ineffective. *p < 0.05, **p < 0.01, ***p < 0.001 vs. respective control (CTR).*

Effects of Q54 and Q48 on sphere formation

Self-renewal capacity is a hallmark of GSC that can be evaluated in-vitro by sphere formation assay. To test the effect of the novel biguanides on GSC self-renewal, we performed a sphere formation assay by treating GBM3, GBM23 and GBM19 GSC cultures for 7 days with Q54, Q48, Q46 (10 and 100 μM) and metformin (1 and 10mM). Biguanide compounds Q54 and Q48 reduced number and size of the formed spheres, while Q46 was again not effective. In particular, Q54 was significantly efficacious on all the GSC tested already at 10 μM, showing a higher potency in the impairment of self-renewal as compared to the activity on GSC proliferation, which occurred with an IC50 of 430 μM.

Conversely, Q48 showed lower efficacy than Q54 at low concentration (10 μM), and in GBM23, it didn't reach a statistical significance in the impairment of sphere formation. However, Q48 100 μM (corresponding to the antiproliferative IC50) showed a highly significant inhibition of spherogenesis (up to 83% in GBM23, 81% in GBM3 and 75% in GBM19). Metformin was effective when used at 10 mM, reflecting its antiproliferative IC50.

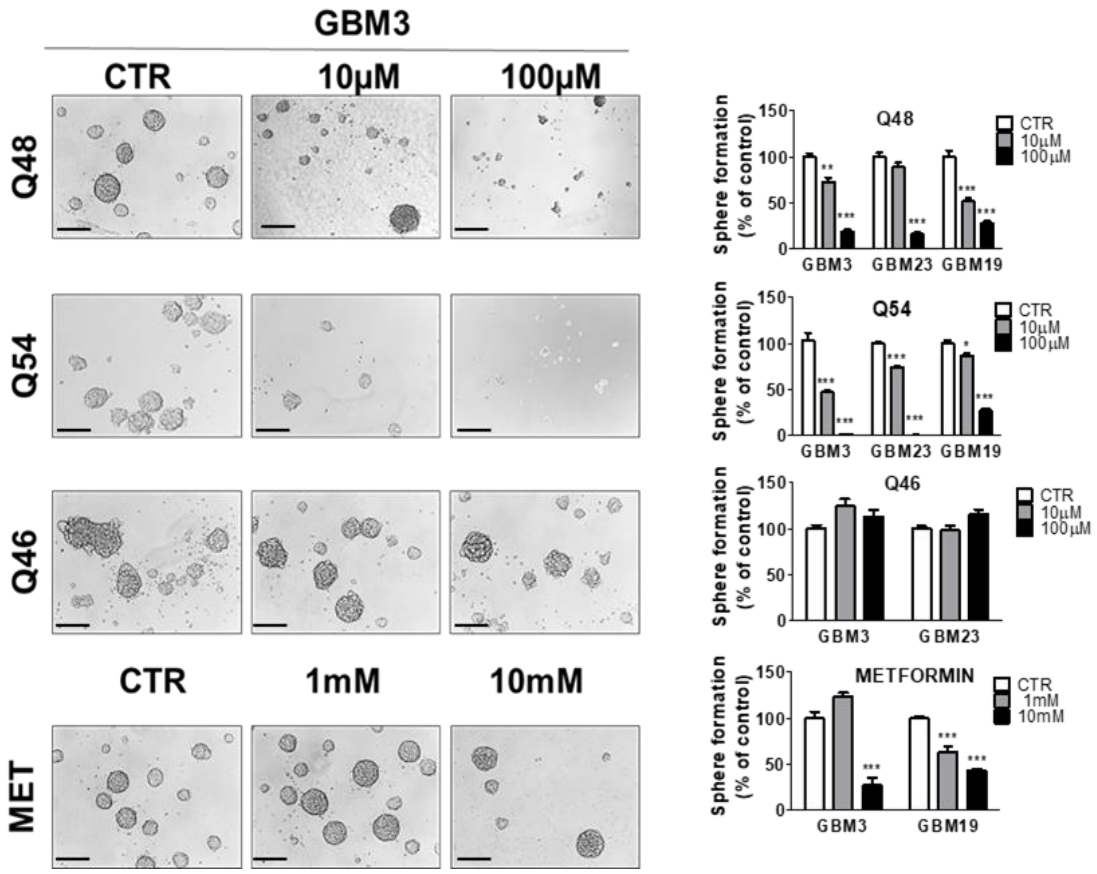

*Figure 11 Effect of novel biguanide derivatives on GSC sphere formation ability. Figure shows sphere-formation assay performed on GBM3 GSCs, treated with Q48, Q54, Q46 (10 and 100 μM) and metformin (1 and 10 mM) for 7 days. Spheres were counted by two independent investigators and for each treatment group (n = 3) was determined the percentage of sphere-forming cells. Representative phase-contrast microscopic images display the number and size of spheres in control (CTR) and with the Q48, Q54, and Q46 treatments (10 and 100 μM) GBM3 cells. Compounds efficacy is compared to metformin (MET) activity, used at 1 and 10 mM. Bar = 150 μm. Bar graphs report sphere number generated after compound treatments, expressed as the mean percentage ± S.D. of respective CTR. *p < 0.05, **p < 0.01, ***p < 0.001 vs. CTR.*

Effects of Q54 and Q48 on migration and invasion

Another distinctive feature of GBM, particularly dependent on GSC activity, is the ability to migrate and invade the surrounding brain parenchyma, giving rise to a rapid tumour relapse. Therefore, we investigate the ability of Q48 and Q54 to affect GSC migration and invasion. Migration assay was performed by a transwell assay: cells were fluorescently labelled by CFDA and their transmigration in the lower chamber towards an FBS-containing medium (used as chemoattractant) was tracked. In control conditions, GBM3, GBM23 and GBM19 GSCs showed high motility toward FBS-containing medium, while Q54 and Q48 (100 μM) impair migration ability of all GSC culture tested (*Figure 12-A*), peaking in GBM3 (− 66% for Q48 and − 75% for Q54). Metformin showed higher efficacy than Q54 and Q48 against GSC migration, although, required a concentration hundred-fold higher (10 mM) to be effective. As expected, Q46 was ineffective in all the tested cultures. Moreover, Q48 and Q54, as well as metformin were able to inhibit GSC invasion from spheroids into Matrigel™ (*Figure 12-B*). Similar effects were observed in 3 independent GSC cultures (GBM3, GBM19, GBM23). Both Q48 and Q54 (100 μM) reached the statistical significance for the anti-invasive activity in all the tested GSC, with the highest efficacy showed by Q48. Metformin (10 mM) significantly inhibited cell invasion in GBM3 and GBM 23, while in GBM19 the inhibitory effects did not reach statistical significance. Q46, used as a negative control, was ineffective in all the tested GSC cultures.

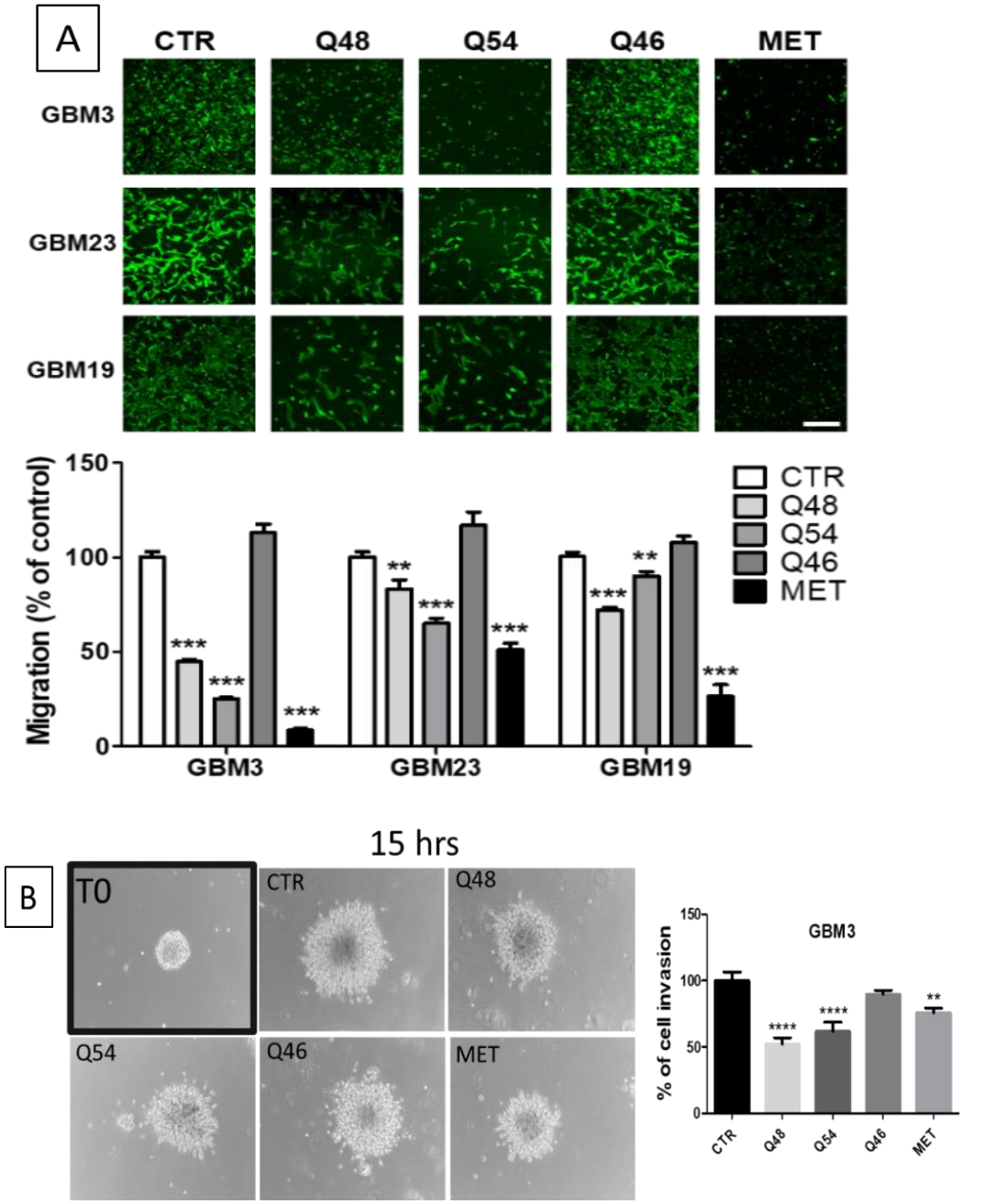

Figure 12 Effect of novel biguanide derivatives on GSC migration and invasion. A: GSC from GBM3, 19, and 23 were treated with Q46, Q48 and Q54 (100 µM), metformin (10 mM), or vehicle (CTR) and fluorescently labelled with CFDA. GSCs were plated in the upper well of fluorescence-blocking membrane transwells, while in the lower wells 10% FBS-containing medium was added as chemoattractant. By confocal microscopy the cells migrated on the bottom surface of the membrane were captured and quantified by ImageJ software. Left panels: Representative images obtained by confocal microscopy of migrated cells on the surface of the transwell membranes.

*Bar = 100 µm. Right panels: Quantification of migrated cells using ImageJ. Data represent the mean ± S.D. (n = 3). **p < 0.01, ***p < 0.001 vs. CTR.*
B: Newly formed spheres from GBM3, 23 and 19 were embedded in Matrigel™ and treated with Q48 (100 µM), Q54 (100 µM), Q46 (100 µM) and metformin (10 mM). The invasion rate was evaluated after 15 h, using the ImageJ software, measuring at least 2 diameters for each sphere. The differences between the average diameter of T15 and T0 of each condition were calculated and compared to control. Left panel: Representative GBM3 images of individual sphere embedded in Matrigel at T0 and after 15 h of treatment (magnification: 10x). Right panel: Bar graphs represent the mean ± S.E.M (n = 25), expressed as percentage of respective controls (CTR) of cell invasion. ∗p < 0.05, ∗∗p < 0.01, ∗∗∗p < 0.001 vs. respective CTR.

Effect of Q54 and Q48 on CLIC1-mediated ion current in GSCs

Metformin, and other biguanide known compounds as phenformin and cycloguanil, exert their antiproliferative activity on GSC through the inhibition of the CLIC-1 mediated ion current[88]. Since Q48 and Q54 contain the biguanide moiety as metformin, we evaluated their activity on CLIC-1, in collaboration with prof. Mazzanti (University of Milano). By perforated patch-clamp experiments, the effects of the novel biguanides on CLIC-1-mediated ion current was evaluated. In current time-course experiments, GBM3 GSCs were sequentially perfused with vehicle (controls) or different concentrations of Q46, Q48, Q54 and metformin, and the known CLIC-1 inhibitor IAA94. The percentage of current inhibition is reported in box plot (*Figure 13*) as ratio of the inhibition induced by each compound and by IAA94, to identify biguanide-insensitive CLIC-1 current, since 100 µM IAA94 completely blocks CLIC-1 current[125]. Q48 and Q54, reduced CLIC-1 activity in a concentration-dependent manner, when tested at concentrations corresponding to IC50 and above, but only Q54 showed an efficacy comparable to metformin (about −80% of CLIC-1 current) for concentrations corresponding to the antiproliferative IC50. As regard potency, Q54 showed higher potency than metformin, achieving the maximal inhibition at 0.5 mM vs. 10 mM of metformin. Q48 inhibited CLIC-1

activity (50%) only starting from a concentration of 0.2 mM and the total inhibition was reached only at 0.5 mM. Since Q48 exerts its antiproliferative activity at concentrations (IC50 0.082 mM) which are not able to completely block CLIC-1 current, these data suggest that Q54 and Q48 exert their antiproliferative effect by targeting CLIC-1, but the high concentration of Q48 required to inhibit CLIC-1, indicates that other molecular targets may contribute to its antiproliferative effect. Q46, as expected from previous experiments, did not affect CLIC1 activity at concentrations up to 1 mM.

Moreover, to evaluate the direct binding ability of Q48 and Q54 to CLIC1, MST experiments were performed by labelling recombinant CLIC1 protein with fluorescent dyes covalently bound to the primary amines (lysine residues) of the protein. In collaboration with Dr. S. Girotto (IIT Genova), thermophoretic-induced fluorescence change of the labelled-CLIC-1 was detected upon addition of increasing concentrations of Q54 and Q48. After sample preparation, data were collected to build a dose-response curve for each compound, providing affinity parameters of Kd = 15.6 ± 1.9 μM and 1.9 ± 0.5 mM, for Q48 and Q54, respectively.

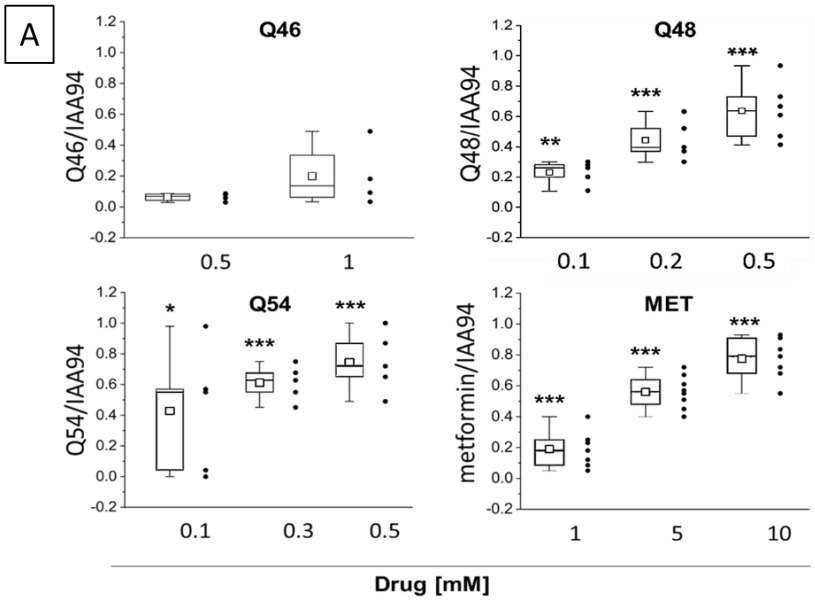

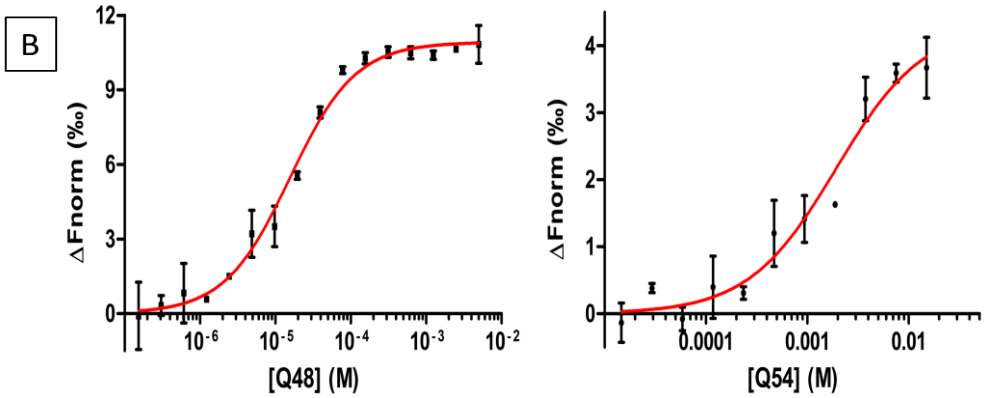

*Figure 13 Effect of novel biguanide derivatives on CLIC1-mediated ion current on GSCs. A: CLIC1-mediated ion current was evaluated by whole-cell patch-clamp electrophysiology analysis in voltage-clamp configuration in GBM3. Current time-course experiments were performed: cell were perfused with vehicle (controls), Q46 (0.5–1 mM), Q48 (0.1–0.5 mM), Q54 (0.1–0.5 mM) and metformin (1–10 mM), followed by IAA94 (100 µM) to identify CLIC1 residual activity. The mean current inhibition is reported in box chart plots as ratio of the biguanide and IAA94 sensitive currents. IAA94 treatment represents the residual CLIC1 activity. The dots next to box charts, indicate the number of cells used for the statistics (range 4–8) for each drug concentration. *p < 0.05, **p < 0.01, ***p < 0.001 vs. respective control cells. B: Microscale Thermophoresis (MST) analysis of CLIC1 binding by Q54 (right) and Q4 8 (left). Titration curve of RED-NHS-labelled CLIC1 (10 nM) with increasing concentrations of novel compounds. MST data are the average of three replicates. The sigmoidal fitting curve (red) was obtained using GraphPad Prism 5.0 software.*

CLIC-1 expression in GSC culture - is CLIC-1 essential for GSC malignant properties?

To measure CLIC-1 expression in GSC, western blot analysis was carried out in a panel of 7 cultures. GBM3, GBM19 and GBM23 which were used for most of the experiments reported in this work, exhibit high content of CLIC-1, in agreement with the observation that the antiproliferative effects we analysed are likely mediated by the impairment of CLIC-1 ion current. Nevertheless, we identified three GSC cultures which although expressing low content of CLIC-1, retain similar malignant tumour features as detected in high-expressing

CLIC-1 cultures (GBM39, GBM44 and GBM50) (*Figure 14-A*). Indeed, low-CLIC-1 expressing cultures were isolated from patients who developed aggressive GBMs and displayed tumorigenic potential in vivo when orthotopically xenografted in mice (mean survival time of mice was 100 days for GBM39 and GBM23, and 120 days for GBM3- *Table 3*), suggesting that CLIC-1 is not essential for GBM development and progression. To verify whether the reduced expression of CLIC-1 interferes with the stemness properties of GSCs, we analysed the expression of stemness marker, the spherogenesis ability and the capacity to differentiate into non-stem cells (when shifted from stem cell-permissive to FBS-containing medium for 15 days). Importantly, we did not observe significant differences with the typical in vitro phenotypical features of high-CLIC-1 expressing GSC cultures *(data not shown)*. Conversely, we noticed by culturing low-CLIC-1 expressing GSCs, a slower in vitro proliferation rate, which was confirmed by comparing the proliferation rate of high CLIC1-expressing cultures (GBM3 and GBM23) to the spontaneously low CLIC1-expressing (GBM39) GSCs for up to 11 days. Growth curves obtained by MTT assay showed that GBM39 in vitro proliferation was slower than GBM3 and GBM23, confirming a role for CLIC-1 in GSC proliferation (*Figure 14-B*). These data indicate that GBM characterized by low CLIC-1 expression retain biological and phenotypical features to the high-expressing CLIC-1 GBM, but the impairment of proliferation rate suggest a role of CLIC-1 in GSC *in-vitro* expansion.

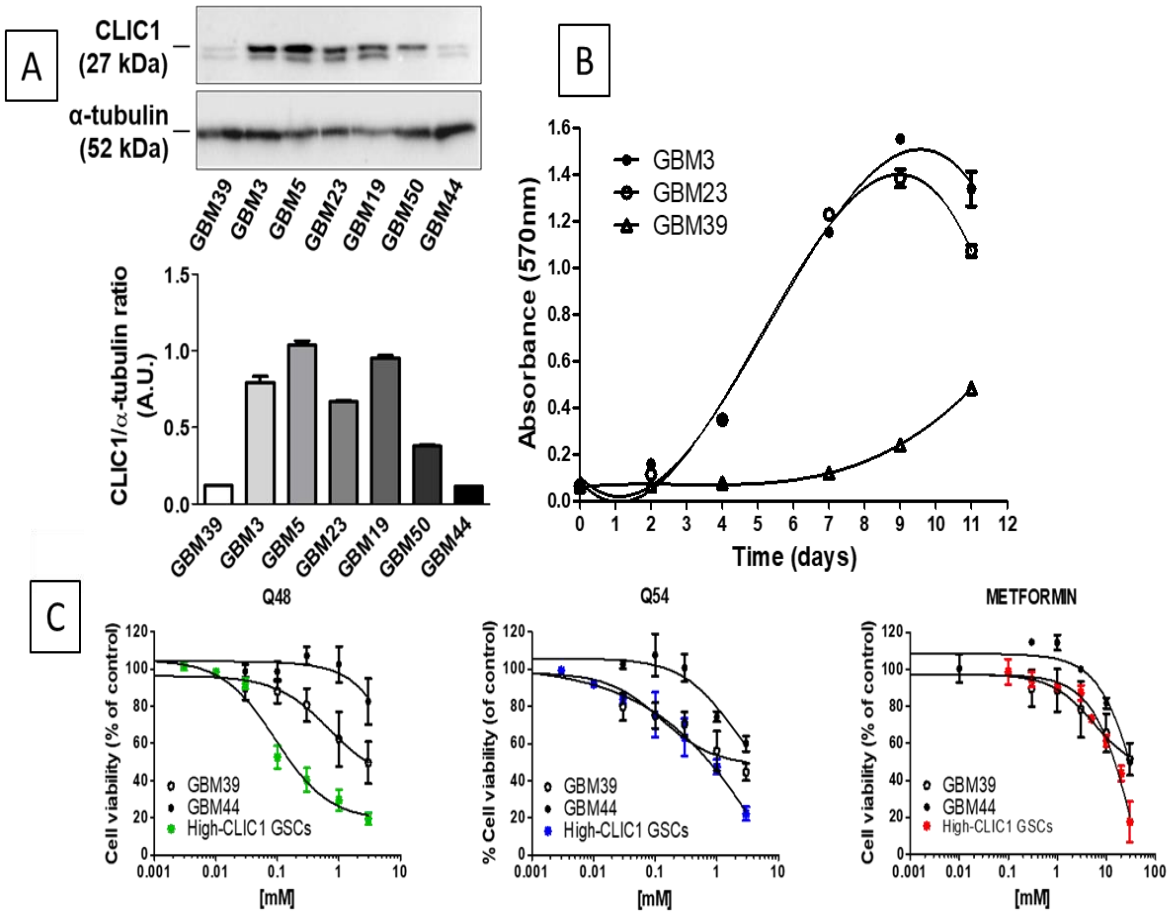

Figure 14 CLIC-1 expression in GBM cultures- A: A: Western blotting analysis of GSC cultures allow the identification of GSC cultures with low CLIC1 protein content. Western blot analysis was performed on total cell lysates from seven GSC cultures. α-tubulin antibody was used as a reference for protein loading. The lower panel shows the resultant densitometric analysis of CLIC1 levels. Data are expressed as mean ± S.D. of CLIC1 densitometry normalized using respective α-tubulin densitometry. GSCs from GBM39 and GBM 44 display low CLIC1 expression as compared to GBM3, 5, 18, and 23. CLIC1 expression in GBM50 was in-between of the two groups. B: Growth curves of low- (GBM39) and high- (GBM3, GBM23) CLIC1-expressing GSCs. MTT assay was used to measure cell viability and proliferation (n = 3). The growth curves were modelled by non-linear third-order polynomial fitting. A significant lower proliferation rate was observed in GSCs isolated from GBM39. C: Antiproliferative activity of Q48, Q54 and metformin in low CLIC1-expressing CLIC1 GSCs. Low-expressing GBM39 and GBM44 were treated for 48 h and analysed by MTT assay. The resulting concentration-response curves were compared with the average response obtained in high-

expressing GBM GSCs. Data represent the pooled mean ± SEM from N = 3 independent experiments.

GSC	Q48		Q54		MET	
	(IC_{50}, mM)	Efficacy* [3mM]	(IC_{50}, mM)	Efficacy* [3mM]	*(IC_{50}, mM)*	Efficacy* [30mM]
GBM39	0.69	50%	0.12	*55%*	117.15	49%
GBM44	n.r.	17%	n.r.	*40%*	68.67	50%
High-CLIC1 GSCs°	*0.082*	*81%*	*0.43*	*78%*	*9.78*	*82%*
*Maximal inhibition of cell viability (%), °overall mean values from GBM3, 5, 19, 23 and 37 pooled concentration-response curves; n.r.=not reached						

Table 2: mean IC50 value (potency) and maximal inhibition (efficacy) reached for each compound obtained from the concentration-response curves.

Antiproliferative effect of Q54 and Q48 in low-expressing CLIC-1 GSCs

We tested the antitumor activity of the novel biguanide derivatives toward low CLIC-1-expressing GSCs (GBM39 and GBM44), in order to correlate the antiproliferative effect to CLIC-1 expression. GBM39 and GBM44 were treated with Q48, Q54 and metformin for 48 h in concentration-response experiments. Growth curves obtained by the analysis of MTT assay displayed a reduced sensitivity to biguanides as compared to high CLIC-1-expressing GSCs (*Figure 14-C*). Indeed, the maximal cell viability reduction was obtained at a concentration of 3 mM for Q48 and Q54, and 30 mM for metformin. Furthermore, cell viability was reduced by only − 50, − 55%, and − 49% in GBM39 and − 17, − 40%, and − 50% in GBM44, respectively, as compared to − 81, − 78%, and − 82% as average effect in CLIC-1-expressing GBMs. The calculated IC50 shows a 10-fold lower potency for Q48 in GBM39 (from 0.082 mM in high expressing-CLIC-1 GBMs to 0.69 mM), while Q54 in GBM39 showed a slightly higher potency (0.12 mM in high expressing-CLIC-1 GBMs

vs. 0.43 mM). IC50 values for Q48 and Q54 in GBM44 cannot be calculated due to the lack of dose-dependent effects. Metformin IC50 shows a 12-fold lower potency both in GBM39 and GBM44 (from 9.8 mM to 117.1 mM in GBM39 and 68.7 mM in GBM44) (*Table 2*). These data point out that CLIC-1 expression is essential for the efficacy of biguanides in general, and of the novel compounds, as antiproliferative agents.

Antiproliferative effect of Q54 and Q48 on 3D culture model

Characterization of the 3D model

To determine the efficacy of the biguanide we developed in this study in GBM 3D models, we firstly characterized GSC-derived 3D cultures in terms of cell growth, cellular organization and cell marker expression. Cell growth macroscopically monitored by an inverted microscope, did not reveal a significant activity within 3 weeks of culture, probably due to the high cellular density occurring within the 3D culture (*Figure 15-A, left panel*). Therefore, we assessed cell proliferation by the incorporation of 5-EdU, founding a continuous proliferative activity that was still lasting also after 30 days of culture. These results clearly demonstrate that cells within the 3D cultures are able to proliferate for a long time without passaging (*Figure 15-A, central panel*). Within the 3D culture, GSC developed a tissue-like layered cellular organization (3 weeks post 3D culture establishment) (*Figure 15-A, right panel*), and similarly to the parental GSCs, used to generate these organoids, retain stem-like marker expression (i.e. Sox-2 and Olig-2). Interestingly, Sox-2 and Olig-2 positive cells mainly compose the edge of the 3D culture, while the internal layers were constituted by cells that express β-III tubulin or GFAP (indicating a more differentiated phenotype) suggesting that the 3D structure favours the development of cellular heterogeneity typical of GBM in patients

(*Figure 15-C,D*). Moreover, proliferating cells (Edu green-labelled cells) were also mainly located in the external layers, corresponding to Sox-2 expressing cells, thus confirming a GSC-like proliferating phenotype, while the internal cells, which are more differentiated, were mainly, non-proliferating (*Figure 15-C*). To confirm that GSCs undergo to a differentiation process within the 3D culture, mRNA analysis was performed (*Figure 15-B*). RT-PCR was carried out on cell lysates from 2D e 3D cultures (15-30 days after Matrigel™ embedding) resulting in a marked increase of CD44 expression (a cell surface protein involved in cell-to-matrix and cell-to-cell interactions) as compared to 2D grown cells. Similar results were observed for MAP2 expression. The ability of GSCs, grown as 3D culture, to acquire cellular heterogeneity, strongly support that the 3D culture model better resemble the phenotype of GBM that occurs in vivo, thus confirming the validity of 3D cultures as a platform for the screening of novel antitumor drugs [126].

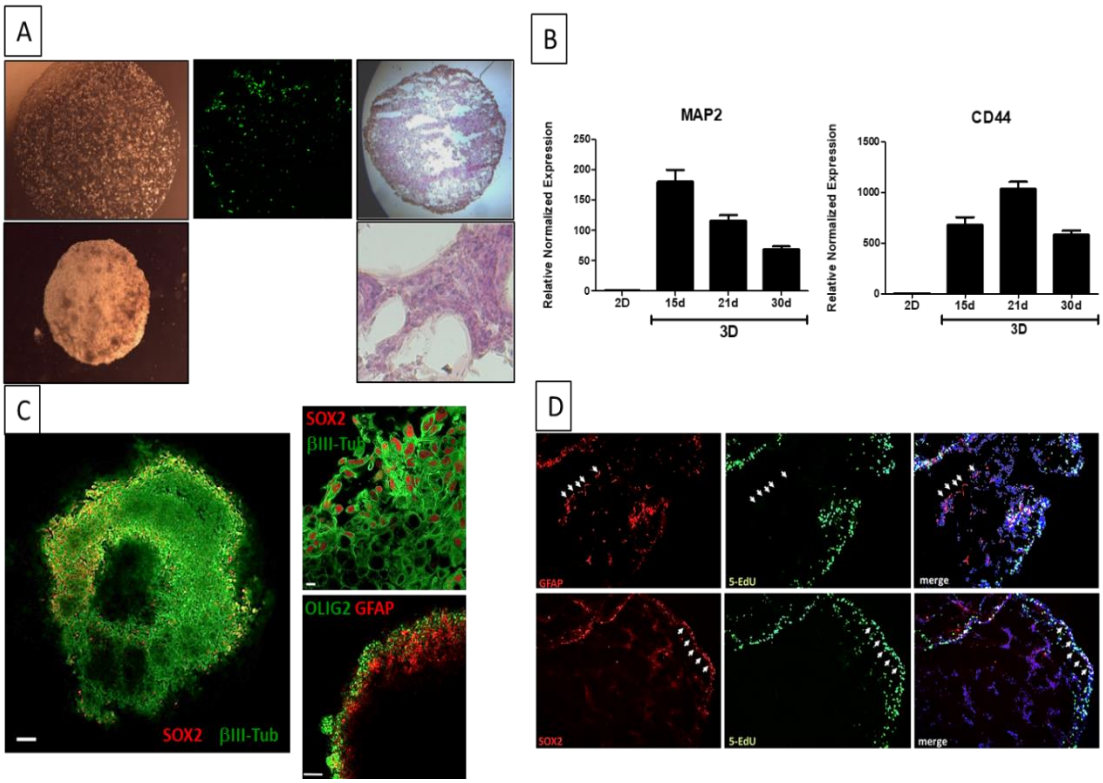

Figure 15 Characterization of GSC 3D organoids. A (from the left panel): representative images of 3D culture growth monitored by a phase-contrast microscope. Images

represent the same GSC 3D culture captured immediately after the embedding in Matrigel™ pearls and after 19 days. Central panel: 5-Edu incorporation assay after 30 days of culture. Cells within the 3D culture can proliferate (fluorescently labelled in green) without passaging for one month. Photos were captured by Stellaris 8 TAU STED confocal microscope (Leica). Right panel: Hematoxylin & eosin staining of GSC organoid sections, after 3 weeks of cultures: cells are organized in a tissue-like layered structure. a: bar = 500 µm; b: bar = 50 µm.

B: Comparison of MAP2 (left) and CD44 (right) mRNA expression in GBM3 GSCs cultivated as 2D monolayer or grown as 3D culture, for 15, 21, and 30 days. Data are obtained by quantitative RT-PCR experiments.

C: Immunofluorescence images of the whole GSC organoid structure labelled with Sox2 (red) and β-III tubulin (green) or Olig2 (green) and GFAP (red) obtained by confocal microscopy. Sox-2 and Olig-2 expressing cells (stemness marker), display a peripheral localization as compared to differentiated cells expressing β-III tubulin and GFAP. Bar=200 µm, 20 µm.

D: Immunofluorescent labelling performed on slices of GSC 3D culture (3 weeks post establishment) for GFAP (red, upper pictures) and Sox2 (red, lower pictures). Incubation with 5-EdU (green) was used to mark actively proliferating cells. Nuclei are counterstained with DAPI (blue). White arrows highlight that most proliferating cells are Sox2-positive and localized at the periphery of the organoid; conversely, most GFAP-positive cells display an inner localization and are not co-labelled by 5-EdU. Bar = 200 µm

Antiproliferative effect of Q54 and Q48 in high-expressing CLIC-1 GSC

The efficacy of the novel biguanides on the GSC 3D cultures was tested after a treatment for 7 days, and the proliferation activity was assessed by 5-EdU incorporation (*Figure 16-A*). As compared to vehicle-treated 3D culture (Ctr), Q54 and Q48 (100 µM) significantly reduced the number of proliferating cells by 95 and 85%, respectively, while metformin required 10 mM concentration to induce similar effects (− 83%). Q46 (1 mM) did not reduce organoid proliferation. Moreover, we assessed the specificity of this effect on GSCs measuring the expression of the stemness marker Sox-2 in 3D cultures challenged with the biguanide compounds. GSC 3D culture were treated for 7 days with Q54 and Q48 (100 µM) and Q46 (1 mM) then sliced and labelled with antibodies against Sox2 and bIII-tubulin in cytoimmunofluorescence

experiments. Q48 and Q54 caused a reduction of Sox2-expressing cells in 3D culture, while no changes in Sox-2 were observed after treatment with Q46 (*Figure 16-B*). The inhibitory effects observed in the proliferation assay and Sox-2 expression confirm the results already observed in 2D cultures (*Figure 8 and 9*).

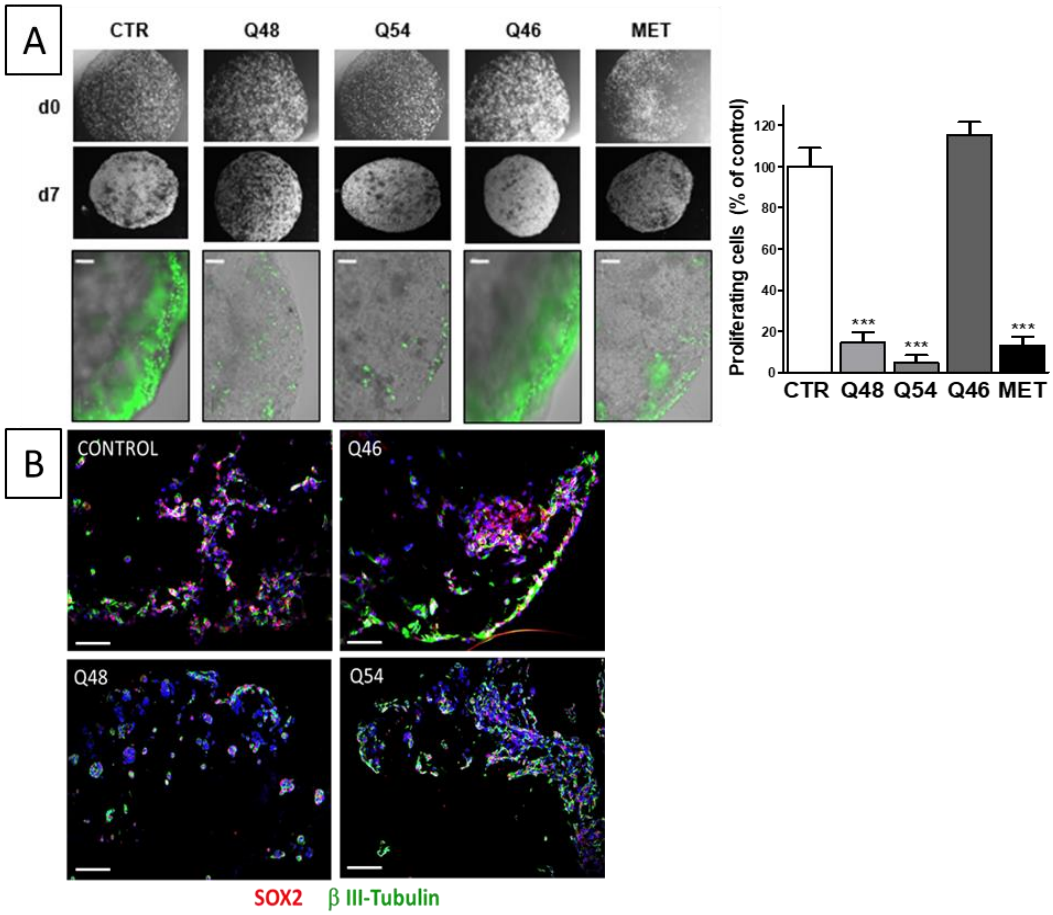

*Figure 16 Q48 and Q54 and metformin impair proliferation in GSC 3D culture and selectively reduce Sox-2 expression A: Representative images of organoids at d0 and d7, prior to treatment (upper pictures). After further 7 days of treatment, proliferating cells were labelled with 5-EdU (green, lower pictures). Bar = 100 µm. The quantification of the changes in proliferation rate (reported as % of control values in the graph) was obtained by measuring the total fluorescence using the ImageJ software. Q48 and Q54 (100 µM) and metformin (10 mM) caused a significant reduction of proliferating cells, while Q46 was not effective. ***p < 0.001 vs. CTR.*
B: Representative images of the changes in the expression of Sox-2 within GSC 3D culture after Q46, Q48, and Q54 treatment evaluated by immunofluorescence (Sox2-expressing cell-red and β-III tubulin-expressing cell-green). Nuclei are counterstained with DAPI (blue). Bar = 200 µm. Q48 and Q54 treatment significantly reduced the

number of Sox2-expressing cells (purple: co-localization of Sox2, red, and nuclei, blue) as compared to vehicle-treated control. Q46 was ineffective.

Antiproliferative effect of Q54 and Q48 in low-expressing CLIC-1 GSC

3D cultures were also generated from low CLIC-1 expressing GSC, even if they showed a slower growth rate, confirming on one hand their tumorigenic ability, and, on the other, the reduced capacity to proliferate in vitro as already observed in the 2D culture condition. The treatment of GBM39 cultured in 3D with Q48 caused a comparable inhibition in GBM3 thus independently from CLIC1 expression levels (*Figure 17-A, B*). This result was unexpected as compared to what was observed in 2D culture, however, it could be due to the longer treatment performed in 3D vs. 2D culture experiments (7 vs. 2 days, respectively) which may induce the interaction with different molecular targets. Q54, as expected, didn't show a significant effect in GBM39 3D culture. Q46 was ineffective confirming its inability to affect GSC proliferation in both 2D and 3D cultures. Interestingly, Q54 activity showed a linear correlation with cell CLIC-1 content (*Figure 14-A*), since in GBM3, highly expressing CLIC-1, a maximal inhibition was observed (−95% of proliferating cells vs. control), in GBM50, which displayed an intermediate CLIC1 content, the effect was in the middle (−50%), and in low CLIC1-expressing GBM39, there was no significant inhibition observed (*Figure 17-C*) ($R^2 = 0.99$).

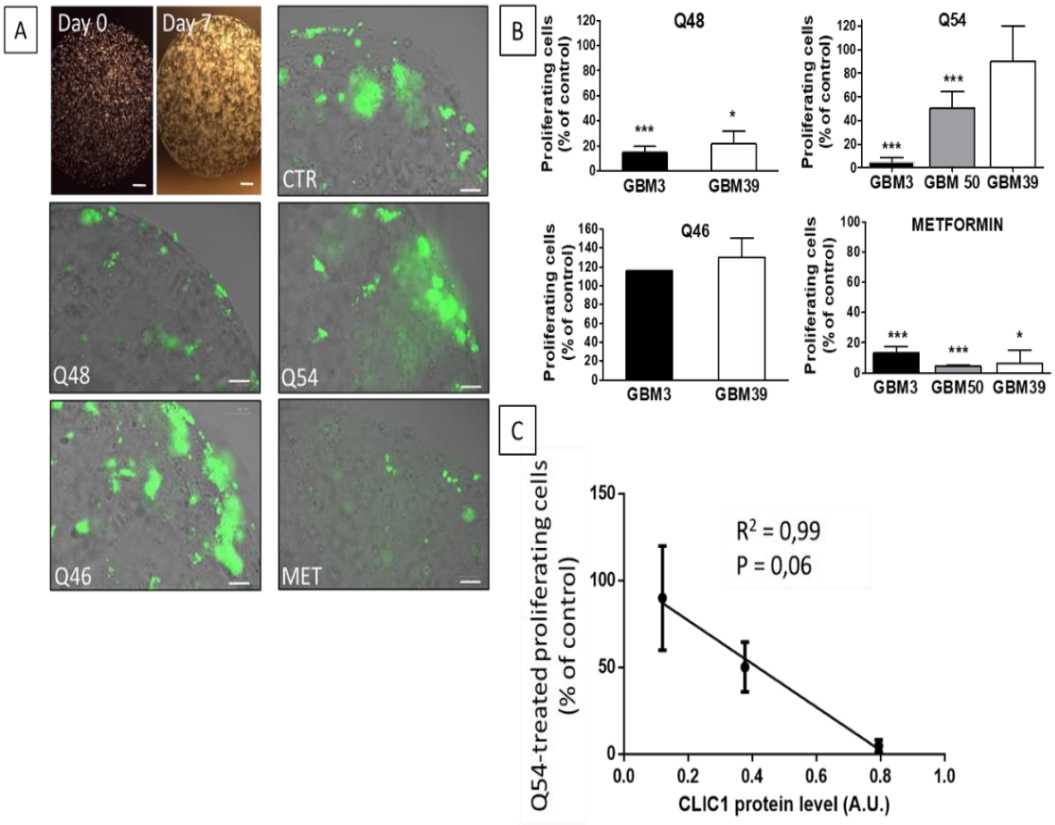

Figure 17 Figure 17 Low CLIC1-expressing GSC (GBM39) are able to grow in 3D culture A: representative images immediately after plating (day 0) and after 1 week (day 7); bar = 300 µm. following pictures: representative images of GBM39 growth as 3D culture, cells in active proliferation were labelled with 5-EdU (green). Vehicle-treated cells (CTR) display a lower proliferative rate than high CLIC-1-expressing organoids (Figure 16). Treatment with Q48 and metformin (7 days) reduced cells proliferation, while Q46 was ineffective. Q54 do not reduce organoid cell proliferation in GBM39. bar = 100 µm.

*B: Quantification of Q48, Q54, Q46 (100 µM), and metformin (10 mM)-dependent changes in 3D culture proliferation rate. Data, obtained measuring the total fluorescence using ImageJ software, are reported as % of control values in the graph. Antiproliferative activity is reported comparing the responses in high CLIC-1-expressing GSCs (GBM3) and low CLIC-1-expressing GSCs (GBM39). Q54 and metformin were also tested on GBM50 which expresses CLIC1 at an intermediate level (Figure 14). Q48 and metformin reduced proliferation in 3D culture independently from CLIC1 expression levels, while Q54 efficacy was directly proportional to the expression of the channel. *p < 0.05, ***p < 0.001 vs. respective control samples.*

C: Linear regression (R2 = 0.99) correlating CLIC1 expression and Q54 antiproliferative activity in GSC-derived organoids

Antiproliferative effect of Q54 and Q48 on zebrafish model

The in-vivo efficacy of the novel biguanide compounds on GBM growth was assessed in the zebrafish model. Zebrafish hindbrain were xenotransplanted with ZsGreen labelled GBM3 GSCs, and Q48, Q54, and Q46 (1 mM), were added to culture water for 3 days. Tumour growth was evaluated by measuring fluorescence intensity and area of the tumour mass using ImageJ software. As already observed in-vitro, Q54 caused a highly significant ($p = 0.0002$) reduction of tumour growth, and Q46 was ineffective. Conversely, Q48, which was highly effective in vitro, in zebrafish model exerted a modest activity that didn't reach statistical significance.

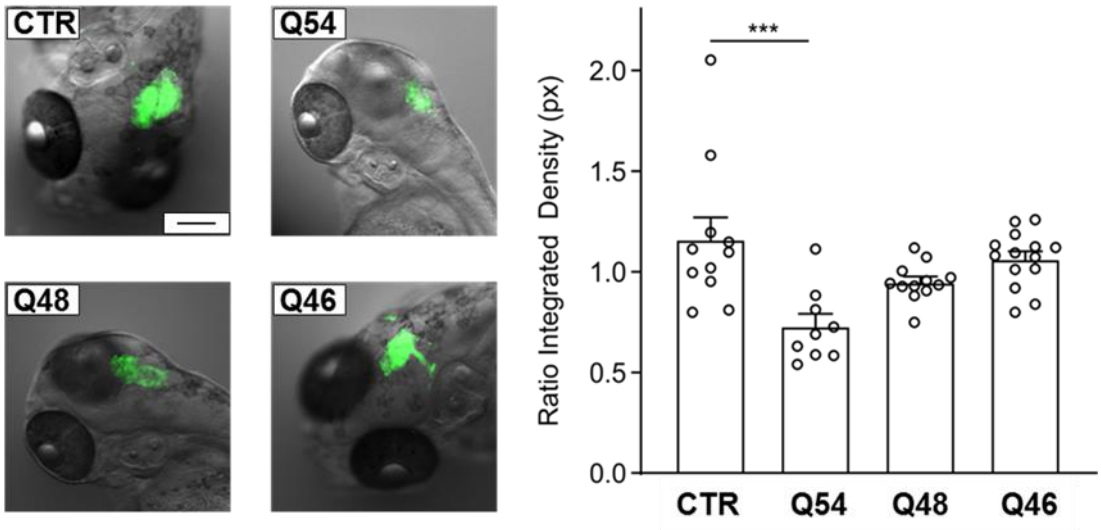

*Figure 18 In-vivo antiproliferative effect of novel biguanides in zebrafish xenotransplanted with GCSs. Representative pictures show the expansion of the tumour mass (72 h post-injection) in zebrafish embryos' brain injected with ZsGreen-positive cells with 1 mM Q54, Q48, and Q46 dissolved in embryos' water. CTR = controls. Scale bar 100 µm. Right graph: Quantification of the integrated density of the tumour mass in control condition or in presence of the compounds. Every experimental point represents the expansion of the tumour mass measured in the single embryo's brain. Data are reported as mean ± SEM; CTR n = 11, Q54 n = 9, Q48 n = 12, Q46 = 14; ***p = 0 .0002.*

Antiproliferative activity of metformin on tumoroid model

Characterization of the 3D model

Tumoroids, which have been obtained and maintained in culture as described in "Material & Methods" section, were firstly characterized in terms of growth rate and cell composition by selective marker expression. We observed that, in the vast majority of cases, cells start to exit from the tissue fragment and invade the surrounding matrix (Matrigel™) within 5 days after the tumoroid establishment (*Figure 19A-Upper*), even if some variability among the different cultures and the different tissue samples in the same specimens was noted, probably due to the characteristic GBM tissue heterogeneity. In about one month, Matrigel™ droplets result totally invaded by tumour cells displaying a reduced size due to both matrix digestions by the cells and its "natural degradation" (*Figure 19A-Lower*). To identify the GBM cell population that compose the tumoroids, their localization, and proliferation ability, immunofluorescence experiments have been performed both on sections (*Figure B*) and on the whole 3D culture (*Figure C*), after 45 days of culture. We detected within the tumoroids the presence of cells labelled by β-III Tubulin (neural differentiation marker), GFAP (astrocyte differentiation marker), Sox-2 (stem-like cell marker), CD31 (marker of endothelial differentiation) and IBA-1 (marker of macrophage/microglia) highlighting that these culture conditions allow the maintenance of different cell subpopulations. To identify the cells in active proliferation we incubated the tumoroids with 5-EdU whose incorporation (green) in an index of DNA synthesis (*Figure 19C and D*).

We observed that, even if after prolonged cultivation (7 months of culture), no macroscopic changes in the tumoroids structure can be observed, but cells are actively proliferating (*Figure 19D*). After 45 days, proliferating cells are still abundantly represented within tumoroids, especially at the edge of the

structure, while after 7 month 5-EdU positive cells, although significantly reduced, were still clearly detectable and sparse within the 3D structure (*Figure 19D, left panel*). Importantly, after 7 months of culture, tumoroids maintain the expression of Sox-2 which co-localize with 5-EdU labelling (yellow), thus indicating the survival and proliferation of the GSC subpopulation (*Figure 19D-right panel*).

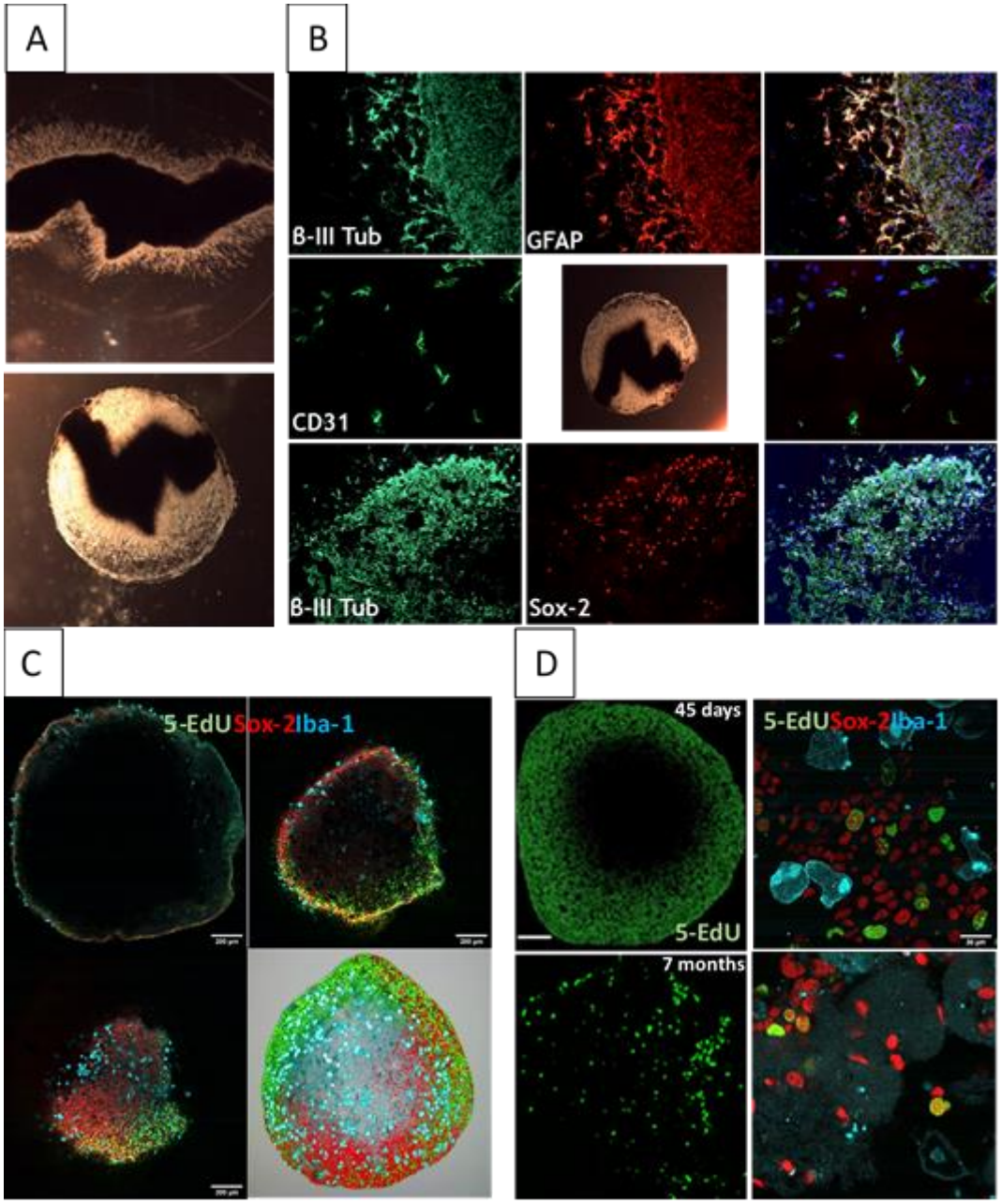

Figure 19 Characterization of tumoroids A: Representative images of one tumoroids growth assessed by an inverted microscope at different time points (upper: 5 days- lower: 20 days). In the upper photo, the tumour fragments (black, in the centre of the tumoroid) and the cells that start to invade are observable, while in the lower one, the tumour fragment is still recognizable but the matrix (Matrigel™) is fully invaded.
B: Immunofluorescent labelling performed on tumoroids slices (45 days post establishment) for (starting from the upper panel) β-III Tubulin (green), GFAP (red) and the colour merge, CD31 (green) and the colour merge, β-III Tubulin (green), Sox-2 (red) and the colour merge. Nuclei are counterstained with DAPI (blue). The expression of different marker within the tumoroids indicates the possibility to maintain in culture different cell subpopulation. Scale bar: 100 µm and 200 µm.
C: Immunofluorescent labelling performed on the whole tumoroids structure (45 days post establishment). By confocal microscopy (Stellaris 8 TAU STED-Leica) whole

tumoroids structure was analysed (the reconstruction, image with grey background, was obtained with Leica software): we identify the localization of cells in active proliferation, labelled by 5-EdU, (green), Sox-2 (red) and Iba-1 (cyan) positive cells. Proliferating cells and Sox-2 positive cells are localized at the edge of the 3D structure. Scale bar: 200 µm

D: Representative images obtained by confocal microscopy on whole tumoroids structure at 45 days (upper panel) and 7 months (lower panel) to assess cell proliferation (green), Sox-2 (red) and Iba-1 (cyan) expression. The left panel was obtained by confocal images reconstruction by ImageJ software and indicate the localization of the proliferating cells. Cells in active proliferation are situated at the edge at 45 days, while at 7 months are sparse within the 3D structure. The expression of Sox-2 is maintaining at 7 months of culture and co-localize with the proliferating cells, while Iba-1 is lost as indicated by the cyan spot in the images (probably cell fragments). Scale bar: 200 µm, 20 µm.

Antiproliferative effect of metformin on tumoroid model

The efficacy of metformin (10mM) in the tumoroids model was established after treatment for 7 days; proliferation activity was assessed by 5-EdU incorporation and images were analysed by ImageJ software. Treated tumoroids showed a massive reduction of proliferation at the edge of the 3D structure, while in the centre, occupied by the tissue fragments, cells retained a certain degree of proliferation rate (images were taken by Zoe™ Cell Imager, Bio-Rad Laboratories, Magnification:20X) (*Figure 20-lower panel*). To image the whole structure, we analysed the tumoroids by Stellaris 8 TAU STED confocal microscope (Leica) (Magnification 10X) (*Figure 20-upper panel*); the core of the tumoroids confirmed a higher proliferation rate than the edge. Fluorescent analysis was performed of the reconstructed confocal images by ImageJ software. Metformin reduced the number of cells in active DNA synthesis by a 35% as compared to control.

The data about tumoroid are currently object of further studies which cannot be completed within the PhD program time-frame.

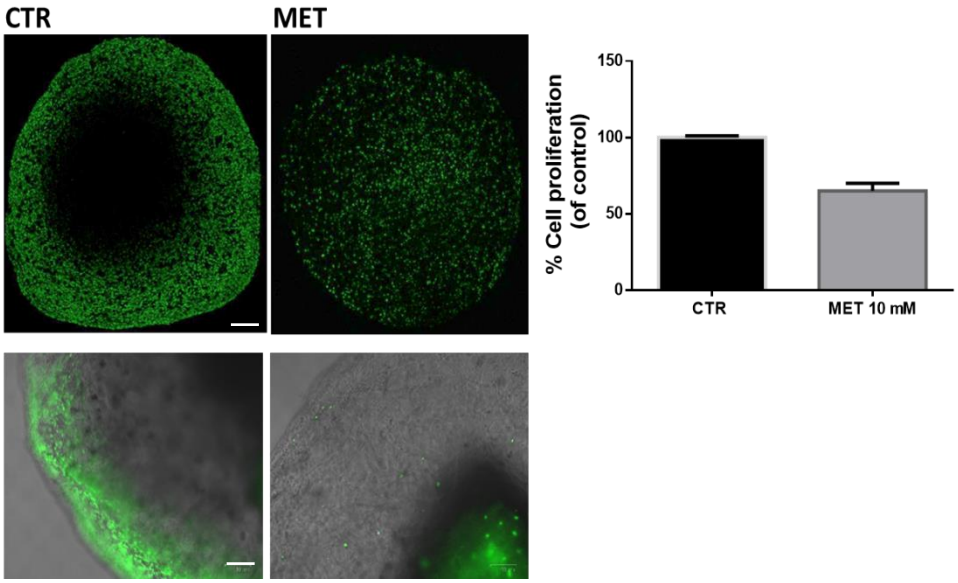

Figure 19 Metformin display antiproliferative activity in tumoroids. Representative images of tumoroids 4 weeks post establishment which were treated with metformin for 7 days (started at week 3) and cells in active proliferation were labelled with 5-EdU (green). Imaging was performed using Zoe™ Cell Imager, Bio-Rad Laboratories (Magnification:20X) (lower panel) and Stellaris 8 TAU STED confocal microscope (Leica) (Magnification 10X) (upper panel). The quantification of the compound-dependent changes in proliferation rate was obtained on the confocal images reconstruction (upper panel) using the ImageJ software. Bar=200 µm, Bar = 100 µm

Discussion

GBM patient survival rate is about 15 months from the diagnosis, during which a progressive deterioration of the quality of life occurs, and since the early 2000s[18], no significant improvements have been obtained. Thus the development of novel therapeutic opportunities is an urgent medical need. In spite of huge research efforts, GBM is still an incurable tumour also due to the lack of appropriate model to recapitulate its high heterogeneity[89]. Metformin, which displays antiproliferative activity on GSC[25,127], has been proposed as a possible option for GBM treatment but the high concentration required (within the mM range)[25,127,128] are very difficult to obtain in patients (plasmatic concentrations after 1.5-2 g/day of metformin, corresponding to a standard treatment for diabetes, are within the μM range)[129], thus new more potent compounds that share the biguanide moiety could be an alternative to metformin[124]. Among the mechanisms proposed for metformin antiproliferative activity[127,128,130], CLIC-1 inhibition is highly correlated to GSC proliferation thus represents a promising target[60,88]. Since CLIC-1 activity is inhibited by both linear and cyclic biguanides[88], we tested a small library of novel biguanide derivatives from metformin (linear structure) or cycloguanil (cyclic structure) evaluating their ability to impair GSC proliferation, self-renewal and invasiveness looking for compounds with higher potency than metformin.

Firstly, we carried out a screening of the ability of novel compounds to inhibit GSC proliferation in concentration response experiments, also evaluating possible off-target activity using cells which not require CLIC-1 for proliferation (i.e. non-stem GBM cells and ucMSCs[60]). As results, within the linear biguanides, we noticed that the substitution with a lipophilic and electron-withdrawing group (4-Cl-Q42 and 3-CF_3-Q50) on the phenyl ring,

displayed high antiproliferative activity, while an apolar electron-donor (4-CH_3-Q49) was correlated to a marked decrease of efficacy. Among the cyclic biguanides, the shift of the chlorine atom from para- (cycloguanil) to meta-position (Q53) has shown a reduced potency, while the Cl substituted in the ortho-position (Q52) prevented the activity, likely due to the steric hindrance which impede the molecule to acquire the appropriate spatial geometry required to interact with CLIC-1. The substitution which showed the best results in terms of higher potency than metformin as far as GSC antiproliferative activity, and selectivity as CLIC-1 blockers was the 4-OMe group on the aromatic ring, that we find on Q48 and Q54. Q48 and Q54 for their higher potency (IC50 = 0.082 and 0.43 mM, respectively, versus 9.78 mM of metformin) and the lower off-target activity (efficacy of about −40% cell viability at the highest concentration tested, toward CLIC1-independent cells, as compared to −80% in GSC) were identified as potential lead compounds. Along with the ability to impair GSC proliferation, Q48 and Q54 inhibit GSC self-renewal (tested as sphere-formation ability), migration, and invasiveness, with efficacy similar to that of metformin, but a 100-fold higher potency. These compounds were able to directly bind to a recombinant form of CLIC-1 with Kd similar to the IC50 observed in the antitumor activity, and to act as CLIC-1 blockers in whole-cell electrophysiology experiments performed on GSC, thus the main molecular target of Q48 and Q54 was identified in CLIC-1. Moreover, we observed that Q46 that did not affect GSC proliferation was also inactive as CLIC-1 blocker, thus supporting the correlation between the inhibition of CLIC1-mediated ion current by Q48, Q54, and their antiproliferative effects. However, while these results clearly correlate the biguanides ability to impair CLIC-1-mediated current with their antiproliferative activity, we have to remark that Q48 was able to completely prevent CLIC-1 activity only at a concentration higher than the antiproliferative IC50 (0.5 vs. 0.082 mM), thus highlighting the possible involvement of additional mechanisms of action in

its antitumor activity. Conversely Q54 activity seems to be solely dependent on the inhibition of CLIC-1-dependent ion current.

Biguanides derivatives were also tested on GSC 3D culture model, and in vivo on zebrafish model[131]. GSC grew as 3D culture develop a tissue-like structure, with a fast-proliferating cells in the external layer expressing stem cell markers, while internally are localized slow-proliferating cells with a differentiated phenotype (i.e. expression of β-III tubulin and GFAP), well mimicking GBM growth in vivo[116]. Treatment with Q48 and Q54 for 7 days inhibited GSC growth within the 3D culture with efficacy similar to metformin, while Q46 was ineffective. To note, as further evidence that these molecules mainly impair GSC, we observed that together with the impairment of GSC hallmarks as self-renewal, migration and invasion, Q48 and Q54 were able to reduce the GBM cell proliferation mainly acting on the GSC component (i.e. Sox-2^+ cells) both in 2D and 3D cultures. In vivo, on zebrafish model, Q54 significantly reduced the growth of GBM3 GSC, xenotransplanted in zebrafish hindbrain, while Q48 which display the highest activity in vitro, caused only a modest inhibition of GSC growth in vivo, which did not reach statistical significance. As already shown in vitro, Q46 was ineffective. Our main hypothesis to explain the low activity of Q48 in vivo is that the zebrafish model requires that the testing molecules be added to the fishes' culture water, and being Q48 much less hydrosoluble than Q54, it might not be able to reach effective concentrations in the animal brain.

Taken together these data display that the inhibition of CLIC-1 reduces GSC proliferation, self-renewal, migration, and invasiveness and that the antiproliferative activity of biguanide compounds is mainly mediated by CLIC-1 inhibition, as demonstrated by the limited inhibition of viability observed in ucMSCs (CLIC-1 independent proliferation). Metformin potency as antitumour activity can be improved, without showing additional toxicity

effects as also shown by the low toxicity exhibited in ucMSCs. Moreover, antitumor effects exerted in 3D GSC culture and in vivo in zebrafish are highly suggestive of efficacy also in more complex systems.

The desirable approach to treat complex pathologies like cancer is a patient tailor-made treatment based on the identification of precise molecular drug targets, in order to improve pharmacological activity and reduce systemic adverse events. Recently, an increasing number of studies and therapies are going towards this direction, focusing on the drug target gene expression of individual patients[132,133].

CLIC-1 is highly expressed in most GBM and it acts as main regulator of GSC growth rate[52]. In this study we analysed the content of CLIC-1 in several GSC cultures, identifying three human GBMs (GBM39, GBM44, and GBM50) inherently expressing low levels of this channel. Interestingly, in patients and in the relative GSCs isolated in vitro, they displayed features similar to the CLIC1 high-expressing counterparts. GBM39, GBM44, and GBM50 could represent a subset of tumours in which CLIC-1 activity is compensated by different intracellular signalling. This observation indicates that, while CLIC-1 functional expression enhances GSC proliferation and tumorigenesis, its activity can be bypassed by different intracellular pathways allowing GBM development and progression. We studied these GBM to assess the specificity of the novel biguanides as CLIC-1 blockers: we found that in 2D culture CLIC-1 low-expressing GSC showed a significant reduction in potency and efficacy of Q48 and Q54 (and metformin). Obviously, the antiproliferative activity is not abolished likely because GSC from these GBMs still express low levels of CLIC-1, which represent the expected molecular target of these compounds. Surprisingly, in GSC 3D culture metformin and Q48 produced a significant antitumor activity also in GBM39 GSCs, independently from CLIC-1 expression, while Q54 efficacy was dependent on CLIC-1 content. Different

reasons may rely under this discrepancy. Firstly, the experimental protocol used in 3D culture requires 7 days of treatment (while the 2D only two days) and may cause an increased antitumor efficacy proportional with the duration of treatment[80], due to the accumulation within tumour tissue and cells (which has been already demonstrated for metformin[134]). Alternatively, this observation, along with the discrepancy between the antiproliferative IC50 and the concentration required to completely block CLIC1-mediated current (0.082 mM vs. 0.5 mM) could highlight the involvement of additional molecular targets of Q48 implicated in the control of GSC proliferation.

For example in the case of metformin, several mechanism of action has been proposed to explain its antiproliferative effect on GSC, such as the inhibition of the Akt pathway[135], the inhibition of mitochondrial energy metabolism, the interference with ROS and transforming growth factor-β signalling or the modulation of the insulin/insulin-like growth factor-1, mitogen-activated protein kinase and AMP-activated protein kinase regulated pathways[136]. Since for metformin and other biguanides[137] in silico studies have proposed an activity on the dihydrofolate reductase (DHFR), we tested the inhibitory activity of metformin, Q54 and Q48 on it, observing that on living GSCs, only Q48 and metformin caused a moderate enzyme inhibition after 72 h of treatment[138] (data are not reported in this thesis). Thus, DHFR inhibition could represent another mechanism of action of some, but not all, biguanide drugs on GSC. Nevertheless, more studies, are needed to elucidate all the possible mechanism of action involved in the antiproliferative effect exerts by the biguanide drug on GSC, for example using technologies such as transcriptomics, able to screen a high number of molecular pathways at the same time.

Since one of the main issues in GBM research is to find the appropriate model to recapitulate the tumour complexity and heterogeneity, in the research work

developed for this thesis, we tested the novel compounds we studied on different GBM models, aiming to obtain better predictive results of the efficacy in vivo. Our results highlight that different models allowed us to obtain distinct information on the new compounds that we could have missed testing the biguanide compound only in one kind of model. For example, Q48 which showed higher efficacy in patient-derived GSC culture both in 2D and in 3D, seems to be less effective in zebrafish, likely due to its reduced water-solubility[138]. Moreover, testing the biguanide compounds on 3D culture of low-expressing CLIC-1 GSC, allow us to note an unexpected high efficacy of Q48, which we do not observe in 2D. Also in this case, we hypothesized a possible accumulation of Q48 within the tissue-like structure and cells or the involvement of additional mechanism of action. These observations pointed out some peculiarities of Q48 that we couldn't observe without these different models and that make us aware that further studies are needed to elucidate these aspects. These data highlight that, to date, is not possible to define a "best model" for GBM research, certainly the aim must be to try to reproduce the GBM heterogeneity and complexity[89,90], and one approach could be to use different models and integrate the obtained data.

Lastly, we started to characterize a new GBM model, the tumoroid. Tumoroids are obtained from GBM fragments embedded in Matrigel™, which can be maintained in culture for several months without passaging. Within tumoroids, after 45 days of culture, we were able to find different cell subpopulations (GSC, endothelial cells, immune cells, astrocytes and neurons) as highlighted by immunofluorescence labelling. Thus, this model could better reproduce the GBM heterogeneity, and could be a suitable platform for high-throughput drug screening, thanks to its easiness obtainment and quite rapid growth. Moreover, from a patient-tailored medicine point of view, tumoroids could represent a turning point, indeed they could be used for testing different

drugs, and then choose the more appropriate therapy to be administered in the patient[139,140].

As regards the potential use of tumoroids as a platform for drug we tested the efficacy of metformin: preliminary results showed an important effect of metformin in the reduction of the proliferation rate also within the tumoroid, even if we observed that metformin antiproliferative activity was mostly exerted on the cells in the periphery of the structure, while the cells located in the centre of the tumoroid seems to be not influenced by the treatment. Conversely in the control condition the cells within the internal portion of the tumour fragment seem non-proliferating. To date, we don't know exactly the reason why the treatment with metformin seems to re-activate a proliferation inside the tumoroids as compared to the control condition; different hypothesis can be drawn: the treatment with metformin mainly impairs the proliferation of the cells that exited from the fragment, while inside the fragment, a selection and reactivation of some cells subpopulation can occur, or since metformin, which is hydrosoluble[134], has been added only at the begin of the experiments it could not reach the fragment with an adequate concentration to induce the antiproliferative effects. This hypothesis seems to do not be in accordance with what we observed in the control condition, in which the tissue fragment seems non-proliferating, but we have to point out that we observed lots of variability among different tumoroids from the same GBM and not all showed non-proliferating tissue fragments. Thus the different behaviour of the inner cells may be non-related to the drug treatment.

Indeed, to date, tumoroids still show some problematic issues: on one side to reproduce tumour cell heterogeneity is a big advantage for GBM research, covering both the intra-tumour and inter-tumour differences, on the other side it came with some technical problems in terms of standardization of the methods and results interpretation which required high number of replicates.

Conclusions

In this work, we show that two novel biguanide compounds, Q48 and Q54, similarly to metformin, impairs GSC proliferation, self-renewal, migration, and invasion, principally acting via CLIC-1 inhibition, in both 2D and 3D models. The novel biguanide derivatives showed a significantly higher potency than metformin as antiproliferative agents, but retaining a GSC-specific activity (and thus likely low off-target toxicity). In particular, the higher potency suggests a possible easy translation in clinical setting. The identification of different expressions of CLIC-1 among different GBM and its correlation to the responsiveness to metformin and the novel biguanide compounds allows us to propose CLIC-1 as a biomarker to predict the susceptibility of distinct GBM to biguanide-based compounds and may be used for the selection of GBM patients which likely could receive benefit from biguanide treatment. The different results obtained for Q48 in 2D GSC cultures, on CLIC-1 low-expressing GBM 3D cultures and on zebrafish highlighted possible additional mechanisms of action for the novel biguanides and metformin, but importantly, point out the importance of using different experimental models. Therefore, the biguanide-based molecule Q48 and Q54 may represent novel and selective treatments for GBM, moreover, we proposed a multi-models approach with the aim to overcome the lack of appropriate models to reproduce GBM heterogeneity and obtain more predictive results of GBM responsiveness to compounds. Moreover, from a precision medicine point of view, we proposed that biguanide compounds are likely more effective in highly-CLIC-1 expressing patients and that tumoroid model, when methodological and standardization issues will be solved, could represent a screening approach for the selection of appropriate patient-based GBM treatment.

Material and Methods

Human GBM Specimens

Tumour specimens were obtained from Neurosurgery department IRCCS-Policlinico San Martino (Genova) after patient's informed consent and Ethical Committee approval. Patient underwent surgery for the first time and never received chemo-radio therapy. The clinical, histopathological and molecular features of patients and tumours, classified as grade IV GBM (n=10) and grade III anaplastic astrocytoma (n=1) according to World Health Organization criteria. Tumour characteristics are reported in table 1. Tumour specimens were immediately mechanically dissociated to isolate a single cells suspension or to embedded fragments in Matrigel.

Table 3 Patients' and tumors' characteristics.

Code	Sex	Age (yrs)	WHO grade	Molecular subtype	IDH and 1p/19q co-deletional status	NOD/SCID mice survival time (days)
GBM 3	M	48	IV	Neural		120
GBM 23	F	70	IV(primary multicentric)	Neural		100
GBM 19	F	41	IV (secondary to oligondoglioma)	Mesenchymal		100
GBM 5	M	67	IV (primary)	Neural		55
GBM 10	F	70	IV			180
GBM 37	F	73	IV			150
GBM 39	M	52	IV			100
GBM 44	F	69	IV		Wt / non-codeleted	n.d.
GBM 50	M	71	III		Wt / non-codeleted	n.d.
GBM 89	M	57	IV		Wt	n.d.
GBM 94	M	41	IV		Wt	n.d.

Glioblastoma stem cells (GSC) and umbilical cord mesenchymal stem cell (ucMSC) primary culture

Patient-derived GBM single cells suspension were cultured in vitro in serum-free medium (stem cell permissive medium) containing:

- 1:1 DMEM-F12 (EuroClone, Milano, Italy) /Neurobasal™ Medium (Gibco-ThermoFisher Scientific, Life Technologies, Monza, Italy), B27™ supplement (Gibco-ThermoFisher Scientific), 2 mM L-glutamine (EuroClone), 1% penicillin-streptomycin (EuroClone), 15 μg/ml insulin (Sigma-Aldrich, Merck Life Science, Milano, Italy), 2 μg/ml heparin (Sigma-Aldrich) and completed with recombinant human bFGF (10 ng/ml; Miltenyi Biotec, Bologna, Italy) and EGF (20 ng/ml; Miltenyi Biotec).

Within 2 weeks, cells gave rise to floating tumor-spheres, but to allow reliable experiments cells were grown as monolayers in flasks coated with growth factor-reduced Matrigel™ (Corning, ThermoFisher Scientific), guaranteeing the maintenance of stem markers, spherogenic properties, differentiation and tumorigenic potential[141]. Tumor-initiating capacity was confirmed by orthotopic xenografts (10,000 cells) in 6–8-weeks old non-obese diabetic severe combined immunodeficient (NOD/SCID) mice.

To induce differentiation, GSCs were shifted for 2 weeks in:

- DMEM-F12 medium supplemented with 10% FBS 2 mM L-glutamine, 1% penicillin-streptomycin (all from EuroClone).

Uc-mesenchymal stem cells (ucMSCs) were isolated from human umbilical cords (uc, n = 4) collected from full-term women, immediately after caesarean section at the Obstetrics and Gynecology Department (International Evangelical Hospital, Genova, Italy), after informed consent and Institutional Ethic Committee approval (register number 2/2010). ucMSCs were isolated as reported[142], cultured in MesenPRO-RS™ Medium (Gibco-ThermoFisher Scientific), and characterized by flow cytometry (MSC Phenotyping Kit, Miltenyi Biotec) following the criteria of the International Society for Cellular Therapy[143].

Establishment of GBM derived 3D cultures

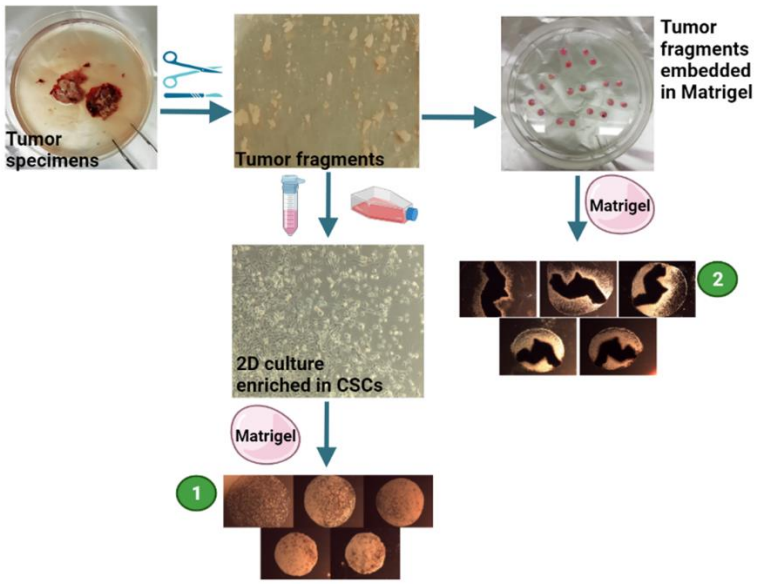

Figure 20 Schematic representation of 3D cultures establishment.

1-GSC 3D culture

Three-dimensional spheroids were obtained as previously described (Hubert, 2016)[116]. Briefly, GSC (5000) were suspended in ice-cold Matrigel™ and seeded in Parafilm™ molds to obtain 10 µL droplets and incubated at 37°C, 5% CO_2 for at least 30 minutes. Droplets were gently washed-off from parafilm molds and transfer to a petri dish and let them grow in stem cells permissive medium. Morphology was assessed through a digital camera Leica ICC50 HD (Leica) mounted on a transmitted light microscope DM IL (Leica).

2-Tumoroids

Upon specimen arrival, they were gently mechanically dissociated and fragments were embedded in 10 µL of ice-cold Matrigel™ droplets and incubated at 37°C, 5% CO_2 for at least 30 minutes. After Matrigel™ polymerization tumoroids were carefully washed-off from molds and let them floated in a serum-free medium already described by Jacob and colleagues[117], with minor modifications containing:

- 50% DMEM:F12 (EuroClone, Milano, Italy), 50% Neurobasal (Gibco-ThermoFisher Scientific, Life Technologies, Monza, Italy), 1X L-glutamine (EuroClone), 1X NEAAs (EuroClone), 1X PenStrep (EuroClone), 1X N2 supplement (Gibco-ThermoFisher Scientific), 1XB27 supplement (Gibco-ThermoFisher Scientific), 1X 2-mercaptoethanol (Thermo Fisher Scientific), and 2.5 μg/ml human insulin (Sigma-Aldrich, Merck Life Science, Milano, Italy).

After 5-7 days cells starts to invade the surrounding matrix as assessed through a digital camera Leica ICC50 HD (Leica) mounted on a transmitted light microscope DM IL (Leica).

Chemical, reagents and antibodies

Metformin, methotrexate, 1-phenylbiguanide hydrochloride (Q46) and 1-(4-chlorophenyl)-biguanide hydrochloride (Q42) are commercially available (Sigma-Aldrich). Q48, Q49, Q50 (linear biguanides) were synthesized by refluxing an ethanolic solution of the proper aniline derivative hydrochloride with dicyandiamide, according to previously published protocols: Q48 and Q49[144], Q50[145].

Q51, Q52, Q53[146], and Q54[147], cycloguanil analogues, were achieved by an acid-catalyzed, three-component synthesis involving an aniline derivative, dicyandiamide and acetone. Elemental analysis of synthesized compounds was performed on a Flash 2000 CHNS (Thermo Scientific) instrument at the Microanalysis Laboratory of Pharmacy Department (University of Genova) to monitor compounds' purity that was observed as >95% for all the newly synthesized compounds.

The following primary antibodies were used:

- Anti-CLIC1 (356.1, SantaCruz Biotechnology, Heidelberg, Germany) dil. 1:750 (WB)

- Anti-Sox2 (sex determining region Y-box 2, L1D6A2, Cell Signaling Technology, EuroClone) dil. 1:100 (IF), 1:1000 (WB)
- Anti-GFAP (glial fibrillary acidic protein, GA5, Cell Signaling Technology, EuroClone) dil. 1:1000 (WB), 1:100 (IF)
- Anti-β-III-Tubulin (18207, Abcam Cambridge, UK) dil. 1:100 (IF)
- Anti-Olig2 (oligodendrocyte transcription factor 2, EPR2673, Abcam) dil. 1:100 (IF)
- Anti-α-tubulin (Sigma-Aldrich) dil. 1:7500 (WB).
- Anti IBA-1 (Ionized calcium-binding adaptor molecule 1, Cell Signaling Technology, EuroClone) dil. 1:100 (IF)

Cell Proliferation assays

MTT reduction assay

MTT (3-(4,5-dimethylthiazol-2-yl)-2,5-diphenyltetrazolium bromide, Sigma-Aldrich) tetrazolium reduction assay was used to test cell viability. GSC were plated at the concentration of 3000 cells/well in 96-well plates. After 48h treatment with test compounds MTT substrate (2.5 mg/ml, in PBS), was added to cells plated and then incubated for 2h. The quantity of formazan crystals formed was evaluated, after being dissolved in DMSO, by recording changes in absorbance at 570 nm using a BioTek ELx800 plate reading spectrophotometer.

5-EdU incorporation

GSC 3D cultures or tumoroids were treated with metformin 10 mM, Q48 and Q54 0.1 mM for 7 days (where indicated) were assessed for changes in cell proliferation. Proliferating cells were detected by using the EduDetectPro Cell Proliferation Kit for Imaging (Base Click GmbH, Neuried, Germany), following the manufacturer's protocol. Fluorescence was detected with Zoe™

Fluorescent Cell Imager (Bio-Rad Laboratories) and fluorescence intensity was measured on captured images using ImageJ software, or with Stellaris 8 TAU STED confocal microscope (Leica).

Cell Count

To evaluate cell viability reduction induced by test compounds the trypan blue exclusion assay was used. GSCs (100,000 cells/well) were seeded in 6-well plates, and after 24h were treated with drugs for further 48h. Viable cells were counted in the presence of Trypan blue 0.4% w/v (Bio-Rad Laboratories, Milano, Italy), using the TC-20™ automated cell counter (Bio-Rad Laboratories) and reported as % of viable cells divided by the total number of counted cells[88].

Sphere-Formation assay

GSCs were seeded in complete medium without Matrigel™, in 48-well plates at 1000 cells/well. After 24h cells drugs were added and spherogenesis was monitored for 7 days. The number of spheres/well was assessed using a digital camera mounted on a transmitted light microscope to image each individual well, and visually calculated by two independent operators.

Migration

Cell migration was performed using Falcon™FluoroBlok™ HTS96 Well Insert Systems (ThermoFisher Scientific) with a light-tight PET membrane with 8 μm pores, able to blocks the transmission light within the range of 400 to 700nm. 15,000 cells/well were fluorescently labelled with Vybrant™ CFDA SE Cell Tracer Kit (Invitrogen- ThermoFisher Scientific), plated on inserts, and allowed to migrate towards FBS-containing medium. After o/n incubation at 37°C/5% CO_2, cells migrated to the bottom of membranes were visualized and captured by confocal laser-scanning microscope (Bio-Rad MRC 1024 ES) at 10×

magnification, and quantified using the ImageJ software (NIH, Bethesda, MA, USA).

Invasion

GSC were seeded without Matrigel™ for one week to let the spheres generate in stem cells permissive medium. After that, spheres were harvested and embedded in 80% of Matrigel™ and 20% of complete medium with Q48 (100 μM), Q54 (100 μM), Q46 (100 μM) and Metformin (10 mM). After Matrigel™ polymerization (45 min), complete medium with Q48, Q54, Q46 and Metformin was added to the dish. Photos of spheres were taken at T0 and after 15 hours using a digital camera Leica ICC50 HD (Leica) mounted on a transmitted light microscope DM IL (Leica). The analysis was performed by ImageJ software (NIH, Bethesda, MA, USA), calculating at least 2 diameters for each sphere. The differences between the average diameter of T15 and T0 of each condition were calculated and compared to control.

Electrophysiology

Patch electrodes (GB150F-8P with filament, Science Products GmbH, Hofheim, Germany) were pulled from hard borosilicate glass on a Brown-Flaming P-87 puller (Sutter Instruments, Novato, CA, United States) and fire-polished to a tip diameter of 1–1.5 μm and an electrical resistance of 5–7 MΩ. As reported[59], patch-clamp electrophysiology was carried out in perforated-patch whole cell configurations. In patch clamp whole cell experiments the voltage protocol consisted of 800 ms pulses from − 40 mV to + 60 mV every 10 s. In time course trials a 60 mV depolarizing voltage step, 800 ms duration was delivered every 5 s. After 5 min, in which the membrane current was stabilized, the cells were perfused with the test compounds. In both experimental conditions current amplitude was measured as trace average between 700 and 750 ms.

Patch clamp solutions were formulated as follow:

- bath solution (mM): 140 NaCl, 5 KCl, 10 HEPES, 1 MgCl2, 2 CaCl2, 5 D-Glucose, pH 7.4;
- pipette solution (mM): 135 KCl, 10 HEPES, 10 NaCl, 1 MgCl2, 2 CaCl2, 5 D-Glucose, pH 7.4.

Evaluation of Q54 and Q48 binding to CLIC1 protein

The binding of Q54 and Q48 to CLIC-1 was performed by the "Istituto Italiano di Tecnologia (IIT)" according to the following protocol[138]:

"Microscale thermophoresis (MST) was used to assess Q48 and Q54 interaction with CLIC1 protein[148]. MST measurements were performed using Monolith NT.115p instrument (NanoTemper Technologies, Munich, Germany). Assays were conducted at 10–20% (BLUE/RED dye) LED excitation power and MST power of 40%. Premium capillaries from NanoTemper Technologies were used. Measurements were carried out at 25 °C in the following buffer: 10 mM HEPES (pH 8.00), 150 mM NaCl, 0.05% Tween20. Recombinant CLIC1 protein was labeled with the Monolith labeling kit RED-NHS (ammine dye NT-647-NHS) and with the Monolith labelling kit BLUE-NHS (ammine dye NT-495-NHS) according to manufacturer instructions (NanoTemper Technologies). MST detects the change in fluorescence of a labeled target along a temperature gradient induced by the activation of an IR laser, upon addition of a ligand[148]. Change in MST signal is expressed as the variation in the normalized fluorescence (Fnorm), defined as Fnorm = F1/F0, where F1 is the fluorescence after a given MST-laser on time and F0 the fluorescence prior to IR laser activation. ΔFnorm is the baseline-corrected normalized fluorescence, frequently expressed in parts per thousand [‰]. The affinity parameters Kd were determined by simultaneously performing the experiment on 16 capillaries, each containing a constant concentration of the labelled target (CLIC1) and increasing concentrations of unlabeled ligand (Q48 or Q54). The recorded gradual change in MST was then plotted as ΔFnorm against the ligand concentration to yield dose-response curves. Labelled CLIC1 concentrations

used were 10 nM or 100 nM for RED or BLUE labelling, respectively. The highest concentrations tested for compound Q48 was 5 mM (1% of DMSO final) and 15 mM for Q54. Obtained data were fitted with sigmoidal models using the GraphPad Prism 5.0 software."

Immunofluorescence

Immunofluorescence of monolayer cultures

GSCs were fixed with 4% paraformaldehyde, permeabilized in PBS/0.1% Triton X-100, blocked with normal goat serum and immunostained with primary antibodies, followed by AlexaFluor 568 and 488 fluorochrome-conjugated secondary antibodies (Invitrogen, ThermoFisher Scientific), as reported. Nuclei were counterstained with DAPI (Sigma-Aldrich). Slides were photographed with a DM2500 microscope (Leica, Milan, Italy) equipped with a DFC350FX digital camera (Leica).

Immunofluorescence of 3D cultures

GSCs 3D culture or tumoroids (organoids) were fixed in 1% paraformaldehyde for 1.5h at RT, washed 2-3 times with PBS 1x and dehydrated overnight at 4°C with 30% sucrose solution. To assess the whole organoid structure, samples were permeabilized with 0.1% Triton X-100 for 20 min and blocked in 10% normal goat serum for 2h at RT, followed by overnight primary antibody incubation. Then, organoids were washed 4 times in PBS 1x for 1.5h each and incubated overnight with secondary antibodies AlexaFluor 568, AlexaFluor 488 (ThermoFisher) and ATTO 647 (Sigma-Aldrich). Organoids were washed 4 times in PBS 1x for 1.5h each and fluorescent images were captured with Stellaris 8 TAU STED confocal microscope (Leica), 3D images were generated using ImageJ software. Alternatively, organoids were frozen in OCT and sectioned at 20 μM. Before, slides were coated with Gelatin (0.1%, Sigma-Aldrich G1890) and Chromium(III) potassium sulphate dodecahydrate (0,01%,

Sigma-Aldrich). Slices were probed overnight with primary antibodies and nuclei were stained with DAPI (1:1000) following a standard immunofluorescence protocol, and then imaged with DM 2500 equipped with DFC 350 FX digital camera (Leica).

Western Blotting

Cells were lysed in a buffer containing 1% Igepal, 20 mM Tris–HCl, pH 8, 137 mM NaCl, 10% glycerol, 2 mM EDTA, 1 mM phenylmethylsulfonyl fluoride, 1 mM sodium orthovanadate, 10 mM NaF (all from Sigma-Aldrich), and the "Complete protease inhibitor mixture" (Roche Diagnostics Monza, Italy). Nuclei were removed by centrifugation and total proteins concentration were measured with Bradford assay (Bio-Rad Laboratories). Proteins were separated by SDS-PAGE, blotted onto PVDF membrane (Bio-Rad Laboratories), and probed with the following antibodies: CLIC-1 (Santa Cruz Biotechnology, Heidelberg, Germany), Sox2 (Abcam) and α-tubulin (Sigma-Aldrich). After incubation with secondary antibodies, to visualize and quantify protein bands, chemiluminescent detection (ChemiDoc™ Imaging System, BioRad Laboratories) was performed.

RNA extraction and quantitative real-time PCR (qRT-PCR)

Total RNA was extracted using the High Pure RNA Isolation Kit (Roche), following the manufacturer's instruction. The cDNA was obtained using the iScript cDNA Synthesis Kit (Bio-Rad)[149].

Single stranded cDNA products were analyzed by real-time PCR using the SsoFastTM EvaGreen mix (Bio-Rad) on a CFX96 Touch real-time PCR (Bio-Rad). Cycling conditions were set at 94°C for 30 s, 60°C for 30 s and 72°C for 30 s, for 37 cycles.

Primer sequences were designed on the mature transcripts:

MAP2:

F = 5′-GAAAGACCAAGAGCCTACCACAG-3′

R = 5′-TCGGTCATGGCTTTCTCCAG-3′

RPLP0:

F:5′-TGTGGGCTCCAAGCAGATGCA-3′

R:5′-GCAGCAGTTTCTCCAGAGCTGGG-3′

CD44:

F: 5′-TGAATATAACCTGCCGCTTTG-3′

R:5′-GCTTTCTCCATCTGGGCCAT-3′

28S:

F:5′-CCCAGTGCTCTGAATGTC AA-3′

R:5′-AGTGGGAATCTCGTTCATCC-3′

Levels of target genes in each sample were normalized on the basis of 28S and RPLP0 amplification and reported as relative values. All qRT-PCR runs included negative controls without mRNA templates and cDNA transcription to check reagents for contaminations.

Zebrafish embryo culture, treatment and in vivo toxicity test

Zebrafish (Danio rerio) adults were raised and maintained following standard methods, according to National (Italian D.lgs 26/2014) and European (2010/63/EU and 86/609/EEC) animal welfare laws. Egg were produced by a breeding stock of mature zebrafish: males and females (ratio 2:1) were kept in a tank under the following conditions: 26°C±1 °C, 14h/10h light/dark cycle. Spawning and fertilization took place within 30min after induction by light. Embryos were collected at 4–5h post-fertilization (hpf) and rinsed with the

culture medium to remove residues on the egg surface. For subsequent experiments healthy embryos were selected. Within the timing in which embryos were analyzed, 120 hpf, experiments are not considered as animal experimentation according to Italian rules (Italian D.lgs 26/2014).

Wild type zebrafish embryos AB were soaked in embryo medium with 0.2 mM 1-phenyl 2-thiourea at twenty-four hpf, and incubated for further 24 h at 28.5 °C. At 48 hpf, embryos were dechorionated, anesthetized with 0.0003% tricaine prior to injection and positioned on a wet agarose 1% pad. Using an Eppendorf FemtoJet microinjector, under the observation by stereoscope (MZ APO, Leica), approximately 150–200 cells (ZsGreen-positive cells) were injected in the hindbrain of each embryo. After transplantation, embryos were incubated for 4 h at 32 °C and checked for the presence of fluorescent cells in the correct site. Then embryos were incubated at 32 °C in fresh medium for the following days. Screened embryos were transferred for the treatments in a 48-well plate with 1 mM compound concentration prior to the incubation at 32 °C. Five days post-fertilization (dpf, 3 days after injection), images of the tumors were captured and the relative integrated density, obtained by the product of the fluorescence intensity and the area of the tumor mass, was calculated as the ratio between the final and the initial tumor integrated density using ImageJ software.

Statistical analysis

All experiments, repeated at least three times and performed in triplicate or quadruplicate, were expressed as mean ± S.D./S.E.M. Statistical analyses and IC50 values, calculated using nonlinear regression curve fit analysis, were done using Prism 5.02 (GraphPad, San Diego CA, USA). Statistical significance between groups was assessed by t-test (unpaired, two-tailed) or one-way

ANOVA followed by post-hoc Dunnett's test, or Tukey multiple comparison test for zebrafish xenograft experiments. A p-value ≤ 0.05 was established as statistically significant.

References

1. Sung, H. *et al.* Global Cancer Statistics 2020: GLOBOCAN Estimates of Incidence and Mortality Worldwide for 36 Cancers in 185 Countries. *CA. Cancer J. Clin.* **71**, 209–249 (2021).

2. Ostrom, Q. T. *et al.* CBTRUS Statistical Report: Primary Brain and Other Central Nervous System Tumors Diagnosed in the United States in 2013–2017. *Neuro. Oncol.* **22**, iv1 (2020).

3. I NUMERI DEL CANCRO IN ITALIA 2020.

4. Louis, D. N. *et al.* The 2016 World Health Organization Classification of Tumors of the Central Nervous System: a summary. *Acta Neuropathol.* **131**, 803–820 (2016).

5. Louis, D. N. *et al.* The 2021 WHO Classification of Tumors of the Central Nervous System: a summary. *Neuro. Oncol.* **23**, 1231–1251 (2021).

6. Nobusawa, S., Watanabe, T., Kleihues, P. & Ohgaki, H. IDH1 Mutations as Molecular Signature and Predictive Factor of Secondary Glioblastomas. *Clin. Cancer Res.* **15**, 6002–6007 (2009).

7. Deorah, S., Lynch, C. F., Sibenaller, Z. A. & Ryken, T. C. Trends in brain cancer incidence and survival in the United States: Surveillance, Epidemiology, and End Results Program, 1973 to 2001. *Neurosurg. Focus* **20**, E1 (2006).

8. McKinnon, C., Nandhabalan, M., Murray, S. A. & Plaha, P. Glioblastoma: clinical presentation, diagnosis, and management. *BMJ* **374**, (2021).

9. Neuropathology for medical education - WebPath. Available at: https://webpath.med.utah.edu/CNSHTML/CNSIDX.html. (Accessed: 25th January 2022)

10. Crespo, I. *et al.* Molecular and Genomic Alterations in Glioblastoma Multiforme. *Am. J. Pathol.* **185**, 1820–1833 (2015).

11. McLendon, R. *et al.* Comprehensive genomic characterization defines human glioblastoma genes and core pathways. *Nature* **455**, 1061–1068 (2008).

12. Meir, E. G. Van *et al.* Exciting New Advances in Neuro-Oncology: The Avenue to a Cure for Malignant Glioma. *CA. Cancer J. Clin.* **60**, 166 (2010).

13. Verhaak, R. G. W. *et al.* An integrated genomic analysis identifies clinically relevant subtypes of glioblastoma characterized by abnormalities in PDGFRA, IDH1, EGFR and NF1. *Cancer Cell* **17**, 98

(2010).

14. Sheikh, Y. & Abdrabou, A. Glioblastoma NOS. *Radiopaedia.org* (2013). doi:10.53347/RID-22779

15. Walker, M. D. *et al.* Evaluation of BCNU and/or radiotherapy in the treatment of anaplastic gliomas. A cooperative clinical trial. *J. Neurosurg.* **49**, 333–343 (1978).

16. Walker, M. D. *et al.* Randomized comparisons of radiotherapy and nitrosoureas for the treatment of malignant glioma after surgery. *N. Engl. J. Med.* **303**, 1323–1329 (1980).

17. Mann, J., Ramakrishna, R., Magge, R. & Wernicke, A. G. Advances in Radiotherapy for Glioblastoma. *Front. Neurol.* **8**, 748 (2017).

18. Stupp, R. *et al.* Radiotherapy plus Concomitant and Adjuvant Temozolomide for Glioblastoma. *N. Engl. J. Med.* **352**, 987–996 (2005).

19. ALLEGATO I RIASSUNTO DELLE CARATTERISTICHE DEL PRODOTTO.

20. Lee, S. Y. Temozolomide resistance in glioblastoma multiforme. *Genes Dis.* **3**, 198–210 (2016).

21. Yu, W., Zhang, L., Wei, Q. & Shao, A. O6-Methylguanine-DNA Methyltransferase (MGMT): Challenges and New Opportunities in Glioma Chemotherapy. *Front. Oncol.* **9**, 1547 (2020).

22. Pistollato, F. *et al.* Intratumoral hypoxic gradient drives stem cells distribution and MGMT expression in glioblastoma. *Stem Cells* **28**, 851–862 (2010).

23. Naz, F., Shi, M., Sajid, S., Yang, Z. & Yu, C. Cancer stem cells: a major culprit of intra-tumor heterogeneity. *Am. J. Cancer Res.* **11**, 5782 (2021).

24. Yang, L. *et al.* Targeting cancer stem cell pathways for cancer therapy. *Signal Transduct. Target. Ther.* **5**, (2020).

25. Würth, R. *et al.* Metformin selectively affects human glioblastoma tumor-initiating cell viability. *https://doi.org/10.4161/cc.23050* **12**, 145–156 (2012).

26. Bonnet, D. & Dick, J. E. Human acute myeloid leukemia is organized as a hierarchy that originates from a primitive hematopoietic cell. *Nat. Med. 1997 37* **3**, 730–737 (1997).

27. Al-Hajj, M., Wicha, M. S., Benito-Hernandez, A., Morrison, S. J. & Clarke, M. F. Prospective identification of tumorigenic breast cancer cells. *Proc. Natl. Acad. Sci. U. S. A.* **100**, 3983–3988 (2003).

28. Li, C. *et al.* Identification of pancreatic cancer stem cells. *Cancer Res.* **67**, 1030–1037 (2007).

29. Ricci-Vitiani, L. *et al.* Identification and expansion of human colon-cancer-initiating cells. *Nat. 2006 4457123* **445**, 111–115 (2006).

30. Reya, T., Morrison, S. J., Clarke, M. F. & Weissman, I. L. Stem cells, cancer, and cancer stem cells. *Nature* **414**, 105–111 (2001).

31. Bajaj, J., Diaz, E. & Reya, T. Stem cells in cancer initiation and progression. *J. Cell Biol.* **219**, (2020).

32. Shibue, T. & Weinberg, R. A. EMT, CSCs, and drug resistance: the mechanistic link and clinical implications. doi:10.1038/nrclinonc.2017.44

33. Lane, S. W., Williams, D. A. & Watt, F. M. Modulating the stem cell niche for tissue regeneration. *Nat. Biotechnol.* **32**, 795 (2014).

34. Liu, R. *et al.* The Prognostic Role of a Gene Signature from Tumorigenic Breast-Cancer Cells. *N. Engl. J. Med.* **356**, 217–226 (2007).

35. Merlos-Suá rez, A. *et al.* Cell Stem Cell The Intestinal Stem Cell Signature Identifies Colorectal Cancer Stem Cells and Predicts Disease Relapse. *Stem Cell* **8**, 511–524 (2011).

36. Galli, R. *et al.* Isolation and characterization of tumorigenic, stem-like neural precursors from human glioblastoma. *Cancer Res.* **64**, 7011–7021 (2004).

37. Ignatova, T. N. *et al.* Human cortical glial tumors contain neural stem-like cells expressing astroglial and neuronal markers in vitro. *Glia* **39**, 193–206 (2002).

38. Oliver, T. G. & Wechsler-Reya, R. J. Getting at the Root and Stem of Brain Tumors. *Neuron* **42**, 885–888 (2004).

39. Bao, S. *et al.* Glioma stem cells promote radioresistance by preferential activation of the DNA damage response. *Nature* **444**, 756–760 (2006).

40. Liu, G. *et al.* Analysis of gene expression and chemoresistance of CD133+ cancer stem cells in glioblastoma. *Mol. Cancer* **5**, 67 (2006).

41. Lathia, J. D., Mack, S. C., Mulkearns-Hubert, E. E., Valentim, C. L. L. & Rich, J. N. Cancer stem cells in glioblastoma. *Genes and Development* **29**, 1203–1217 (2015).

42. Gimple, R. C., Bhargava, S., Dixit, D. & Rich, J. N. Glioblastoma stem cells: Lessons from the tumor hierarchy in a lethal cancer. *Genes and Development* **33**, 591–609 (2019).

43. Mellinghoff, I. K. *et al.* Molecular Determinants of the Response of Glioblastomas to EGFR Kinase Inhibitors. *N. Engl. J. Med.* **353**, 2012–2024 (2005).

44. Lombardi, G. *et al.* Regorafenib in Recurrent Glioblastoma Patients: A Large and Monocentric Real-Life Study. *Cancers (Basel).* **13**, (2021).

45. Vredenburgh, J. J. *et al.* Phase II Trial of Bevacizumab and Irinotecan in Recurrent Malignant Glioma. *Clin. Cancer Res.* **13**, 1253–1259 (2007).

46. Diaz, R. J. *et al.* The role of bevacizumab in the treatment of glioblastoma. *J. Neurooncol.* **133**, 455–467 (2017).

47. Weller, M. *et al.* Vaccine-based immunotherapeutic approaches to gliomas and beyond. *Nat. Rev. Neurol. 2017 136* **13**, 363–374 (2017).

48. Stupp, R. *et al.* Effect of Tumor-Treating Fields Plus Maintenance Temozolomide vs Maintenance Temozolomide Alone on Survival in Patients With Glioblastoma: A Randomized Clinical Trial. *JAMA* **318**, 2306 (2017).

49. Lacouture, M. E. *et al.* Prevention and Management of Dermatologic Adverse Events Associated With Tumor Treating Fields in Patients With Glioblastoma. *Front. Oncol.* **10**, 1045 (2020).

50. Chamberlain, M. C., Cloughsey, T., Reardon, D. A. & Wen, P. Y. A novel treatment for glioblastoma: integrin inhibition. *https://doi.org/10.1586/ern.11.188* **12**, 421–435 (2014).

51. Nabors, L. B. *et al.* A Safety Run-in and Randomized Phase II Study of Cilengitide Combined with Chemoradiation for Newly Diagnosed Glioblastoma (NABTT 0306). *Cancer* **118**, 5601 (2012).

52. Peretti, M. *et al.* Chloride channels in cancer: Focus on chloride intracellular channel 1 and 4 (CLIC1 AND CLIC4) proteins in tumor development and as novel therapeutic targets. *Biochim. Biophys. Acta - Biomembr.* **1848**, 2523–2531 (2015).

53. Wulfkuhle, J. D. *et al.* Proteomics of Human Breast Ductal Carcinoma in Situ 1. (2002).

54. Chen, C. De *et al.* Overexpression of CLIC1 in human gastric carcinoma and its clinicopathological significance. *Proteomics* **7**, 155–167 (2007).

55. Tang, H. Y. *et al.* A xenograft mouse model coupled with in-depth plasma proteome analysis facilitates identification of novel serum biomarkers for human ovarian cancer. *J. Proteome Res.* **11**, 678–691 (2012).

56. Wei, X. *et al.* Chloride intracellular channel 1 participates in migration

and invasion of hepatocellular carcinoma by targeting maspin. *J. Gastroenterol. Hepatol.* **30**, 208–216 (2015).

57. Wang, L. *et al.* Elevated expression of chloride intracellular channel 1 is correlated with poor prognosis in human gliomas. *J. Exp. Clin. Cancer Res.* **31**, 1–7 (2012).

58. Setti, M. *et al.* Functional Role of CLIC1 Ion Channel in Glioblastoma-Derived Stem/Progenitor Cells. *JNCI J. Natl. Cancer Inst.* **105**, 1644 (2013).

59. Peretti, M. *et al.* Mutual Influence of ROS, pH, and CLIC1 Membrane Protein in the Regulation of G1–S Phase Progression in Human Glioblastoma Stem Cells. *Mol. Cancer Ther.* **17**, 2451–2461 (2018).

60. Gritti, M. *et al.* Metformin repositioning as antitumoral agent: selective antiproliferative effects in human glioblastoma stem cells, via inhibition of CLIC1-mediated ion current. *Oncotarget* **5**, 11252–11268 (2014).

61. Würth, R. *et al.* Drug-repositioning opportunities for cancer therapy: novel molecular targets for known compounds. *Drug Discov. Today* **21**, 190–199 (2016).

62. Kumar, V. & Chhibber, S. Thalidomide: An Old Drug with New Action. *http://dx.doi.org/10.1179/joc.2011.23.6.326* **23**, 326–334 (2013).

63. Bianchi, G., Richardson, P. G. & Anderson, K. C. Promising therapies in multiple myeloma. *Blood* **126**, 300–310 (2015).

64. Galiè, N. *et al.* Sildenafil Citrate Therapy for Pulmonary Arterial Hypertension. *N. Engl. J. Med.* **353**, 2148–2157 (2005).

65. EMA. Allegato I Riassunto delle caratteristiche del prodotto Revatio. 1–33 (2020).

66. Miner, J. & Hoffhines, A. The Discovery of Aspirin's Antithrombotic Effects. *Texas Hear. Inst. J.* **34**, 179 (2007).

67. Phillips, I., Langley, R., Gilbert, D. & Ring, A. Aspirin as a Treatment for Cancer. *Clin. Oncol.* **25**, 333–335 (2013).

68. Moon, C. M. *et al.* Nonsteroidal anti-inflammatory drugs suppress cancer stem cells via inhibiting PTGS2 (cyclooxygenase 2) and NOTCH/HES1 and activating PPARG in colorectal cancer. *Int. J. Cancer* **134**, 519–529 (2014).

69. Hay, M., Thomas, D. W., Craighead, J. L., Economides, C. & Rosenthal, J. Clinical development success rates for investigational drugs. *Nat. Biotechnol. 2014 321* **32**, 40–51 (2014).

70. Gupta, S. C., Sung, B., Prasad, S., Webb, L. J. & Aggarwal, B. B. Cancer

drug discovery by repurposing: teaching new tricks to old dogs. *Trends Pharmacol. Sci.* **34**, 508–517 (2013).

71. Sotelo, J., Briceño, E. & López-González, M. A. Adding chloroquine to conventional treatment for glioblastoma multiforme: A randomized, double-blind, placebo-controlled trial. *Ann. Intern. Med.* **144**, 337–343 (2006).

72. Würth, R., Barbieri, F. & Florio, T. New Molecules and Old Drugs as Emerging Approaches to Selectively Target Human Glioblastoma Cancer Stem Cells. *Biomed Res. Int.* **2014**, (2014).

73. Evans, J. M. M., Donnelly, L. A., Emslie-Smith, A. M., Alessi, D. R. & Morris, A. D. Metformin and reduced risk of cancer in diabetic patients. *BMJ* **330**, 1304–1305 (2005).

74. Hadad, S. *et al.* Evidence for biological effects of metformin in operable breast cancer: A pre-operative, window-of-opportunity, randomized trial. *Breast Cancer Res. Treat.* **128**, 783–794 (2011).

75. Zhou, G. *et al.* Role of AMP-activated protein kinase in mechanism of metformin action. *J. Clin. Invest.* **108**, 1167–1174 (2001).

76. Yue, W. *et al.* Metformin combined with aspirin significantly inhibit pancreatic cancer cell growth in vitro and in vivo by suppressing anti-apoptotic proteins Mcl-1 and Bcl-2. *Oncotarget* **6**, 21208–21224 (2015).

77. Orecchioni, S. *et al.* The biguanides metformin and phenformin inhibit angiogenesis, local and metastatic growth of breast cancer by targeting both neoplastic and microenvironment cells. *Int. J. Cancer* **136**, E534–E544 (2015).

78. Barbieri, F. *et al.* In vitro and in vivo antiproliferative activity of metformin on stem-like cells isolated from spontaneous canine mammary carcinomas: Translational implications for human tumors. *BMC Cancer* **15**, (2015).

79. Sesen, J. *et al.* Metformin Inhibits Growth of Human Glioblastoma Cells and Enhances Therapeutic Response. *PLoS One* **10**, e0123721 (2015).

80. Gritti, M. *et al.* Metformin repositioning as antitumoral agent: selective antiproliferative effects in human glioblastoma stem cells, via inhibition of CLIC1-mediated ion current. *Oncotarget* **5**, 11252–11268 (2014).

81. Marini, C. *et al.* Direct inhibition of hexokinase activity by metformin at least partially impairs glucose metabolism and tumor growth in experimental breast cancer. *Cell Cycle* **12**, 3490–3499 (2013).

82. Iglesias, D. A. *et al.* Another surprise from metformin: Novel mechanism

of action via k-Ras influences endometrial cancer response to therapy. *Mol. Cancer Ther.* **12**, 2847–2856 (2013).

83. Eikawa, S. *et al.* Immune-mediated antitumor effect by type 2 diabetes drug, metformin. *Proc. Natl. Acad. Sci. U. S. A.* **112**, 1809–1814 (2015).

84. Hirsch, H. A., Iliopoulos, D., Tsichlis, P. N. & Struhl, K. Metformin selectively targets cancer stem cells, and acts together with chemotherapy to block tumor growth and prolong remission. *Cancer Res.* **69**, 7507–7511 (2009).

85. Vazquez-Martin, A., Oliveras-Ferraros, C., Del Barco, S., Martin-Castillo, B. & Menendez, J. A. The anti-diabetic drug metformin suppresses self-renewal and proliferation of trastuzumab-resistant tumor-initiating breast cancer stem cells. *Breast Cancer Res. Treat.* **126**, 355–364 (2011).

86. Lonardo, E., Cioffi, M., Sancho, P., Crusz, S. & Heeschen, C. Studying pancreatic cancer stem cell characteristics for developing new treatment strategies. *J. Vis. Exp.* **2015**, (2015).

87. Kim, N. Y., Lee, H. Y. & Lee, C. Metformin targets Axl and Tyro3 receptor tyrosine kinases to inhibit cell proliferation and overcome chemoresistance in ovarian cancer cells. *Int. J. Oncol.* **47**, 353–360 (2015).

88. Barbieri, F. *et al.* Inhibition of Chloride Intracellular Channel 1 (CLIC1) as Biguanide Class-Effect to Impair Human Glioblastoma Stem Cell Viability. *Front. Pharmacol.* **9**, (2018).

89. Azzarelli, R. Organoid Models of Glioblastoma to Study Brain Tumor Stem Cells. *Front. Cell Dev. Biol.* **8**, 16 (2020).

90. Paolillo, M., Comincini, S. & Schinelli, S. In Vitro Glioblastoma Models: A Journey into the Third Dimension. *Cancers (Basel).* **13**, (2021).

91. Zhou, W. *et al.* Periostin secreted by glioblastoma stem cells recruits M2 tumour-associated macrophages and promotes malignant growth. *Nat. Cell Biol. 2014 172* **17**, 170–182 (2015).

92. Chen, Z. *et al.* Cellular and Molecular Identity of Tumor-Associated Macrophages in Glioblastoma. *Cancer Res.* **77**, 2266–2278 (2017).

93. Guan, X., Hasan, M. N., Maniar, S., Jia, W. & Sun, D. Reactive Astrocytes in Glioblastoma Multiforme. *Mol. Neurobiol. 2018 558* **55**, 6927–6938 (2018).

94. Xia, S. *et al.* Tumor microenvironment tenascin-C promotes glioblastoma invasion and negatively regulates tumor proliferation. *Neuro. Oncol.* **18**, 507–517 (2015).

95. de Gooijer, M. C., Guillén Navarro, M., Bernards, R., Wurdinger, T. & van Tellingen, O. An Experimenter's Guide to Glioblastoma Invasion Pathways. *Trends Mol. Med.* **24**, 763–780 (2018).

96. Timerman, D. & Yeung, C. M. Identity confusion of glioma cell lines. *Gene* **536**, 221–222 (2014).

97. Carla Da Hora, C., Schweiger, M. W., Wurdinger, T. & Tannous, B. A. Patient-Derived Glioma Models: From Patients to Dish to Animals. (2019). doi:10.3390/cells8101177

98. Tanaka, S. *et al.* Genetically distinct glioma stem-like cell xenografts established from paired glioblastoma samples harvested before and after molecularly targeted therapy. *Sci. Reports 2019 91* **9**, 1–9 (2019).

99. Wang, C. *et al.* Mimicking brain tumor-vasculature microanatomical architecture via co-culture of brain tumor and endothelial cells in 3D hydrogels. *Biomaterials* **202**, 35–44 (2019).

100. Laks, D. R. *et al.* Large-scale assessment of the gliomasphere model system. *Neuro. Oncol.* **18**, 1367–1378 (2016).

101. Lancaster, M. A. & Knoblich, J. A. Organogenesis in a dish: modeling development and disease using organoid technologies. *Science* **345**, (2014).

102. Clevers, H. Modeling Development and Disease with Organoids. *Cell* **165**, 1586–1597 (2016).

103. Rahmani, W. *et al.* Attenuation of SARS-CoV-2 Infection by Losartan in Human Kidney Organoids. *iScience* 103818 (2022). doi:10.1016/J.ISCI.2022.103818

104. Qian, X. *et al.* Brain-Region-Specific Organoids Using Mini-bioreactors for Modeling ZIKV Exposure. *Cell* **165**, 1238–1254 (2016).

105. Bartfeld, S. *et al.* In Vitro Expansion of Human Gastric Epithelial Stem Cells and Their Responses to Bacterial Infection. *Gastroenterology* **148**, 126-136.e6 (2015).

106. Lancaster, M. A. & Huch, M. Disease modelling in human organoids. *Dis. Model. Mech.* **12**, (2019).

107. Lancaster, M. A. *et al.* Cerebral organoids model human brain development and microcephaly. doi:10.1038/nature12517

108. Sato, T. & Clevers, H. Growing self-organizing mini-guts from a single intestinal stem cell: Mechanism and applications. *Science (80-.).* **340**, 1190–1194 (2013).

109. Sato, T. *et al.* Single Lgr5 stem cells build crypt-villus structures in vitro without a mesenchymal niche. *Nat. 2009 4597244* **459**, 262–265 (2009).

110. Dekkers, J. F. *et al.* Characterizing responses to CFTR-modulating drugs using rectal organoids derived from subjects with cystic fibrosis. *Sci. Transl. Med.* **8**, (2016).

111. Tatullo, M. *et al.* Organoids in Translational Oncology. *J. Clin. Med.* **9**, 1–16 (2020).

112. Van De Wetering, M. *et al.* Prospective Derivation of a Living Organoid Biobank of Colorectal Cancer Patients. *Cell* **161**, 933–945 (2015).

113. Sachs, N. *et al.* A Living Biobank of Breast Cancer Organoids Captures Disease Heterogeneity. *Cell* **172**, 373-386.e10 (2018).

114. Yan, H. H. N. *et al.* A Comprehensive Human Gastric Cancer Organoid Biobank Captures Tumor Subtype Heterogeneity and Enables Therapeutic Screening. *Cell Stem Cell* **23**, 882-897.e11 (2018).

115. Wang, C., Tong, X. & Yang, F. Bioengineered 3D Brain Tumor Model To Elucidate the Effects of Matrix Stiffness on Glioblastoma Cell Behavior Using PEG-Based Hydrogels. *Mol. Pharm.* **11**, 2115–2125 (2014).

116. Hubert, C. G. *et al.* A Three-Dimensional Organoid Culture System Derived from Human Glioblastomas Recapitulates the Hypoxic Gradients and Cancer Stem Cell Heterogeneity of Tumors Found In Vivo. *Cancer Res.* **76**, 2465–2477 (2016).

117. Jacob, F. *et al.* A Patient-Derived Glioblastoma Organoid Model and Biobank Recapitulates Inter- and Intra-tumoral Heterogeneity. *Cell* **180**, 188-204.e22 (2020).

118. Ogawa, J., Pao, G. M., Shokhirev, M. N. & Verma, I. M. Glioblastoma Model Using Human Cerebral Organoids. *Cell Rep.* **23**, 1220–1229 (2018).

119. Bian, S. *et al.* Genetically engineered cerebral organoids model brain tumor formation. *Nat. Methods 2018 158* **15**, 631–639 (2018).

120. Linkous, A. *et al.* Modeling Patient-Derived Glioblastoma with Cerebral Organoids. *Cell Rep.* **26**, 3203 (2019).

121. Azzarelli, R., Ori, M., Philpott, A. & Simons, B. D. Three-dimensional model of glioblastoma by co-culturing tumor stem cells with human brain organoids. *Biol. Open* **10**, (2021).

122. Hofer, M. & Lutolf, M. P. Engineering organoids. *Nat. Rev. Mater.* **6**, 1 (2021).

123. Yi, H. G. *et al.* A bioprinted human-glioblastoma-on-a-chip for the

identification of patient-specific responses to chemoradiotherapy. *Nat. Biomed. Eng. 2019 37* **3**, 509–519 (2019).

124. Barbieri, F. *et al.* Repurposed Biguanide Drugs in Glioblastoma Exert Antiproliferative Effects via the Inhibition of Intracellular Chloride Channel 1 Activity. *Front. Oncol.* **9**, (2019).

125. Tonini, R. *et al.* Functional characterization of the NCC27 nuclear protein in stable transfected CHO-K1 cells. *FASEB J.* **14**, 1171–1178 (2000).

126. Wensink, G. E. *et al.* Patient-derived organoids as a predictive biomarker for treatment response in cancer patients. *NPJ Precis. Oncol.* **5**, (2021).

127. Sato, A. *et al.* Glioma-initiating cell elimination by metformin activation of FOXO3 via AMPK. *Stem Cells Transl. Med.* **1**, 811–824 (2012).

128. Sahra, I. Ben *et al.* Metformin, independent of AMPK, induces mTOR inhibition and cell-cycle arrest through REDD1. *Cancer Res.* **71**, 4366–4372 (2011).

129. Graham, G. G. *et al.* Clinical pharmacokinetics of metformin. *Clin. Pharmacokinet.* **50**, 81–98 (2011).

130. Bridges, H. R., Jones, A. J. Y., Pollak, M. N. & Hirst, J. Effects of metformin and other biguanides on oxidative phosphorylation in mitochondria. *Biochem. J.* **462**, 475–487 (2014).

131. Gaudenzi, G. *et al.* Patient-derived xenograft in zebrafish embryos: a new platform for translational research in neuroendocrine tumors. *Endocrine* **57**, 214–219 (2017).

132. Pernik, M. N. *et al.* Patient-Derived Cancer Organoids for Precision Oncology Treatment. *J. Pers. Med.* **11**, (2021).

133. Habib, A., Pease, M., Kodavali, C. V., Amankulor, N. & Zinn, P. O. A contemporary update on glioblastoma: molecular biology, current management, and a vision towards bio-adaptable personalized care. *J. Neurooncol.* **151**, 103–112 (2021).

134. Baldassari, S. *et al.* Development of an Injectable Slow-Release Metformin Formulation and Evaluation of Its Potential Antitumor Effects. *Sci. Rep.* **8**, (2018).

135. Würth, R. *et al.* Metformin selectively affects human glioblastoma tumor-initiating cell viability: A role for metformin-induced inhibition of Akt. *Cell Cycle* **12**, 145–156 (2013).

136. Grytsai, O., Myrgorodska, I., Rocchi, S., Ronco, C. & Benhida, R. Biguanides drugs: Past success stories and promising future for drug

discovery. *Eur. J. Med. Chem.* **224**, (2021).

137. Gabel, S. A. *et al.* A Structural Basis for Biguanide Activity. *Biochemistry* **56**, 4786–4798 (2017).

138. Barbieri, F. *et al.* Chloride intracellular channel 1 activity is not required for glioblastoma development but its inhibition dictates glioma stem cell responsivity to novel biguanide derivatives. *J. Exp. Clin. Cancer Res.* **41**, 53 (2022).

139. Xu, H., Jiao, D., Liu, A. & Wu, K. Tumor organoids: applications in cancer modeling and potentials in precision medicine. *J. Hematol. Oncol.* **15**, 58 (2022).

140. Loong, H. H. F. *et al.* Patient-derived tumor organoid predicts drugs response in glioblastoma: A step forward in personalized cancer therapy? *J. Clin. Neurosci.* **78**, 400–402 (2020).

141. Griffero, F. *et al.* Different response of human glioma tumor-initiating cells to epidermal growth factor receptor kinase inhibitors. *J. Biol. Chem.* **284**, 7138–7148 (2009).

142. Bajetto, A. *et al.* Different effects of human umbilical cord mesenchymal stem cells on glioblastoma stem cells by direct cell interaction or via released soluble factors. *Front. Cell. Neurosci.* **11**, (2017).

143. Dominici, M. *et al.* Minimal criteria for defining multipotent mesenchymal stromal cells. The International Society for Cellular Therapy position statement. *Cytotherapy* **8**, 315–317 (2006).

144. King, H. & Tonkin, I. M. Antiplasmodial action and chemical constitution; guanidines and diguanides. *J. Chem. Soc.* 1063–1069 (1946). doi:10.1039/JR9460001063

145. Shapiro, S. L. *et al.* 3726 Substituted Arylbiguanides.

146. Modest, E. J. Chemical and Biological Studies on 1,2-Dihydro-s-triazines. II. Three-Component Synthesis. *J. Org. Chem.* **21**, 1–13 (1956).

147. Bami: Studies in dihydrotriazines: 1-aryl-2, 4-diamino-1,... - Google Scholar. Available at: https://scholar.google.com/scholar_lookup?journal=J+Sci+Ind+Res&title=Studies+in+dihydrotriazines:+1-aryl-2,4-diamino-1,6-dihydro-6,6-dialkyl-1,3,5-triazines&author=HL+Bami&volume=14C&publication_year=1955&pages=231-236&. (Accessed: 1st March 2022)

148. Seidel, S. A. I. *et al.* Microscale thermophoresis quantifies biomolecular interactions under previously challenging conditions. *Methods* **59**, 301–

315 (2013).

149. Banelli, B. *et al.* The histone demethylase KDM5A is a key factor for the resistance to temozolomide in glioblastoma. *Cell Cycle* **14**, 3418–3429 (2015).

List of publications

1. Barbieri F, **Bosio AG**, Pattarozzi A, Tonelli M, Bajetto A, Verduci I, Cianci F, Cannavale G, Palloni LMG, Francesconi V, Thellung S, Fiaschi P, Mazzetti S, Schenone S, Balboni B, Girotto S, Malatesta P, Daga A, Zona G, Mazzanti M, Florio T. Chloride intracellular channel 1 activity is not required for glioblastoma development but its inhibition dictates glioma stem cell responsivity to novel biguanide derivatives. J Exp Clin Cancer Res. 2022 Feb 8;41(1):53. doi: 10.1186/s13046-021-02213-0. PMID: 35135603; PMCID: PMC8822754.

2. Thellung S, Corsaro A, **Bosio AG**, Zambito M, Barbieri F, Mazzanti M, Florio T. Emerging Role of Cellular Prion Protein in the Maintenance and Expansion of Glioma Stem Cells. Cells. 2019 Nov 18;8(11):1458. doi: 10.3390/cells8111458. PMID: 31752162; PMCID: PMC6912268.

Convention and abstract submission

- European organoids symposium 2019, Milano 23rd -24th September 2019
- The Future of Medicines Starts Now 2019 (2nd edition) Genova, 26th-27th September 2019

- BraYn- 2nd Brainstorming Research Assembly for Young Neuroscientists, 14th-15th-16th November 2019. **Poster presentation**: Cellular prion protein controls stem cell-like properties of human glioblastoma cancer stem cells. (Alessia G. Bosio et al.)

- 39° Congresso Nazionale SIF **Abstract:** Chloride intracellular channel 1 inhibition dictates antitumor effects of old and new biguanide compounds in glioblastomastem cells. (F. Barbieri, A. G. Bosio, et al.)

- "Organoids: Modelling Organ Development and Disease in 3D Culture" -21st ,22nd, 23rd,24th October 2020.

- 40° Congresso Nazionale SIF **Abstract:** Targeting the Chloride Intracellular Channel -1 activity pinpoints a molecular vulnerability in human glioblastoma stem cells: antitumor effects of novel linear and cyclic biguanides (F. Barbieri, A. G. Bosio, et al.)

- BraYn- 4th Brainstorming Research Assembly for Young Neuroscientists 20th, 21st, 22nd October 2021. **Poster presentation:** Patient derived 3D glioblastoma-culture models: characterization and potential applications in drug screening. (Alessia G. Bosio et al.)

Acknowledgments

Firstly, I would like to express my gratitude to Prof. Florio and to all the Pharmacology Lab for believing in me in 2017 (when I barely knew how to use a pipette) and then, giving me the opportunity to start my PhD. Sincere thanks to Prof. Florio and Prof. Federica Barbieri for having guided me during my PhD with continuous support and patience, and for their help in writing my PhD thesis.

I would like to thank Martina for being the best colleague for this « journey » I could ever ask for, I already miss our brainstormings, but I know to have found a friend. A big thanks to all my lab mates Alessandro, Stefano, Irene and Mario for all the interesting discussions during these three years, tips and continuous collaboration. A very special mention to Alessandra and Adriana for teaching me almost everything since when I started to attend the lab, for all their tips and for all the time we spent together. I know that it will be difficult to find another place with the same sense of teamwork, trust and collaboration as was in my lab!

I would like to thank Dott.ssa Elena Gatta for helping me look inside my organoids, making beautiful photos with the confocal microscope Stellaris.

Lastly, I would like to thank my family, my mum, my dad and my « *two Richards* » for believing in me and above all, pushing me to follow my dreams: there is no better demonstration of love.